# MAGNETOM Flash

Issue Number 81 · 2/2022
Pediatric Edition

siemens-healthineers.com/magnetom-world

Page 26
**"Quick MRI" Pediatric Brain Imaging at 3T: A child-tailored approach**
*Andrea Righini, et al.*

Page 30
**BLADE Diffusion Brain MRI in Children**
*Aaron S McAllister, Ramkumar Krishnamurthy*

Page 42
**Deep Resolve in Pediatric MRI**
*Johan Dehem*

Page 50
**Liver Magnetic Resonance Elastography in Children**
*Elżbieta Jurkiewicz, et al.*

Page 60
**Pediatric Whole-Body MRI: How I Do It**
*Bac Nguyen, Lil-Sofie Muller*

Page 70
**3T Cardiac MRI and Acute Myocarditis in the Context of Second-dose mRNA Vaccine**
*Erin Robins, Claire Harris*

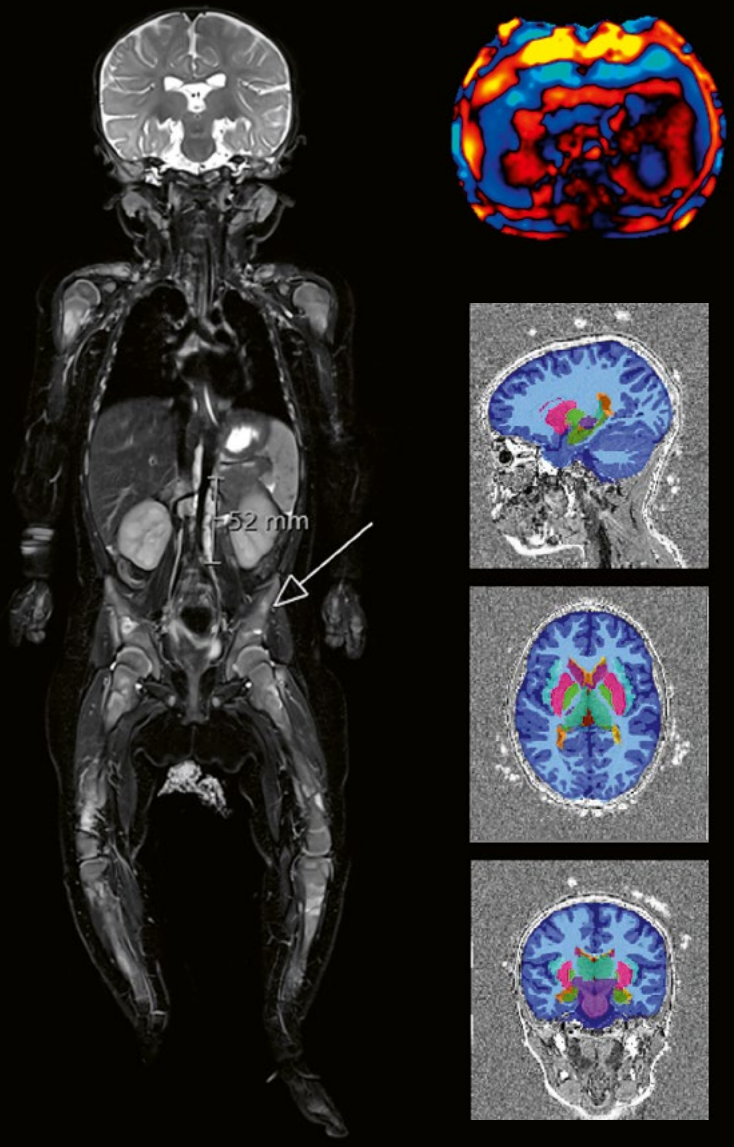




SIEMENS Healthineers

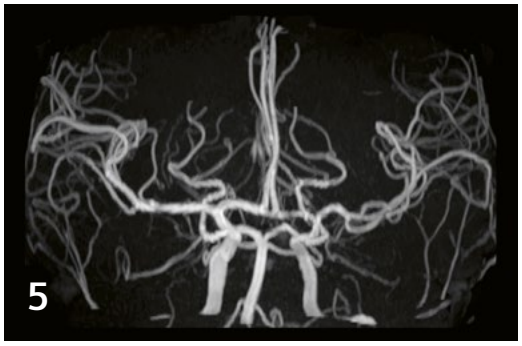


Scanning faster

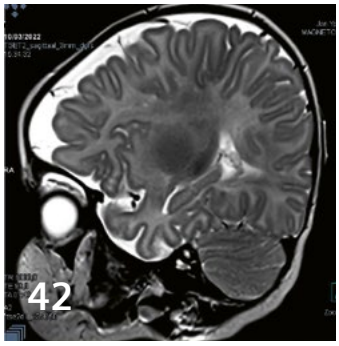


Deep Resolve Quiet


Help your little patients lose their fear with Lottie

## Neurological Imaging


5 **Scanning Faster: Application in Pediatric Neuroimaging**
Michael Kean
Royal Children's Hospital, Melbourne, Australia

26 **Abbreviated Turbo Spin Echo T2- and FLAIR-weighted Sequences to Complement Multiplanar HASTE Images in "Quick MRI" Pediatric Brain Imaging at 3 Tesla: A child-tailored approach**
Andrea Righini, et al.
Children's Hospital V. Buzzi, Milan, Italy

30 **2D BLADE Turbo Gradient- and Spin-Echo versus 2D Spin-Echo Echo-Planar Diffusion-Weighted Brain MRI in Children**
Aaron S McAllister, Ramkumar Krishnamurthy
Nationwide Children's Hospital, Columbus, OH, USA

34 **MP2RAGE-based Inline Morphometric and Regional T1 Assessment[1] in Pediatric Patients: Initial Clinical Experience and Potential Benefits**
Baptiste Morel, et al.
University of Tours, France

42 **Deep Resolve in Pediatric MRI**
Johan Dehem
Jan Yperman Ziekenhuis, Ieper, Belgium


[1] *Work in progress. The application is currently under development and not for sale in the U.S. and in other countries. Its future availability cannot be ensured.*

## Abdominal Imaging


50 **Liver Magnetic Resonance Elastography in Children**
Elżbieta Jurkiewicz, et al.
The Children's Health Memorial Institute, Warszawa, Poland


## Whole-body Imaging


56 **PET-MRI Patterns in Pediatric Patients with Neurofibromatosis Type 1 (NF1) and NF1-associated Malignant Peripheral Nerve Sheath Tumors (MPNSTs)**
Valentina Bodanza, Diego Cecchin, et al.
University Hospital of Padova, Italy

60 **Pediatric Whole-Body MRI: How I Do It**
Bac Nguyen, Lil-Sofie Muller
Oslo University Hospital, Rikshospitalet, Oslo, Norway


## Cardiovascular Imaging


70 **3T Cardiac MRI and Acute Myocarditis in the Context of Second-dose mRNA Vaccine. A Case Study**
Erin Robins, Claire Harris
Perth Children's Hospital, Nedlands, Western Australia


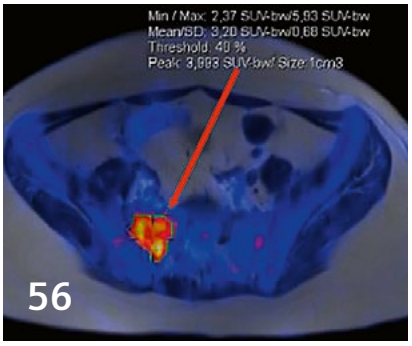


PET-MRI Patterns in NF1 and MPNSTs

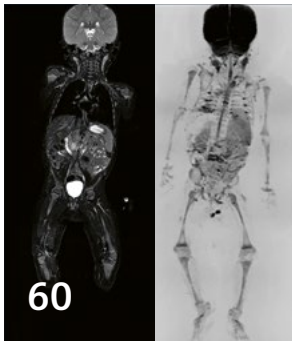


Pediatric Whole-Body MRI

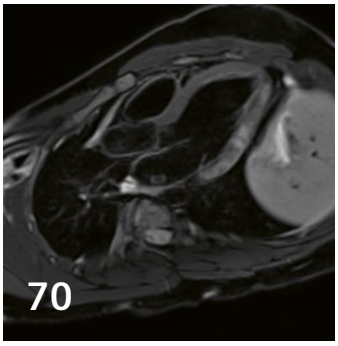


Cardiac MRI and Acute Myocarditis

## Patient Experience

76 **Pediatric Patient Experience: Reshaping the World of Magnetic Resonance Imaging for Children**
Gabriele Hahn
University Hospital Carl Gustav Carus, Technische Universität Dresden, Germany

## Meet Siemens Healthineers

82 **Introducing Pedro Itriago Leon**
MR collaborations manager
Houston, TX, USA

We appreciate your comments.
Please contact us at magnetomworld.team@siemens-healthineers.com

## Editorial Board



## Review Board

Siemens Healthineers extends its appreciation to all the radiologists, technologists, physicists, experts, and scholars who donate their time and energy – without payment – in order to share their expertise with the readers of MAGNETOM Flash.

MAGNETOM Flash – Imprint



Publisher:
**Siemens Healthcare GmbH**
Magnetic Resonance,
Karl-Schall-Str. 6, D-91052 Erlangen, Germany

**Editor-in-chief:**
Antje Hellwich
(antje.hellwich@siemens-healthineers.com)

**Editorial Board:**
Jane Kilkenny; Nadine Leclair, M.D.;
Christianne Leidecker, Ph.D.;
Rebecca Ramb, Ph.D.; Wellesley Were

**Review Board:**
Gaia Banks, Ph.D.; André Fischer, Ph.D.;
Daniel Fischer; Christian Geppert, Ph.D.;
Raphael Schwarz, Ph.D.; Gregor Thörmer, Ph.D.

**Copy Editing:**
Sheila Regan, Jen Metcalf, UNIWORKS,
www.uni-works.org
(with special thanks to Kylie Martin)

**Layout:**
Agentur Baumgärtner,
Friedrichstr. 4, D-90762 Fürth, Germany

**PrePress and Image Editing, Production:**
Clemens Ulrich, Paul Linssen,
Siemens Healthcare GmbH

**Printer:**
Schmidl & Rotaplan Druck GmbH,
Hofer Str. 1, D-93057 Regensburg, Germany

Note in accordance with § 33 Para.1 of the German Federal Data Protection Law: Despatch is made using an address file which is maintained with the aid of an automated data processing system.

MAGNETOM Flash is sent free of charge to Siemens Healthineers MR customers, qualified physicians, technologists, physicists and radiology departments throughout the world. It includes reports in the English language on magnetic resonance: diagnostic and therapeutic methods and their application as well as results and experience gained with corresponding systems and solutions. It introduces from case to case new principles and procedures and discusses their clinical potential. The statements and views of the authors in the individual contributions do not necessarily reflect the opinion of the publisher.

The information presented in these articles and case reports is for illustration only and is not intended to be relied upon by the reader for instruction as to the practice of medicine. Any health care practitioner reading this information is reminded that they must use their own learning, training and expertise in dealing with their individual patients. This material does not substitute for that duty and is not intended by Siemens Healthcare to be used for any purpose in that regard. The drugs and doses mentioned herein are consistent with the approval labeling for uses and/or indications of the drug. The treating physician bears the sole responsibility for the diagnosis and treatment of patients, including drugs and doses prescribed in connection with such use. The Operating Instructions must always be strictly followed when operating the MR system. The sources for the technical data are the corresponding data sheets. Results may vary.

Partial reproduction in printed form of individual contributions is permitted, provided the customary bibliographical data such as author's name and title of the contribution as well as year, issue number and pages of MAGNETOM Flash are named, but the editors request that two copies be sent to them. The written consent of the authors and publisher is required for the complete reprinting of an article.

We welcome your questions and comments about the editorial content of MAGNETOM Flash. Please contact us at magnetomworld.team@siemens-healthineers.com

Manuscripts as well as suggestions, proposals and information are always welcome; they are carefully examined and submitted to the editorial board for attention. MAGNETOM Flash is not responsible for loss, damage, or any other injury to unsolicited manuscripts or other materials. We reserve the right to edit for clarity, accuracy, and space. Include your name, address, and phone number and send to the editors, address above.

**MAGNETOM Flash is also available online:**

**www.siemens-healthineers.com/magnetom-world**

# Scanning Faster: Application in Pediatric Neuroimaging

**Michael Kean**

Chief MR Technologist at The Royal Children's Hospital / Murdoch Children's Research Institute, Melbourne, Australia

How many of the MR community can remember neuroimaging pre-MRI or pre-CT, when highly skilled neuroradiologists performed air studies to outline the ventricles or CSF pathways to visualize the impact of intracranial or intraspinal pathology on normal anatomy? That was my introduction to pediatric neuroimaging in 1979.

How far we have come in such a short time is an extraordinary accomplishment, and the review by Runge [1] looking at the 50 years of innovation in imaging puts it all in perspective.

As a member of the MR community, I celebrated 30 years of pediatric MRI during the early phases of the COVID-19 pandemic, and every new advance in hardware, clinical applications, and pulse sequences still continues to amaze me – with a diverse and eclectic group of scientists and engineers working within academia and Siemens Healthineers taking us to places most of us never dreamed possible. If I reflect on my early days with my first Siemens system in the early 1990s I would never have imagined just how far this amazing imaging modality would develop. My first system was a MAGNETOM 63SP 4000 with no array coils, fast spin echo was only just being talked about, MPRAGE didn't exist, the gradient strength was 10 mT/m with an almost glacial slew rate of 10 T/m/s. When you compare that to our latest scanner, a MAGNETOM Prisma$^{fit}$ with 80/200 gradients, it brings to reality how far we have come (Fig. 1).

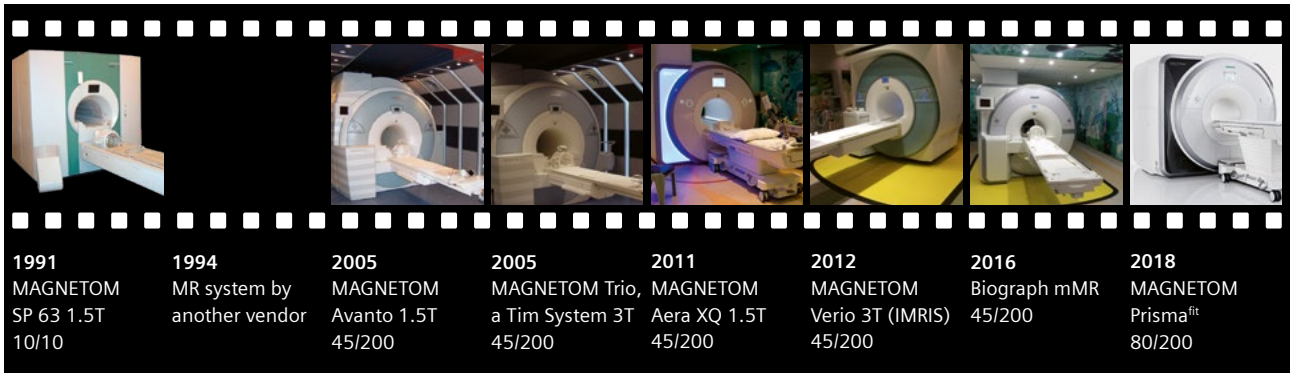


**1** Evolution of MRI systems utilized by The Royal Children's Hospital for scanning pediatric patients from 1991 to present. Gradient strength represented by max gradient amplitude (mT/m) / slew rate (T/m/s).

[1] *MR scanning has not been established as safe for imaging fetuses and infants less than two years of age. The responsible physician must evaluate the benefits of the MR examination compared to those of other imaging procedures. Note: This disclaimer does not represent the opinion of the author.*

The use of MRI in the evaluation of pediatric neuroimaging has grown over the past 30 years, going from a clinical problem-solving tool after an equivocal CT to the imaging modality of choice in the majority of pediatric neuroimaging protocols.

This change in clinical focus has been due largely to the increasing availability of the modality and an explosion of technical advancements in areas such as field strength, system hardware, coil design, image reconstruction, pulse sequences, and more user-intuitive operating systems that have unleashed the potential to reduce scan times and, in some instances, correct for motion.

The requirement to make MR faster is driven by many factors within the clinical or research community. These range from patient compliance, pressure on the MR facility to scan more patients in a shorter time based on the rising costs of healthcare or unacceptable waiting lists, the requirement to add newer sequences into the protocol, and a reduction in sedation or anesthesia times.

The most common question for MR users is: Why can't we scan faster? And the processes that underlie that very simple but emotive question are complex and there is no one solution. To answer that question, we need to look at the basic equation that defines scan time in MRI, and at the complexity of interrelated components that define it. The scan time in MRI in its most basic form is

Equation 1

$$T_A = TR \cdot N_{Ave} \cdot N_y \cdot N_z$$

with TR being the repetition time, and $N_{Ave}$, $N_y$, and $N_z$ being the the number of averages, phase encoding steps and partition encoding steps or slices, respectively. All these individual components contribute to image contrast, spatial resolution, and foremost the signal-to-noise ratio (SNR). While the latter may be affected by many factors, such as the coil, the object to be imaged, and relaxation, it is fundamentally defined by the voxel size $V_{Voxel}$ and the time that is used to sample data $T_S$ [2]:

Equation 2

$$SNR \propto V_{Voxel} \cdot \sqrt{T_S} \propto V_{Voxel} \cdot \sqrt{N_{Ave} N_y N_z}$$

The fact that SNR is not abundant in MRI leads, as can easily be seen from the above equation, to the well-known trade-off between spatial resolution, scan time, and SNR. Any small change of the above parameters will likely have an impact on image quality and it is ultimately the image quality that determines our success or failure on our quest to reduce scan times.

However, what is ultimately determined to be a diagnostic image of sufficient spatial resolution, signal-to-noise, and contrast-to-noise to adequately display the anatomical structure or pathology is not standardized. Our acceptance of image quality is mainly based on a radiologist's perception and their qualitative or semi-quantitative assessment of the data. Rofsky [3] wrote an editorial in JMRI in 2015 looking at this issue and its implications for how we construct our MR imaging protocols.

The goal for the MR team is to redefine the protocol to reduce the scan time whilst maintaining image quality consistent with the internal standards of the department, system hardware, and needs of the patient. In our attempts to make scan times shorter, the historical perception was that to successfully shorten scan times we needed to compromise on image quality. This is an unacceptable compromise, and we should be investigating methodologies that either produce images of an equivalent standard as our basic protocols or in some instances a higher quality, understanding the complexities involved in reducing our scan times (Fig. 2).

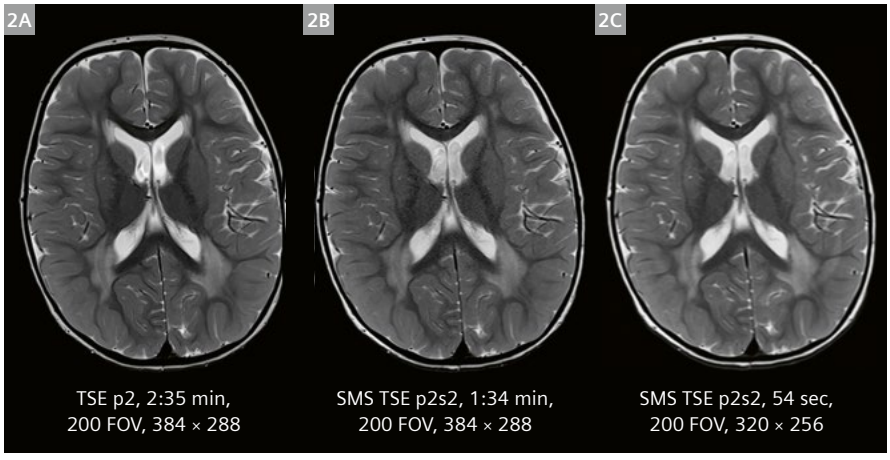


**2** Three T2 images acquired with different scan times demonstrating that it is possible to balance a scan time reduction whilst maintaining diagnostic integrity.

Our longstanding collaboration with Siemens Healthineers has been instrumental in refining the internal parameters of new research applications or pre-product sequences and translating them into standard-of-care pediatric imaging. One of the most significant of these was the development of our Code Stroke protocol, in which MRI and not CT is considered as the first-line imaging modality in pediatric stroke (Fig. 3). But as we know, as soon as this article is published there will be newer and faster options available to the MR community and the acquisitions presented in this article will be considered slow.

Understanding the pulse sequence and the reconstruction method is crucial to a facility's ability to make informed adjustments within the protocol to reflect the speed and image quality they require. Many of these faster scanning sequences or iterative reconstruction techniques have the potential to introduce artifacts into the images, so it is imperative that all the information about the method is available locally, prior to implementing significant change.

So reducing scan time is just not as simple as changing one parameter. It is essential that we as end users understand the reliance on maintaining overall image quality and the potential consequences of producing unacceptable image quality based on these changes.

How many times has a member of the team come back from a meeting such as ISMRM with a new ultrafast scanning protocol, but when you try it the images look bad? Most of the time, not all the information is available during the presentation and often crucial information isn't shared. It's like baking a cake with only half the recipe and you must guess the rest. My advice would be: In your earliest foray into these new techniques, don't go jumping into the freezing lake. Instead, take it slowly and ease your way in. Initially work within the protocol tree from Siemens Healthineers. Or if it's a C2P agreement between two sites, adopt their protocol as they have done all the development work; once you have some local experience with the sequence, then and only then should you modify the parameters.

Every MRI scanning facility has its own definition of what is acceptable image quality, and that is ultimately how we all must define the success or failure of implementing any new sequence or reconstruction methodology designed to facilitate more efficient or faster scanning.

I would strongly advise all MR facilities to run their own side-by-side comparison of any new sequence or reconstruction technique before redefining your standard protocols. The qualitative evaluation of the data should include these questions:

1. Maintaining image sharpness – is there more image blurring?
2. Artifacts – comparable to previous protocol, or are there new artifacts based on the internals of the new sequence?
3. Maintenance of soft-tissue contrast that you would expect?
4. Is there more noise in the image than you are used to?
5. Is there image distortion of the anatomy within the FOV?
6. Are you getting the reduction in scan time you would expect?
7. How does it affect patient compliance?
8. Reconstruction times – are these slowing your booking allocations?

During the early 1990s, turbo spin echo was introduced based on the work by Hennig et al. [4]. It made significant reductions to scan times, but as a consequence drew a

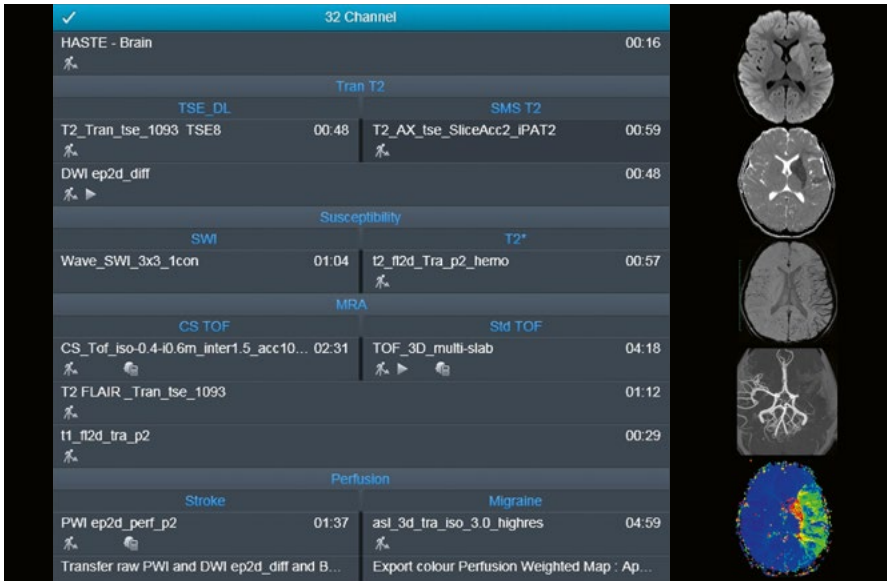


**3** A screenshot of the Code Stroke protocol. MAGNETOM Prisma$^{fit}$ with *syngo* MR E11C software using a 32-channel coil incorporating our latest modification to the protocol using advanced sequences.

considerable amount of criticism from the MR community because the image contrast, apparent image sharpness, and the appearance of fat wasn't the same as conventional spin echo imaging, leading to multiple comparative studies appearing in the literature [5, 6]. The experience gained from the very passionate debate brought about by this significant advance in MR sequences has served as a reminder to the members of the MR community who lived through it how slow we are to change. To quote John Maynard Keynes: "The difficulty lies not so much in developing new ideas as in escaping from old ones".

In the late 1990s and early 2000s, there were several major developments that had a significant impact on our ability to scan faster, and further refinements of these techniques have been the mainstay of our clinical and research imaging protocols. The development of multi-element phased array coils for brain and spine imaging enabled the development of parallel acquisition techniques. The introduction of techniques to undersample data using the characteristics of the individual coil elements in the coil array to reconstruct the data, i.e., SENSE by Pruessman et al. [7, 8] and GRAPPA by Griswold et al. [9], form the building blocks of our current parallel imaging techniques. The undersampling of data in the phase encoding direction within the imaging slice will directly impact the scan time as shown by Equation 1, but at the same time will reduce overall SNR (see Equation 2). In addition to that, we must account for noise amplification due to imperfections during the image reconstruction process. The equation for the SNR in parallel imaging is given by

Equation 3

$$SNR_{PAT} = \frac{SNR}{g\sqrt{R}}$$

where SNR refers to the SNR of non-accelerated data, R to the acceleration factor, and *g* to the geometry factor or *g*-factor. The latter essentially describes the capability of the coil array to reconstruct the given image in its specific orientation from undersampled data by exploiting the intrinsic spatial information encoded in their individual receiver sensitivities. The observed *g*-factor varies across the reconstructed image and is influenced by the coil geometry, i.e., by the number and location of the individual coil elements in the array with respect to the imaging volume, the phase encoding direction, the coil loading, and the applied acceleration factor R.

Apart from this *g*-factor noise amplification, parallel imaging has the potential to generate different and distinct types of image artifacts, which are often dependent on the parallel imaging technique used [10, 11]. Understanding the formation and characteristics of those artifacts can be complicated [12, 13], but is crucial.

The incorporation of parallel imaging into imaging protocols is standard nowadays, and acceleration factors of up to 3 can typically be achieved without impacting the resultant SNR and image quality.

In 3D imaging, the earliest implementations of parallel imaging only utilized data undersampling in the phase encoding direction. As demonstrated by Breuer et al. [14, 15], looking at parallel imaging from a more volumetric perspective opens up opportunities for modifying or distinctively controlling the aliasing that arises from the undersampling of *k*-space. The technique, which became known by the acronym CAIPIRINHA makes efficient use of the encoding capabilities of the coil array by exploiting the coil sensitivity variations not only along the phase encoding direction but also along the partition encoding direction, which results in reduced *g*-factors when compared to standard in-plane parallel imaging.

As we travel through the history of MRI, there are several very distinct periods of time in which vendors competed based on their ability to redefine the technology, and these translated to imaging protocols that produced scans of higher quality in less time.

The introduction of higher field strengths and higher density coil combinations redefined how we scanned our patients. It unleashed the potential of the significant increase in signal-to-noise and overcame some of the limitations of standard parallel imaging.

In 2005 we took delivery of our 3T MAGNETOM Trio, A Tim System, and 6 months later our 32-channel head coil [16]. These two components took our imaging to the next level. The combination of the high-SNR, high-coil-density array and 3 Tesla enabled us to confidently accelerate our acquisitions with higher acceleration factors whilst maintaining exquisite image quality.

As history has shown, nothing stands still in MRI. The evolution of new sequences or hardware from benchtop to clinic can be extremely short, and this has enabled the ongoing refinement of our clinical protocols.

The fundamental principle of CAIPIRINHA can also be applied in 2D imaging, where it has become a cornerstone of what today is known as simultaneous multi-slice (SMS) or multiband (MB) imaging [16, 17]. Notably, the simultaneous acquisition of multiple slices was explored well before the advent of parallel imaging. Mueller [18], Glover (with POMP) [19], and Larkman [20] investigated the concept in the context of acceleration and this early work underpinned the development of the SMS or MB sequences we use today.

By simultaneously exciting multiple slices rather than undersampling *k*-space, SMS doesn't shorten the time that is used to sample data. As such, it doesn't suffer the reduction in SNR generally associated with conventional

parallel imaging. In particular, SMS has proven useful for applications that intrinsically suffer from limited slice coverage or where long TRs or breath-holds render fast sequential scanning impossible [21–25].

The earliest adopters of these new SMS sequences were academic research centers that were probing the inner workings of the brain using DWI, and resting state and functional MRI. Depending on the encoding strategy, the excitation of multiple slices within the imaging volume comes with some inherent issues, such as interslice leakage degrading imaging, slice aliasing, Nyquist ghosts, and SAR. Given that TSE and DWI acquisitions are already relatively high-SAR sequences at 3T, sequence developers looked at methods to address the issue of peak RF load.

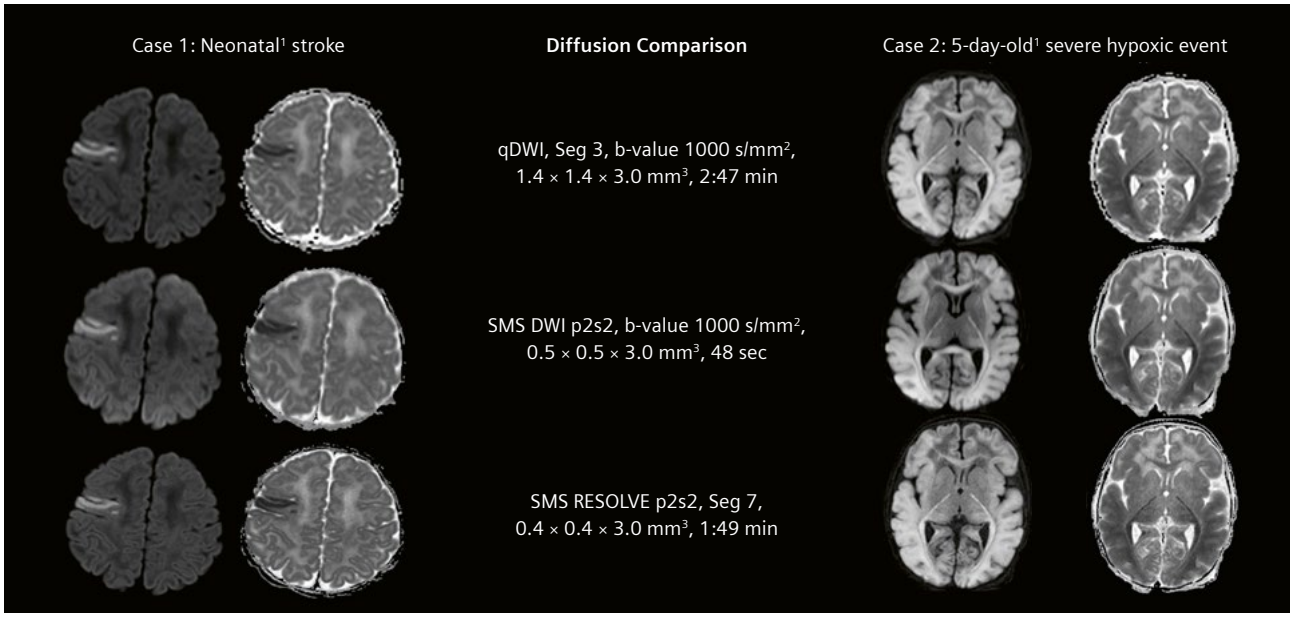


**4** A comparison of different diffusion-weighted imaging (DWI) sequences demonstrating equivalent diagnostic sensitivity.

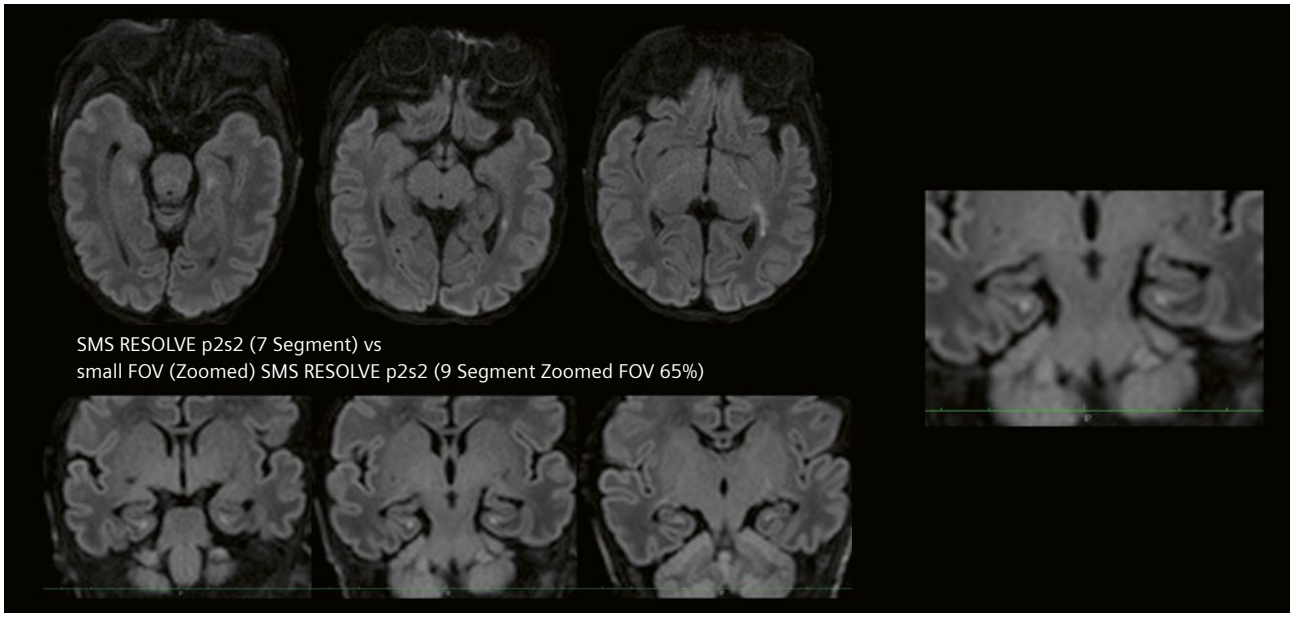


**5** An example of SMS RESOLVE diffusion-weighted imaging (DWI) in a baby[1] with hypoxic ischemic encephalopathy (HIE). The images demonstrate the flexibility of the sequence to perform high diagnostic quality acquisitions in transverse and coronal.

One of the methods was to modify the original VERSE [26] pulse to meet the demands required of SMS imaging.

Our unit's first foray into SMS imaging was in 2012 and involved adapting the C2P sequence from CMRR to enhance our research studies (resting state and fMRI) and multi-direction multi-shell high b-value DTI examinations for epilepsy surgical planning. Although over the past 10 years there have been multiple modifications and enhancements to the SMS sequences, they still form an important component of our patient care.

In regards to clinical imaging, the introduction of SMS ssDWI acquisitions and later SMS RESOLVE has altered our clinical protocols. Currently we only perform accelerated ssDWI acquisitions in Code Stroke or for patients requiring a quick DWI. The use of SMS RESOLVE [24, 27, 28] is standard in all our other protocols, due to the reduction in scan time when compared to standard RESOLVE. The resultant scan time is equivalent to a ssDWI with the added benefits of significantly reduced image degradation at bone–air interfaces and areas of calcification or hemorrhage, and reduced T2* blurring based on the segmented acquisition. The beauty of the acquisition is that you can balance the number of segments and acquisition time to improve image quality in non-transverse acquisitions. We also opted to use the advanced shimming mode to further enhance our image quality (Figs. 4, 5).

With the diffusion imaging sorted, we turned our attention to implementing SMS TSE [29, 30] sequences into our standard neuroimaging protocols at 3T, primarily focusing on our epilepsy protocol. The T2 acquisitions in the protocol were required to cover the whole brain with a resolution of 0.2 × 0.2 × 2.5 $mm^3$ and a scan time less

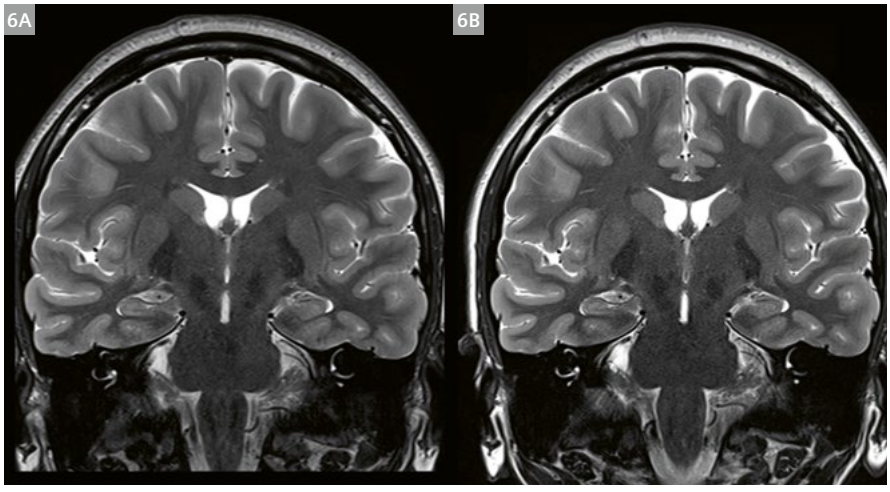


**6** Two coronal T2 TSE acquisitions with matched slice thickness (2.5 mm) and resolution parameters (0.2 × 0.2 × 2.5 $mm^3$) demonstrating similar image quality. Image **(6B)** appears to have a higher spatial resolution but this is due to a slightly higher level of noise in the final image. **(6A)** Std T2 p2 TSE with **(6B)** SMS T2 TSE p2s2.

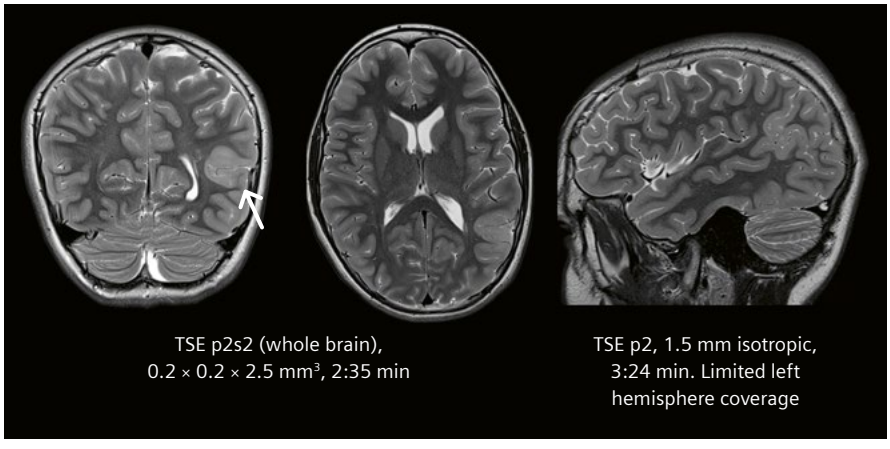


**7** Clinical example from our epilepsy Dot protocol demonstrating the image quality using SMS p2s2 turbo spin echo (TSE) in a case of suspected bottom-of-sulcus dysplasia (BOSD), using MAGNETOM Prisma$^{fit}$ with *syngo* MR E11C and the 32-channel Head Coil.

than the current standard TSE. The implementation of SMS into the diffusion components of our protocols was relatively straight forward, but SMS TSE was far more challenging in terms of addressing the SAR issues, interslice aliasing, matching similar image contrasts, and patient compliance. At our institution, we keep the scanner in normal mode and SAR management proved challenging; it required a reduction in flip angle and the utilization of normal or low SAR RF. The RF associated with the multi-slice excitation also has an impact on the image contrast and especially on the signal intensity of CSF through magnetization transfer effects. In the initial phase of trialing the sequence, the radiologists preferred the non-accelerated version, but increasing TR and TE values brought the image contrasts closer and made them acceptable to the radiologists whilst still reducing scan times by 45% (Figs. 6, 7). SMS is an extremely flexible addition to the pulse sequence and can be used with PAT or without. Most of the initial trials regarding the introduction of SMS or MB into clinical T2 imaging was using the standard TSE sequence. However, a variant was used for diffusion in cholesteatomas using the turbo gradient spin echo (TGSE) sequence, and the parameters could be modified to obtain T2 TGSE SMS BLADE acquisitions. This was extremely useful in reducing the scan time of T2 BLADE (Fig. 8). We currently use SMS TSE in non-longitudinal studies such as general screening,

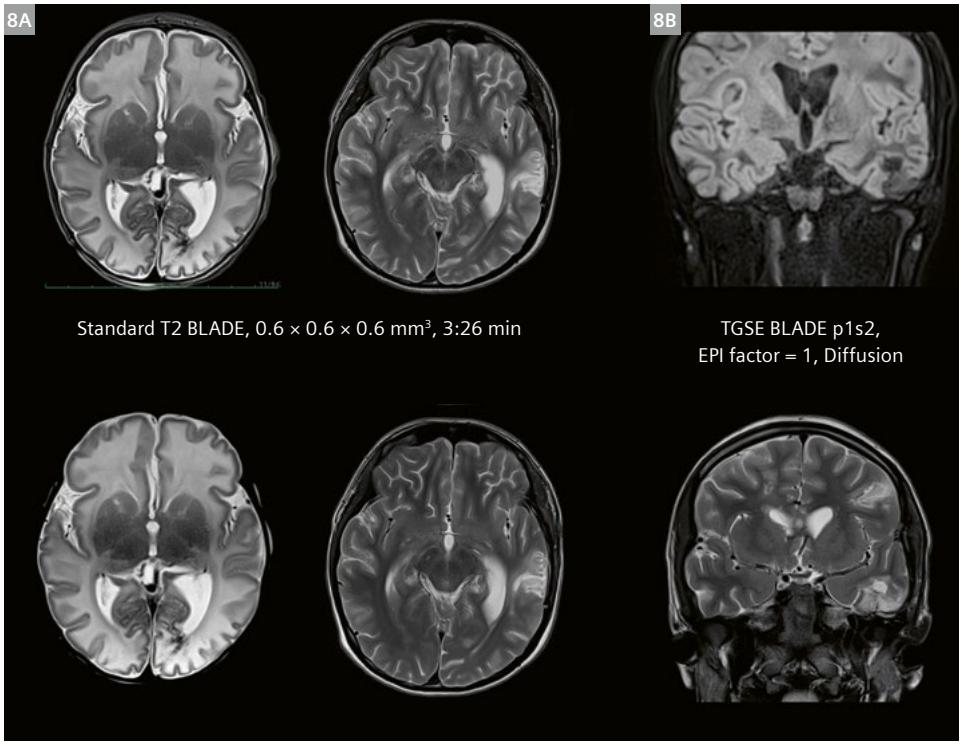


**8** Two clinical examples of using TGSE SMS BLADE to reduce scan time.
**(8A)** Neonate with multiple congenital vascular malformations.
**(8B)** Follow-up postarterial stroke including coronal DWI.

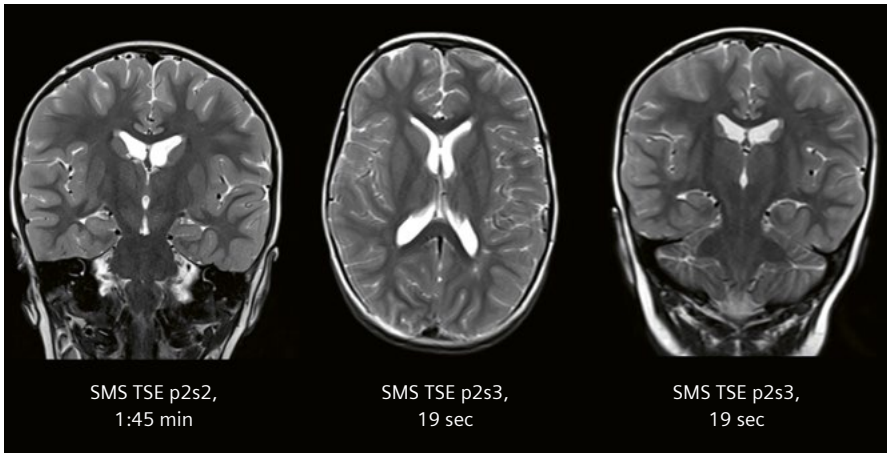


**9** Due to referrer preferences, MRI is proving to be the examination of choice in pediatrics to look at hydrocephalus and shunt malfunction in patients with hydrocephalus – in reality: How fast can we go?

hydrocephalus follow-up, and Code Stroke. Not all our 3T scanners have the SMS option, so tumor monitoring still requires standard TSE. We have developed an extremely quick 3-plane T2 protocol using SMS TSE to evaluate shunt dysfunction in patients with hydrocephalus (Fig. 9).

The next phase of MRI technical developments heralded the arrival of higher density 4G coils, in particular the 64-channel coil [31] for head and neck imaging, and MAGNETOM Prisma$^{fit}$ with its industry-leading gradients with a maximum gradient amplitude of 80 mT/m and a slew rate of 200 T/m/s. The ongoing development at Siemens Healthineers culminating in MAGNETOM Prisma$^{fit}$ was covered by Schmitt [32] in a recent article in MAGNETOM Flash. In our efforts to reduce scan times the narrative is normally focussed on novel pulse sequences and complex image reconstruction algorithms but the complex interactions of the gradient sub-system that drives many of these advances is often ignored. Many of our standard clinical protocols utilize complex diffusion scans or fast scanning applications require the gradient sub-system to deliver acquisitions that produce smaller field of view (FOV), higher spatial resolution, shorter echo spacing (ESP), and minimum echo times (TE) to minimize image blurring and distortion artifacts.

3D imaging is the mainstay of numerous protocols within our institution, ranging from MR angiography, high-resolution T1 and FLAIR in our epilepsy protocols, and post-contrast black blood imaging in our neuro-oncology protocols, to volumetric T1 and T2 in research studies, or a basic T1 in screening brains.

Historically these acquisitions, even with standard PAT and the inclusion of 3D acceleration, have long resulted in many studies being degraded by patient motion.

In 2007 Michael Lustig et al. [33, 34] introduced their work on Compressed Sensing (CS). The technique, initially proposed as a concept to accurately reconstruct signals from small numbers of random measurements, exploits the inherent redundancy of MRI data and thus facilitates significant scan time reductions. CS requires that the acquired image is compressible. In other words, it needs to have a sparse representation in a well-known transform domain. If this condition is met, and *k*-space is undersampled such that the undersampling artifacts have a noise-like appearance in this transform domain, the image can be reconstructed using a nonlinear iterative optimization [35–37]. The level of scan acceleration is governed by the compressibility of the image rather than the factors that affect standard parallel imaging and may highly depend on the application and the basic SNR conditions at hand. While CS is typically suited to 3D applications and excellent results are obtained in 2D functional cardiac studies, the sparsity requirements are often not met with static 2D sequences.

Our first introduction to CS imaging was with 3D TOF MRA [38–40], which has a high degree of sparsity that gives us the possibility to use higher acceleration factors based on the inherent differences in MR contrast based on the TOF acquisition. We learned very quickly that CS was a very different entity from standard acceleration techniques and it presented us with many challenges on the road to

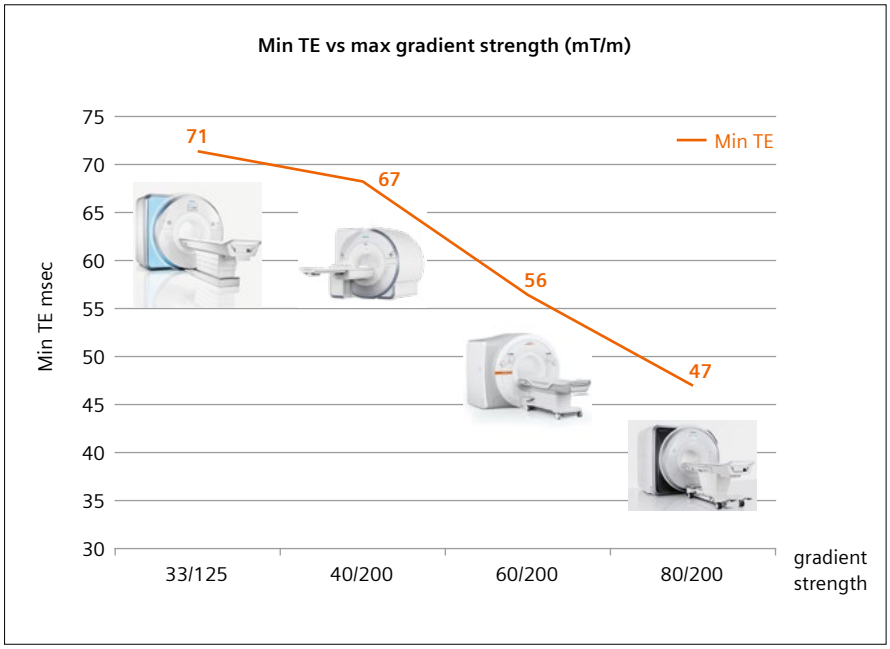


**10** A comparison of the minimum TE obtained across several clinical systems with differing gradient performance (maximum gradient amplitude and slew rates) using a standardized acquisition protocol: TR 5 sec minTE, FOV 380 × 81%, Res 128 × 100%, p2, 1.5 × 1.5 × 5.0 mm$^3$, Monopolar Bw 2442 Hz, Normal RF, Max Performance Gradients, b-values 50/400/800 s/mm$^2$.

clinical acceptance – including very slow reconstruction times due to the complex image reconstruction pipeline. As with all our research sequences, we performed intensive cross-technique comparisons to optimize the data quality. We were introduced to new image reconstruction parameters that had dramatic effects on image quality. Many hours of retrospective data reconstruction were undertaken and involved varying the number of iterations and regularization factor to find the best trade-off between data consistency and mathematical data optimization. If the regularization factor was set too high, the images appeared over-filtered. If it was set too low, the images were noisy. We also found that if we changed the number of iterations, the regularization factor needed to be adjusted (Fig. 11). This process was undertaken for the acceleration factors, and our preferences for these were determined by clinical presentation. We opted for two acceleration factors: one of 7.2 for vascular follow-up cases and for moyamoya and vasculitis scans; and one of 10.2 in AVM and Code Stroke. This resulted in considerable reductions in scan times (Figs. 12–14). An added bonus from the reconstruction process was an increase in spatial resolution, which went from 0.3 × 0.3 × 0.5 $mm^3$ (5:48 min) using standard 3D TOF to 0.4 × 0.4 × 0.4 $mm^3$ (3:20 min) using 3D CS TOF (Fig. 15).

The translation of 3D CS TOF acquisition, although challenging at times, presented us with fewer challenges than developing protocols for our other 3D sequences. Each 3D acquisition posed different challenges in relation to overall image quality and our perceptions of how far we could take the acceleration factors. The beauty of optimizing CS protocols is that you can retrospectively reconstruct the data by modifying the regularization factor and number of iterations until you have reached that level of data consistency. The optimization of the CS T2 SPACE acquisition was the most straightforward and resulted in significant reductions in scan time. Similar to the 3D CS TOF, an added bonus was an increase in spatial resolution from 0.9 × 0.9 × 0.9 $mm^3$ (5:20 min) for the standard 3D T2 SPACE to 0.8 × 0.8 × 0.8 $mm^3$ (2:30 min) for the compressed sensing version (Fig. 16).

*[2]CS MPRAGE is work in progress. The application is currently under development and is not for sale in the U.S. and in other countries. Its future availability cannot be ensured.*

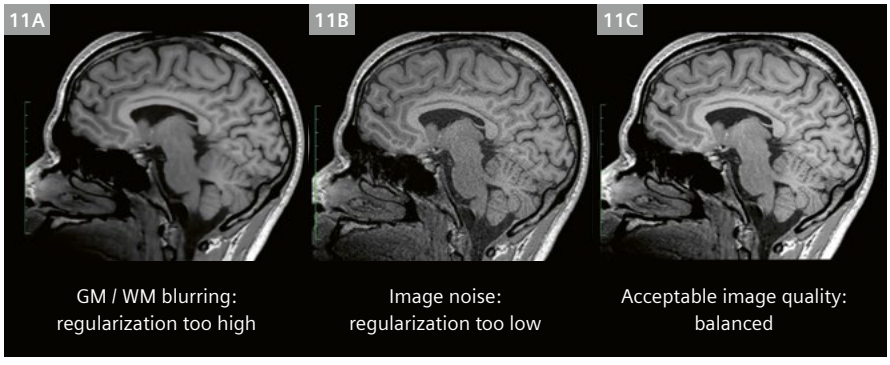


**11** These images demonstrate the importance of optimizing the regularization factor in Compressed Sensing (CS) reconstruction and the impact it has on image quality. The images shown are CS MPRAGE[2] acquired on a MAGNETOM Prisma$^{fit}$ with *syngo* MR E11C with a spatial resolution of 0.8 mm isotropic acquired in 2:30 min using a standard 32-channel Head Coil.

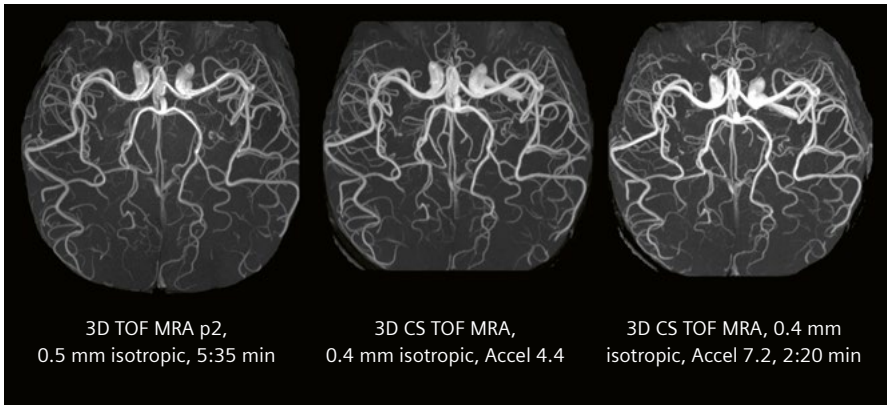


**12** The image quality achieved in our internal quality assurance testing prior to our implementation of Compressed Sensing 3D Time of Flight (CS 3D TOF) into our standard protocols. The images shown are acquired on a MAGNETOM Prisma$^{fit}$ with *syngo* MR E11C using a standard 32-channel Head Coil with previously determined regularization factor and number of iterations. These images represent the image quality achieved at differing levels of acceleration when compared to our standard 3D TOF MRA.

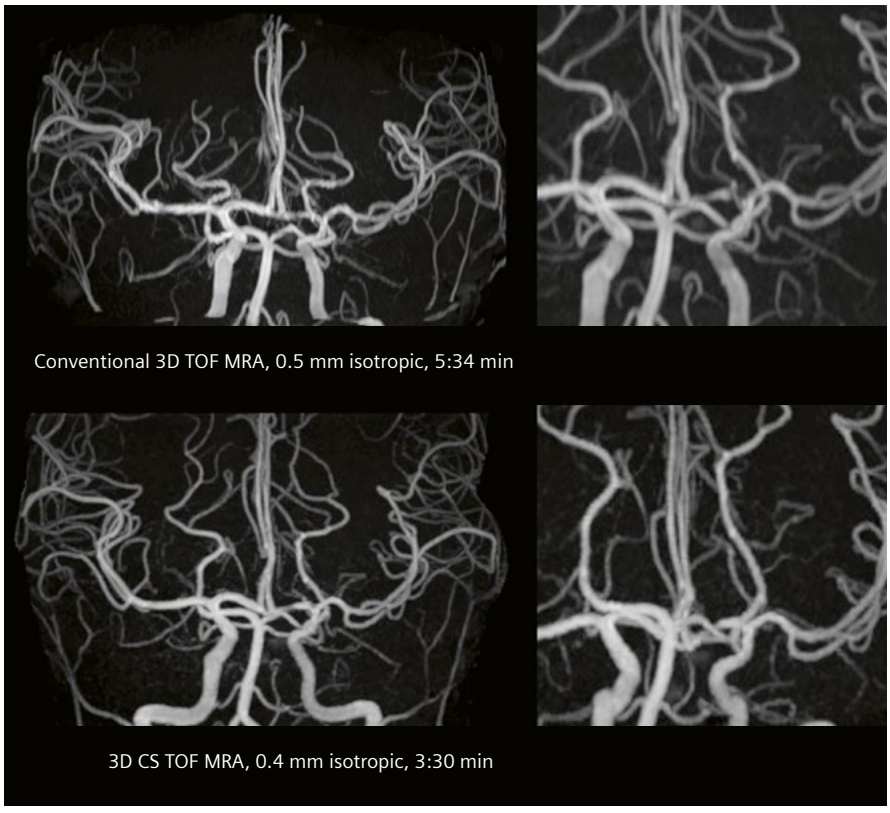


**13** A comparison of two MRA techniques in a follow-up study of intracranial vasculitis.

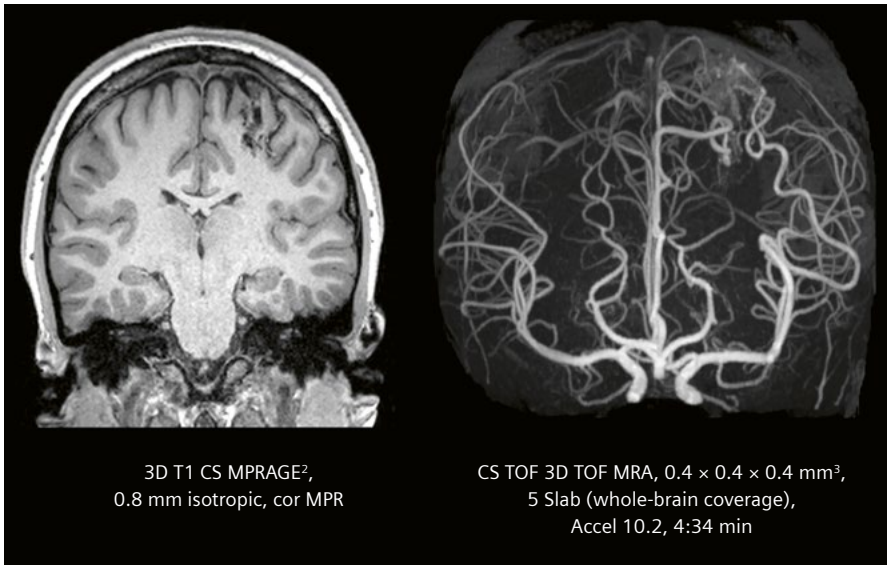


**14** A clinical case of pre-operative planning in a patient with an arteriovenous malformation (AVM) acquired using CS MPRAGE² and CS 3D TOF MRA. The MRA was acquired with an acceleration of 10.2, which is our standard acceleration factor for AVMs balancing whole-head vessel coverage in an acceptable scan time whilst maintaining high quality data.

Our center has a very busy epilepsy surgery program and we have become reliant upon high-resolution fat-suppressed 3D SPACE FLAIR for our comprehensive imaging protocol in these patients [41, 42]. High resolution? Our previous standard of care protocol acquired 0.9 × 0.9 × 0.9 $mm^3$ p2 FLAIR in 6:20 minutes, so the challenge was to see if we could obtain the same degree of scan time reduction as we did with T2 SPACE. Based on the information we obtained working with the T2 SPACE, it was clear that this wouldn't be possible. We settled on a protocol that provided a modest reduction in scan time, but as we experienced with the T2 SPACE, the SNR in acquisition enabled us to obtain a higher resolution of 0.8 × 0.8 × 0.8 $mm^3$ (4:10 min) for the CS version compared to 0.9 × 0.9 × 0.9 $mm^3$ (6:20 min) for the standard 3D T2 SPACE (Fig. 17).

3D T1 MPRAGE acquisitions are an integral component when constructing our pediatric brain protocols, and the flexibility to modify scan parameters based on the patient's age, clinical presentation, and compliance whilst preserving image quality is critical. If we apply our original question – can we reduce scan time whilst maintaining image quality that is equal to or better than the original? – I believe that with the majority of applications for MPRAGE we have met the brief, with the exception of epilepsy, where the image sharpness at the cortical grey matter–white matter junctions is slightly inferior to standard MPRAGE imaging, which reduces our diagnostic confidence

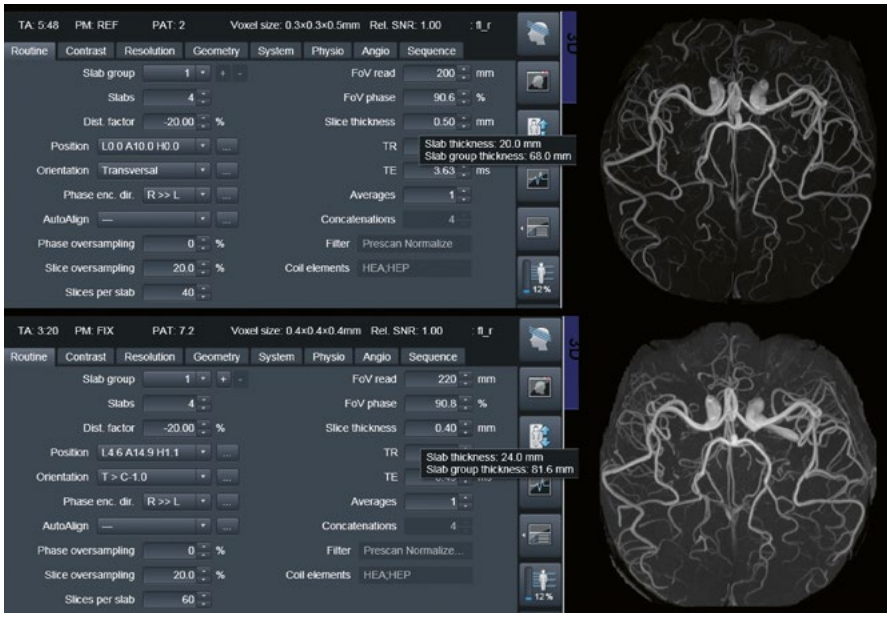


**15** A screenshot of our Dot protocols for MRA demonstrating the protocol variations between our old standard 3D TOF MRA and the updated Compressed Sensing 3D Time of Flight (CS 3D TOF). The screenshots demonstrated the difference in spatial resolution, acceleration (shown as PAT) which equates to scan time reduction, volume coverage, and importantly image quality.

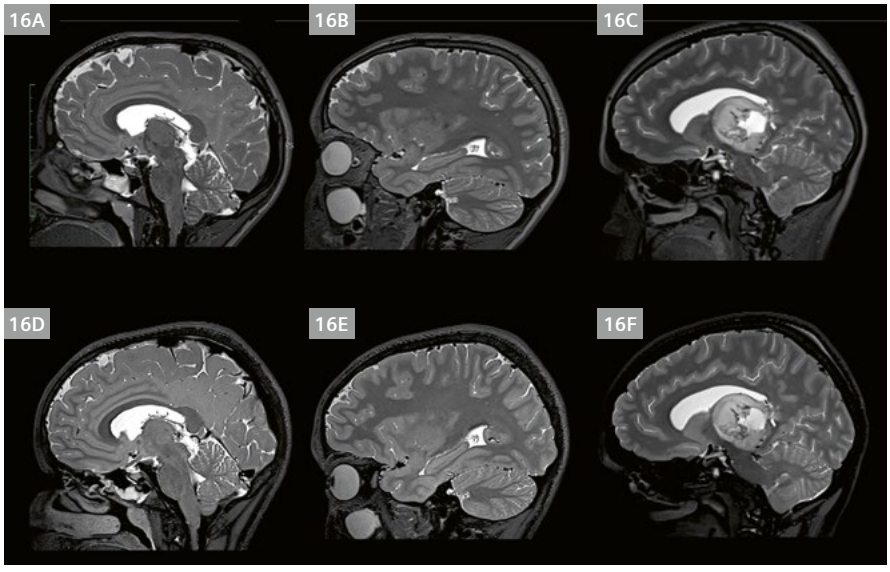


**16** MAGNETOM Prisma$^{fit}$ with *syngo* MR E11C and 32-channel Head Coil, 3D T2 SPACE, 0.9 mm isotropic, 5:20 min vs. 3D T2 CS SPACE, 0.8 mm isotropic, 2:30 min. **(16A, B, D, E)** 13-year-old normal control research participant. **(16C, F)** High-grade glioma.

in finding small cortical dysplasias (Figs. 18, 19). In contrast studies, the Compressed Sensing version of MPRAGE had the same degree of diagnostic accuracy when compared to standard MPRAGE [43, 44] (Fig. 20).

Our most challenging and definitely most frustrating task was the implementation of post-contrast, fat-suppressed black blood T1 SPACE in oncology. The sensitivity and specificity when evaluating metastatic disease in pediatric brain tumors dictates that this sequence is included in our protocols. Our initial attempts at developing this protocol failed due to inconsistent image quality resulting from a lack of inherent image contrast that introduced

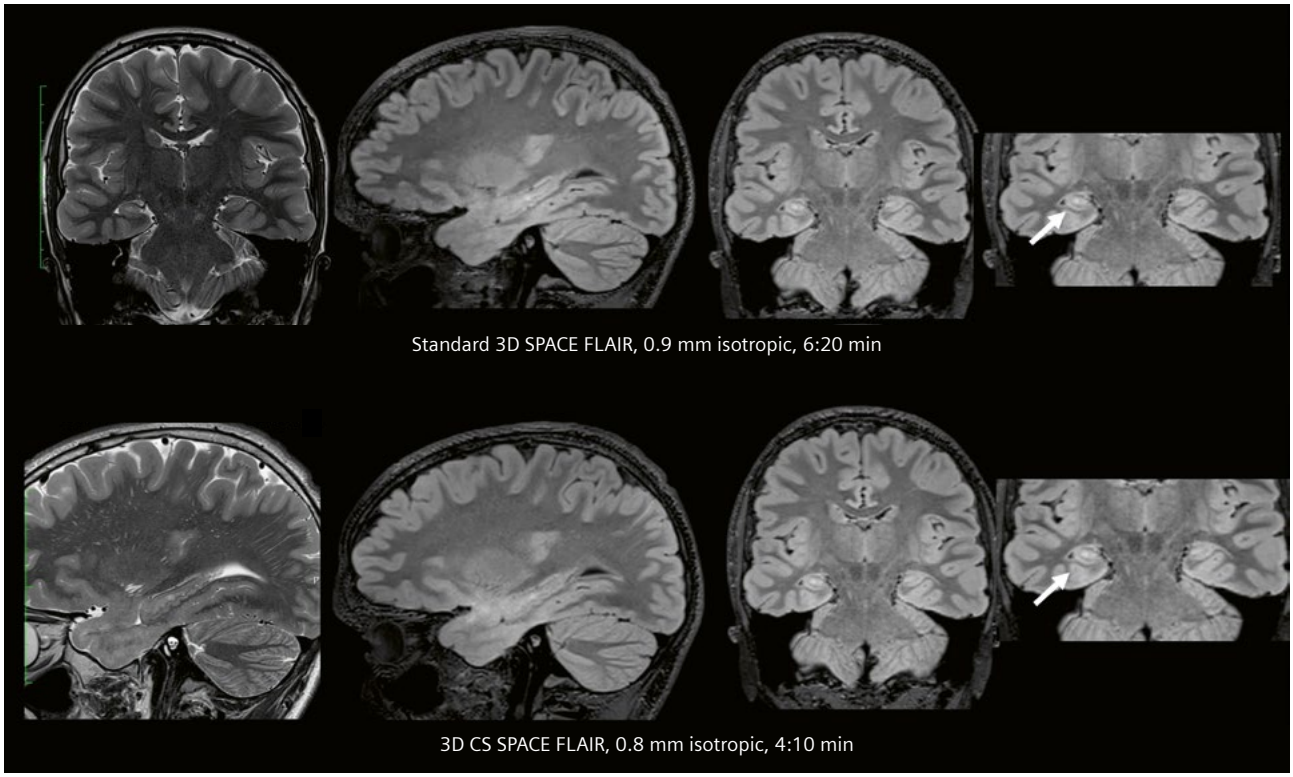


**17** Comparison of 3D T2 FS SPACE and 3D T2 FS CS SPACE in a 16-year-old female with hippocampal lesion on outside imaging. Acquired on 3T MAGNETOM Prisma$^{fit}$ with *syngo* MR E11C and the 32-channel Head Coil.

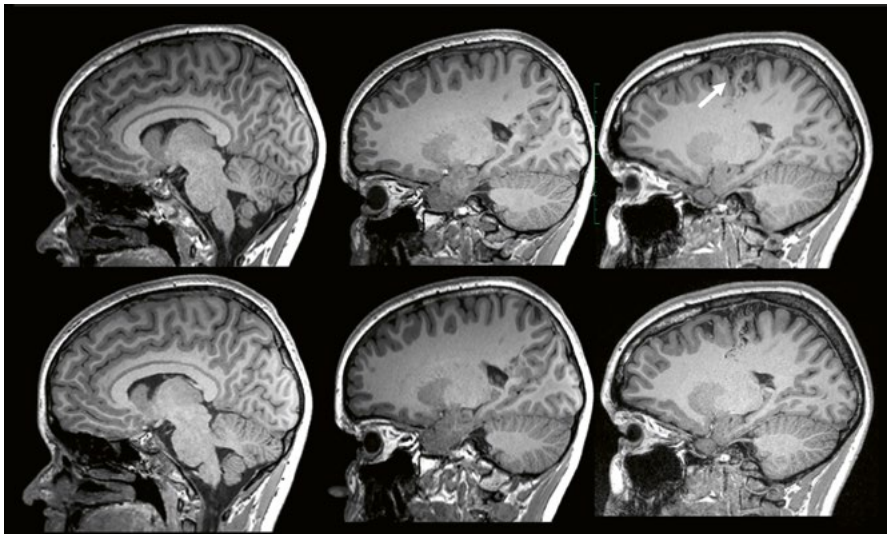

**18** Comparison of standard 3D MPRAGE p2, 0.9 mm isotropic, 4:20 min (top row) and 3D CS MPRAGE, acceleration factor 3.5, 0.8 mm isotropic, 2:30 min (bottom row) in a patient with an AVM (arrow) demonstrating higher spatial resolution in a shorter scan time.

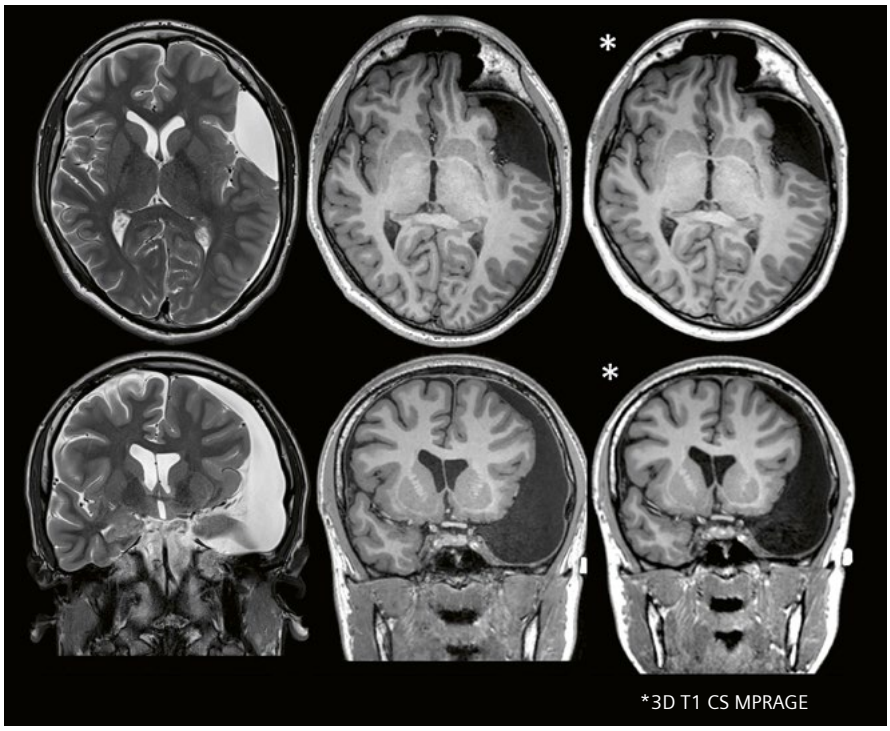


**19** A clinical example of a patient with an arachnoid cyst comparing 3D MPRAGE p2, 0.9 mm isotropic, 4:20 min, and 3D CS MPRAGE[2], acceleration factor 3.5, 0.8 mm isotropic, 2:30 min, resolution in a shorter scan time. The T2 images were acquired with SMS TSE.

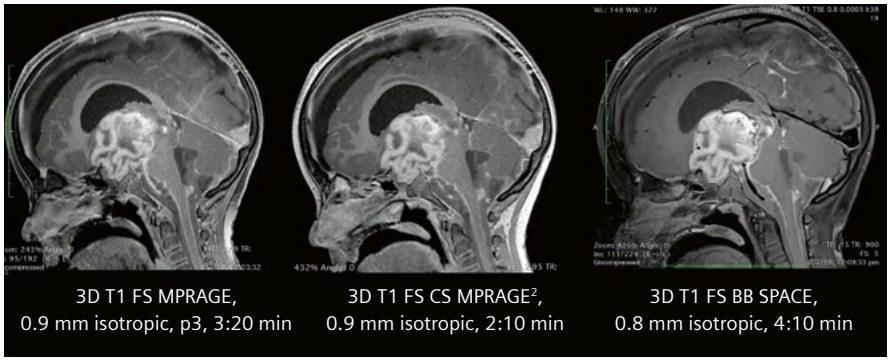


**20** A side-by-side comparison of three fat-suppressed (FS) 3D T1 volumetric sequences in a patient with metastatic pilocytic astrocytoma following the administration of 0.05 ml/kg 1 mmol gadolinium contrast agent.

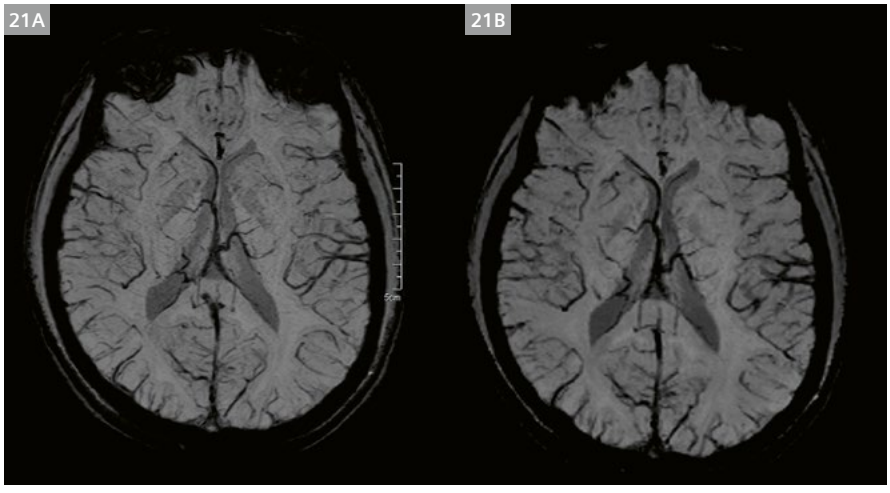


**21** Our first clinical case comparing our standard susceptibility-weighted sequence (SWI) to 3D Wave CAIPI SWI. The standard SWI protocol **(21A)** uses a parallel imaging (PAT) factor of 3 and a minimally higher interpolated spatial resolution (0.6 × 0.6 × 1.8 $mm^3$) acquired in 3:05 minutes compared to **(21B)** the Wave CAPI SWI (0.7 × 0.7 × 1.5 $mm^3$) acquired with an acceleration of 3 × 2 and a resultant scan time of 1:32 min.

artifacts from a lack of data fidelity due to undersampling effects, motion and pulsatile artifacts, and ultimately lower acceleration rates.

On reflection, the introduction of Compressed Sensing into our standard protocol has achieved our goals by reducing scan times whilst maintaining imaging quality and diagnostic integrity [45–48]. But outside of a scan time perspective, CS also represents a paradigm shift in MRI. Unlike conventional imaging, the image reconstruction operation is non-linear, which renders this process less comprehensible. Artifacts and pitfalls may be much harder to detect and understand. The variation in our ability to reduce scan times was dictated by the weighting of the sequence (T1, T2) and the level of sparsity from the inherent tissue contrasts rather than the system hardware. The technique does require optimization of critical reconstruction parameters to maintain data fidelity when compared to standard acquisitions, and the introduction of different artifacts based on low-sparsity data and movement needs to be recognized and where necessary repeated. In some cases, a non-accelerated acquisition will produce data of higher consistency and the skill is to determine when to make that call. Remember that going faster isn't always the best option – understand the limitations and consequences of all the options you choose for scanning your patient.

The earliest attempts to accelerate 3D imaging by applying parallel imaging in both phase encoding directions produced images of varying degrees of quality and it was not until the development of CAIPIRINHA and more recently Wave CAIPI [49, 50] that it has been possible to produce high-quality data in reduced scan times without the use of computer-intensive iterative reconstruction techniques. CAIPIRINHA can be applied to SPACE and VIBE sequences within the standard 3D tree, Wave CAIPI is available also for GRE with SWI and for research applications in MPRAGE[2] and SPACE[2] [49]. This produces imaging protocols with significant reductions in time depending on the matrix coil, which ultimately defines the limitations on acceleration in both phase encoding directions. A review of the literature [51–56] supports our conclusions that the implementation of Wave CAIPI sequences into standard pediatric imaging protocols is possible and the reduction in scan times is consistent with other techniques without

[2]*Work in progress. The applications are currently under development and not for sale in the U.S. and in other countries. Their future availability cannot be ensured.*

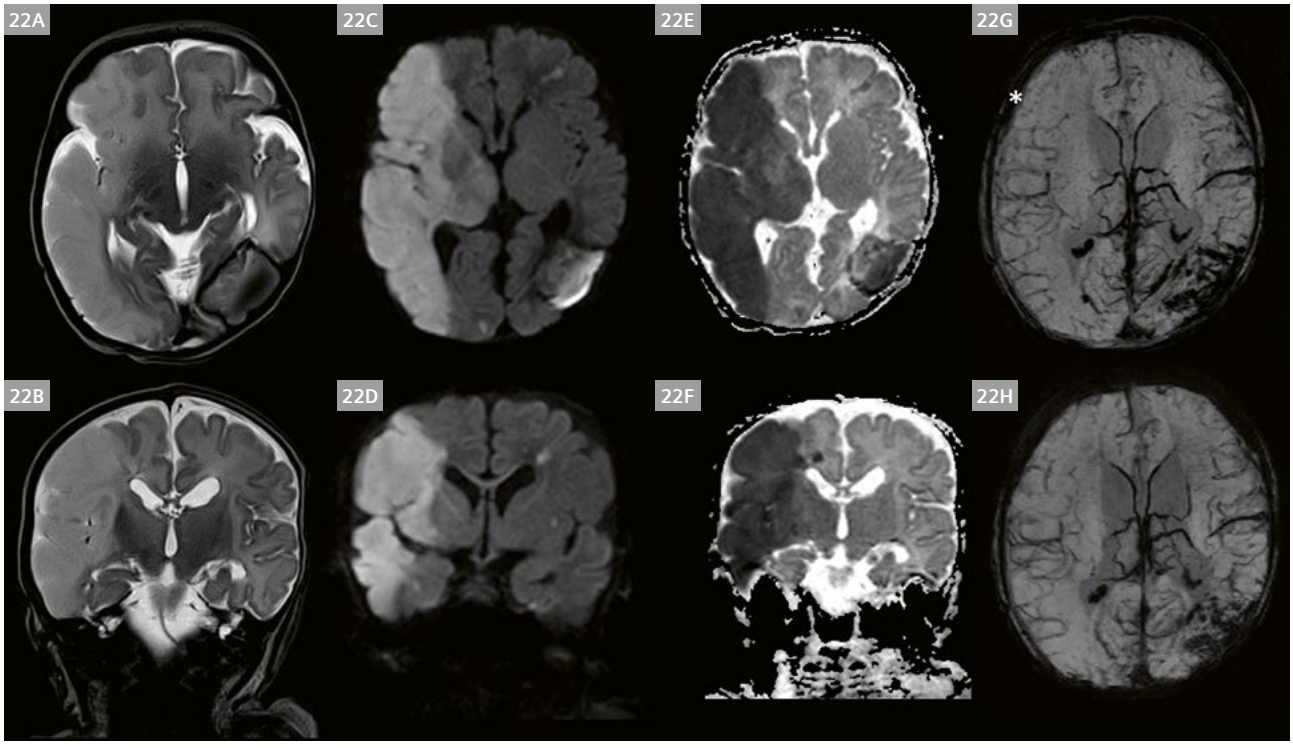


**22** Clinical case of a 2-week-old baby[1], complex congenital heart disease (CHD) post 1st phase corrective surgery – clinical presentation floppy. Comparing our standard susceptibility-weighted sequence (SWI) to 3D Wave CAIPI SWI. The standard neonatal SWI protocol **(22A)** uses a parallel imaging (PAT) spatial resolution (0.6 × 0.6 × 1.6 $mm^3$) acquired in 3:47 min compared to **(22B)** the Wave CAPI version (0.6 × 0.7 × 1.6 $mm^3$) acquired with an acceleration of 2 × 2 and a resultant scan time of 2:30 min.
**(22A,B)** BLADE T2, 0.6 × 0.6 × 2.5 $mm^3$; **(22C–F)** SMS RESOLVE DWI b 1000 s/$mm^2$, **(22G)** SWI p2, 0.6 × 0.6 × 1.6 $mm^3$, 3:47 min; **(22H)** Wave CAIPI SWI 2 × 2, 0.6 × 0.6 × 1.6 $mm^3$, 2:30 min

the long reconstruction times attributed to the iterative reconstruction methods. We currently use tgre_wave with SWI and MPRAGE[2]. Depending on the resolution required, the minimum reduction in scan time is 50% and higher in some other instances. In standard applications of Wave CAIPI SWI we use an acceleration factor of 3 × 2, but in neonatal[1] cases we use a more modest 2 × 2 as shown in the images. We haven't fully evaluated the application of Wave CAIPI SPACE[2] to pediatrics, as we have primarily focused our work on the compressed sensing applications (Figs. 21, 22).

Currently our preferred choices are 3D TOF, T2 SPACE, and FS SPACE FLAIR where we use Compressed Sensing and for MPRAGE and SWI we use the Wave CAIPI sequences

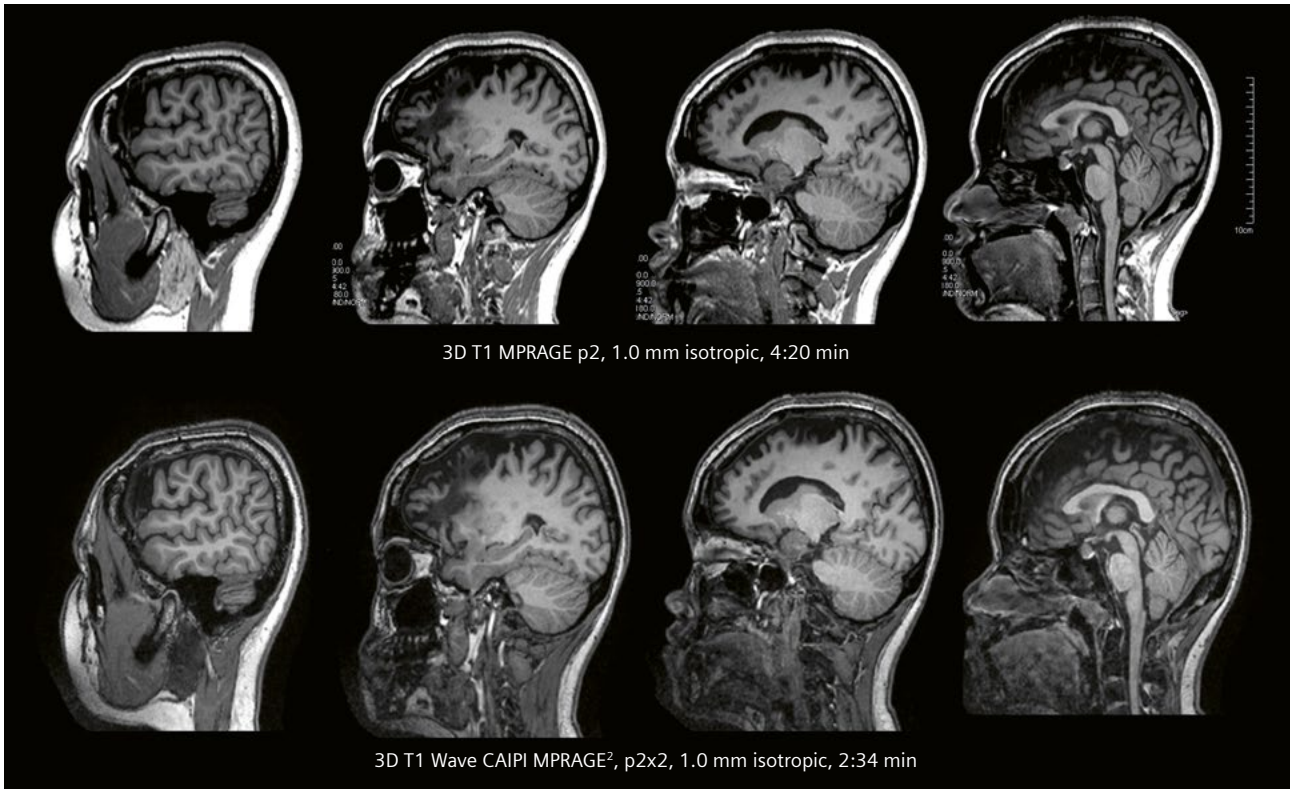


**23** Clinical case of stroke follow-up in a 17-year-old girl with moyamoya disease comparing our standard 3D T1 MPRAGE (p2, 1 mm isotropic, 4:20 min) protocol to 3D Wave CAIPI MPRAGE[2] with a moderate PAT factor (p2x2, 1 mm isotropic, 2:34 min).

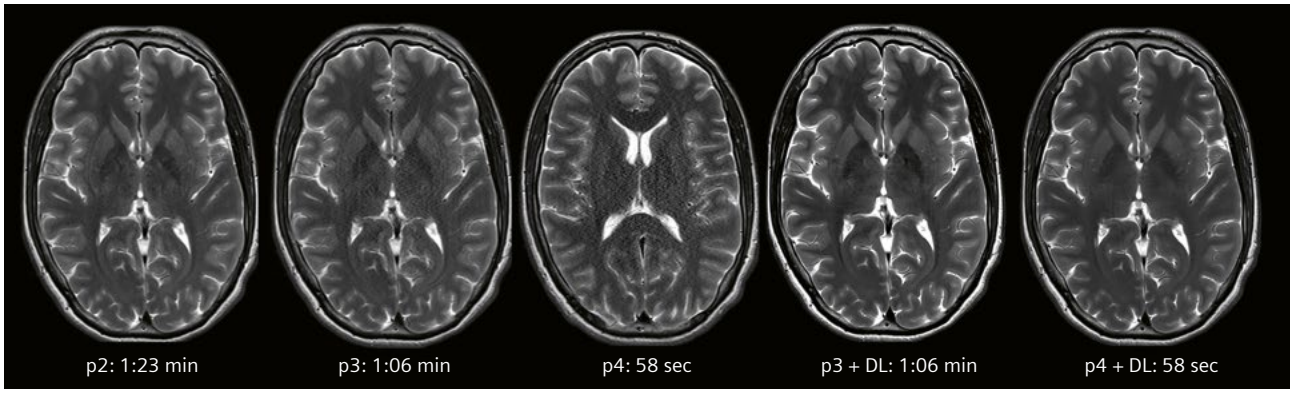


**24** This is an illustration of the effect of varying the parallel imaging factor (PAT) on the scan time and subsequent reduction in signal-to-noise (SNR). All parameters remained locked except for the PAT factor. A deep learning algorithm (DL) was applied during image reconstruction to denoise the images and improve image quality.

(Fig. 23). We currently still prefer to use standard MPRAGE for neonatal imaging.

The most recent innovation and potentially the most exciting is the use of artificial intelligence (AI) image reconstruction techniques to denoise and sharpen our data in our quest to reduce scan times. Two recent articles published in MAGNETOM Flash by Behl [57] and Hammernik [58] describe the potential to dramatically reduce imaging time while maintaining image quality by using deep learning techniques. We know from the literature and every MR lecture we attend that the final MR image is a compromise between three tightly associated factors:

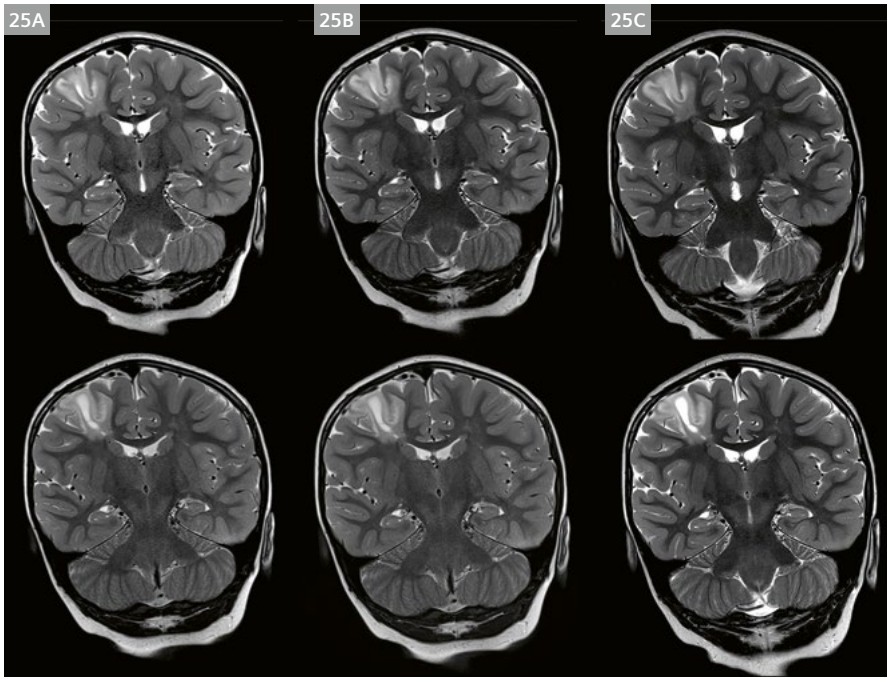


**25** Clinical case of patient presenting with seizures requiring MRI for evaluation of suspected focal cortical dysplasia (FCD).
Three whole-brain coronal T2 scans were acquired where spatial resolution was matched (0.2 × 0.2 × 2.5 $mm^3$).

**25A**: TSE p2, 4:23 min
**25B**: SMS TSE p2s2, 2:36 min
**25C**: TSE p4 DL, 2:27 min

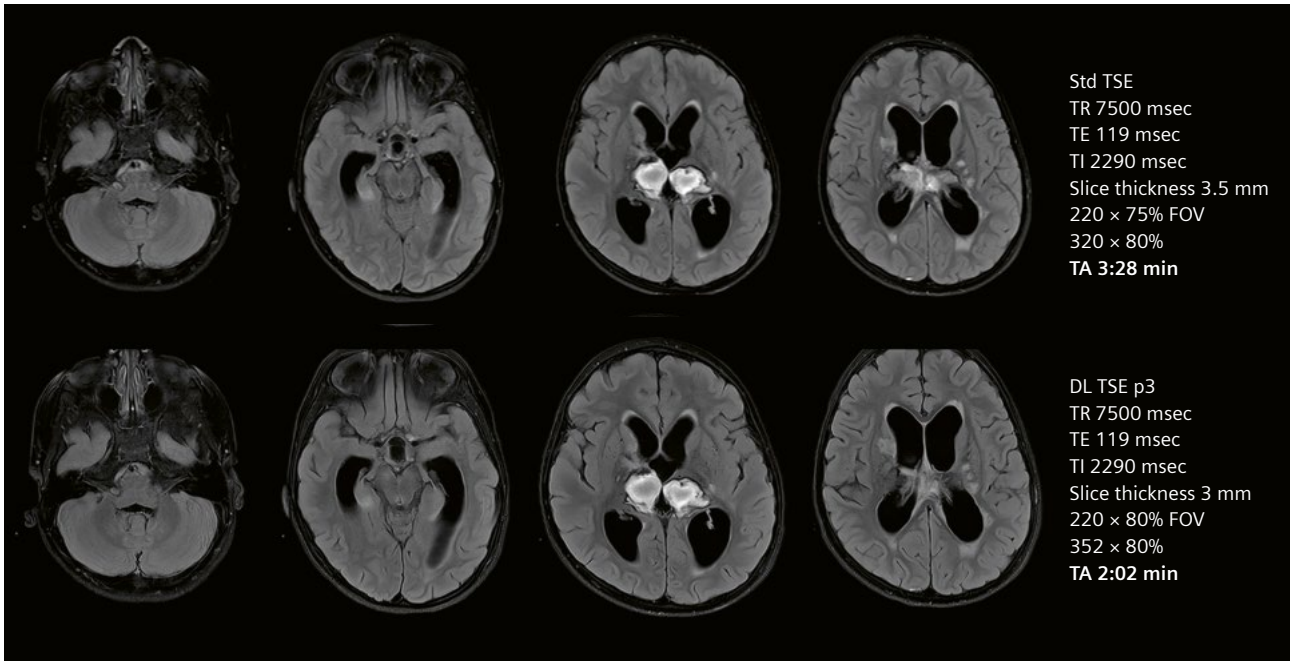


**26** Clinical example comparing standard (std) 2D FS FLAIR and 2D FS FLAIR with deep learning (DL) in a patient with bilateral infarcts from venous sinus thrombosis.

SNR, resolution, and acquisition time. Minor modifications of one factor significantly affect the others – and AI or deep learning (DL) reconstruction methods have the potential to minimize these effects [59, 60].

We know that the use of PAT options introduces noise within the image, and the use of high-density coils introduces an inhomogeneous distribution of noise, which combined will degrade image quality. Deep learning solutions have the potential to denoise these images and dramatically improve image quality (Fig. 24).

By using deep learning we can increase the resolution, introduce higher PAT factors, or reduce the number of averages. We can intentionally create an image with more noise present in the data and use DL in the reconstruction phase to produce images of diagnostic quality. These techniques have enabled us to reduce the scan times of our 2D acquisitions that were previously not suitable for iterative reconstruction techniques (Fig. 25). 2D FLAIR acquisitions are used in many pediatric brain protocols and, based on conventional TSE acquisition strategies, they are considered slow when compared to other TSE sequences. The use of higher PAT factors and denoising of the image using DL has enabled a minimum 50% reduction in scan time (Figs. 26–28). This reduction in scan time is like all our 2D TSE sequences, but users should be aware that because we are potentially increasing the degree of data undersampling by using higher PAT factors, there is the potential for ringing artifacts, more prominent pulsatile effects, and more evident image degradation from movement.

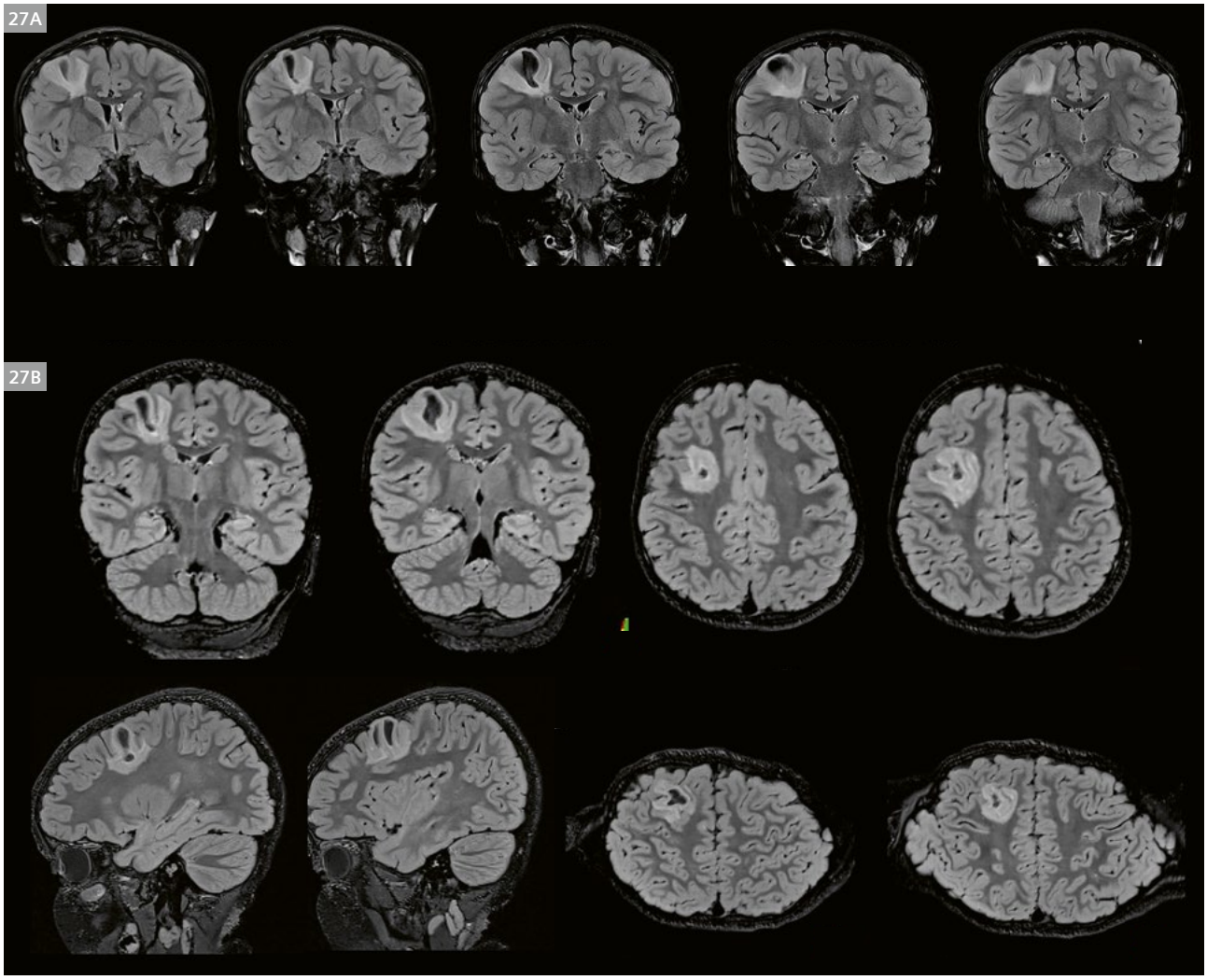


**27** Same patient as in Figure 26, comparing DL 2D TSE FLAIR with 3D SPACE FS FLAIR CS. Patient presenting with seizure, clinical question: Focal Cortical Dysplasia (FCD)?
**(27A)** DL 2D T2 TSE FLAIR, 0.4 × 0.4 × 3.0 $mm^3$, 2:23 min
**(27B)** 3D SPACE FS FLAIR CS, 0.8 × 0.8 × 0.8 $mm^3$, 3:48 min

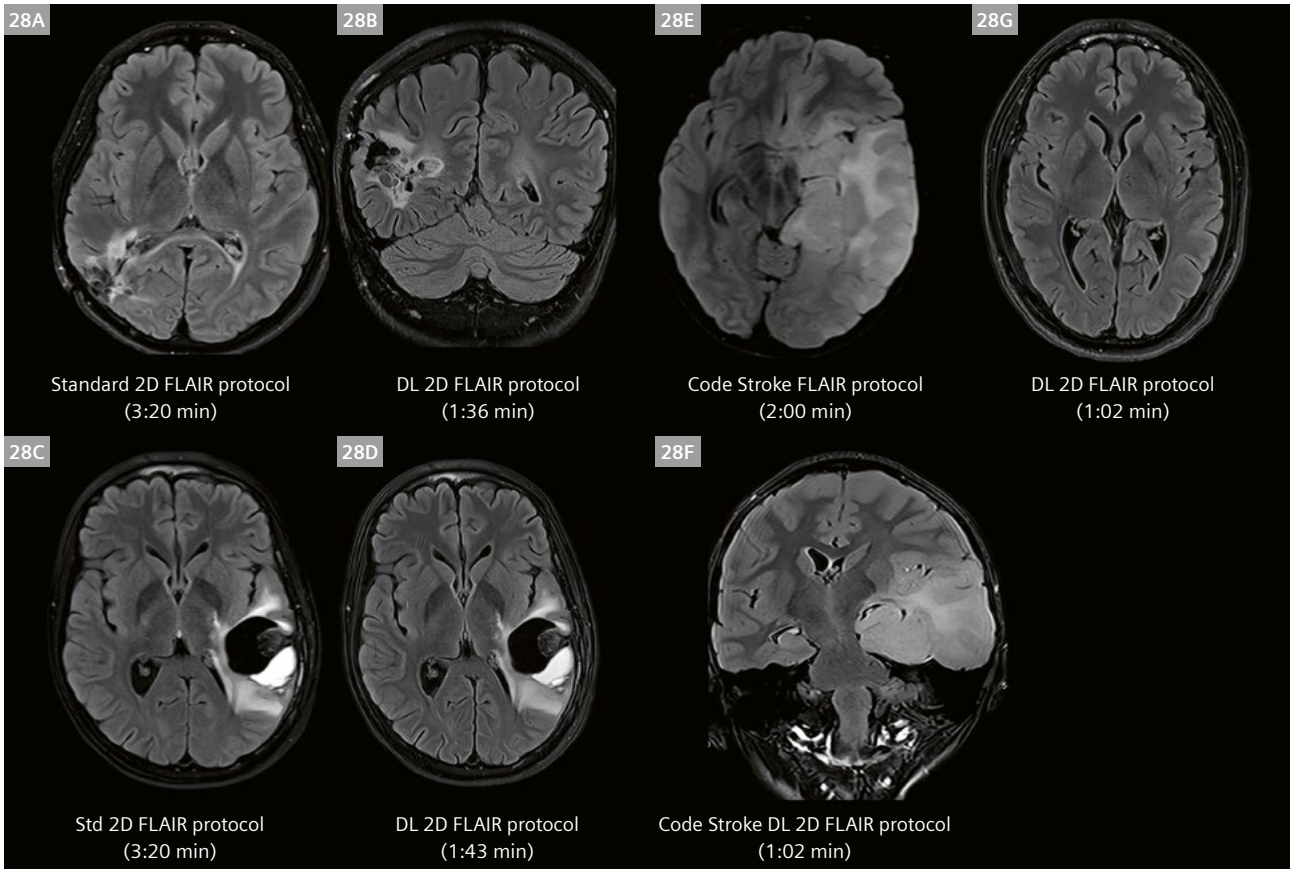


**28** Standard 2D FS FLAIR has been one of the roadblocks to faster clinical brain protocols. These examples **(28A, B)** post operative DNET **(28C, D)** post operative Ewings sarcoma and **(28E, F)** Code Stroke that turned out to be high grade glioma demonstrate the utility of applying deep learning (DL) to 2D FLAIR to provide a strategy to reduce scan times and improve image quality. **(28G)** is an example of our 1 min Code Stroke FLAIR protocol.

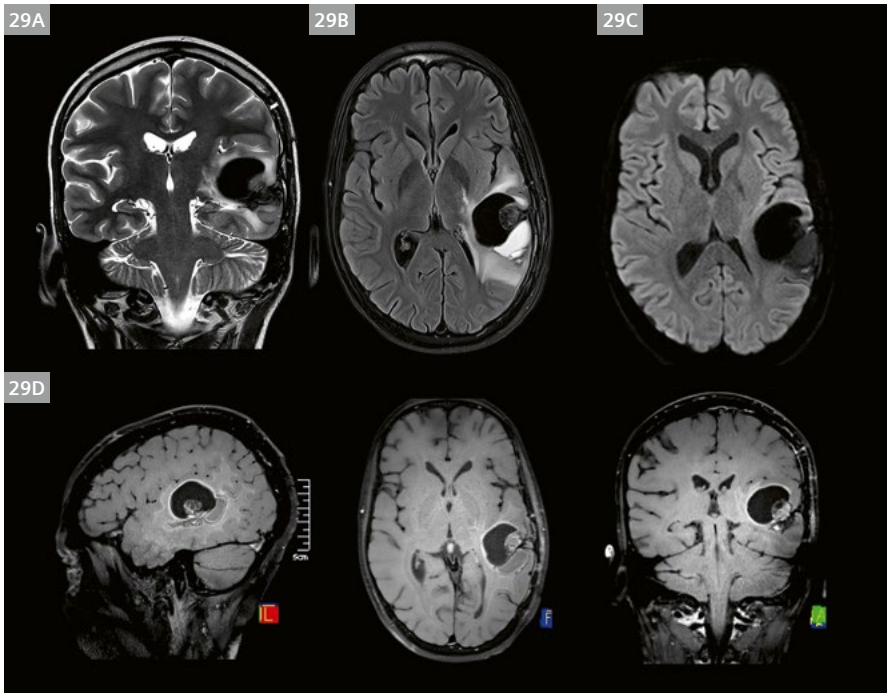


**29** Putting it all together into a clinical neuro-oncology protocol. Recurrent supra tentorial Ewings Sarcoma.

**29A**: T2 TSE DL p3,
0.2 × 0.2 × 2.5 $mm^3$, 2:20 min
**29B**: T2 FS FLAIR DL, 1:43 min
**29C**: SMS RESOLVE p2s2 DWI,
b-value 1000 $s/mm^2$
**29D**: CS FS T1 SPACE BB,
0.8 mm isotropic, 4:12 min

## Conclusion

The introduction of faster scanning techniques into routine pediatric protocols is possible and the scan time reductions can be significant. Whilst there may not be a single solution for each clinical protocol, the tools are available to customize your sequences to match the requirements of your department (Fig. 29). The MR team must have a basic understanding of the technique and, importantly, of any limitations associated with it before blindly implementing it into your daily protocols. There is the potential to introduce new artifacts with many of these methods, so you need to have a basic understanding of the underlying pulse sequence and reconstruction processes so you can perform quality assurance on your images. A caveat to introducing faster techniques is that some of the options available may use gradient-intensive pulse sequences that could produce a different acoustic noise profile or higher volume and induce more vibration that may disturb some patients.

## Disclaimer

All images and author comments relate to the research versions of the Compressed Sensing, Wave CAIPI, and deep learning applications scanned on a MAGNETOM Prisma$^{fit}$ with *syngo* MR E11C software.

## Acknowledgments

The author acknowledges and recognizes the Wurundjeri people as the Traditional Custodians of the land in which we are located. We respect all Aboriginal and Torres Islander peoples and honor their cultural and spiritual relationships of the land and water, and their rich contribution to society.
Staff of the Children's MRI and PET Centre.
Staff and patients of RCH.
Siemens Healthineers Erlangen, Germany; Dr Heiko Meyer and the Neuroimaging team for having the confidence in our unit to enable multiple collaboration projects; Michaela Schmidt, Dr Christoph Forman and Dr Peter Speier for their help with CS 3D TOF MRA; Dr Daniel Staeb, Dr Kieran O'Brien, Jonathan Richer, and Peter Zammit from Siemens Healthineers Australia for their ongoing scientific support.

The author also acknowledges the support provided through our C2P agreement with the CMRR at the University of Minnesota, Minneapolis, MN, USA, for the SMS TSE and MB diffusion sequences.

**References**

1 Runge VM, Aoki S, Bradley WG Jr, Chang KH, Essig M, Ma L, et al. Magnetic Resonance Imaging and Computed Tomography of the Brain-50 Years of Innovation, With a Focus on the Future. Invest Radiol. 2015;50(9):551–556.
2 Macovski A. Noise in MRI. Magn Reson Med. 1996;36(3):494–497.
3 Rofsky NM. The importance of image quality: in the eyes of the beholder? J Magn Reson Imaging. 2015;41(4):861–865.
4 Hennig J, Nauerth A, Friedburg H. RARE imaging: a fast imaging method for clinical MR. Magn Reson Med. 1986;3(6):823–833.
5 Prenger EC, Beckett WW, Kollias SS, Ball WS Jr. Comparison of T2-weighted spin-echo and fast spin-echo techniques in the evaluation of myelination. J Magn Reson Imaging. 1994;4(2):179–184.
6 Patola WB, Coulter BA, Chipperfield PM, Lingawi SS. A comparison of conventional spin-echo and fast spin-echo in the detection of multiple sclerosis. J Magn Reson Imaging. 2001;13(5):657–667.
7 Pruessmann KP, Weiger M, Scheidegger MB, Boesiger P. SENSE: sensitivity encoding for fast MRI. Magn Reson Med. 1999;42(5):952–962.
8 Pruessmann KP, Weiger M, Börnert P, Boesiger P. Advances in sensitivity encoding with arbitrary k-space trajectories. Magn Reson Med. 2001;46(4):638–651.
9 Griswold MA, Jakob PM, Heidemann RM, et al. Generalized autocalibrating partially parallel acquisitions (GRAPPA). Magn Reson Med. 2002;47(6):1202–1210.
10 Yanasak NE, Kelly MJ. MR imaging artifacts and parallel imaging techniques with calibration scanning: a new twist on old problems. Radiographics. 2014;34(2):532–548.
11 Glockner JF, Hu HH, Stanley DW, Angelos L, King K. Parallel MR imaging: a user's guide. Radiographics. 2005;25(5):1279–1297.
12 Polimeni JR, Wiggins GC, Wald LL. Characterization of artifacts and noise enhancement introduced by GRAPPA reconstructions. Proc Intl Soc Mag Reson Med. 2008; p. 1286.
13 Larkman DJ, Nunes RG. Parallel magnetic resonance imaging. Phys Med Biol. 2007;52(7):R15–55.
14 Breuer FA, Blaimer M, Heidemann RM, Mueller MF, Griswold MA, Jakob PM. Controlled aliasing in parallel imaging results in higher acceleration (CAIPIRINHA) for multi-slice imaging. Magn Reson Med. 2005;53(3):684–691.
15 Breuer FA. CAIPIRINHA – Revisited. ↗ MAGNETOM FLASH 2015;63(3):7–15.
16 Wiggins GC, Triantafyllou C, Potthast A, Reykowski A, Nittka M, Wald LL. 32-channel 3 Tesla receive-only phased-array head coil with soccer-ball element geometry. Magn Reson Med. 2006 Jul;56(1):216–223.
17 Setsompop K, Gagoski BA, Polimeni JR, Witzel T, Wedeen VJ, Wald LL. Blipped-controlled aliasing in parallel imaging for simultaneous multislice echo planar imaging with reduced g-factor penalty. Magn Reson Med. 2012; 67(5):1210–1224.
18 Müller S. Simultaneous multislice imaging (SIMUSIM) for improved cardiac imaging. Magn Reson Med. 1989;10(1):145–155.
19 Glover GH. Phase-offset multiplanar (POMP) volume imaging: a new technique. J Magn Reson Imaging. 1991;1(4):457–461.
20 Larkman DJ, Hajnal JV, Herlihy AH, Coutts GA, Young IR, Ehnholm G. Use of multicoil arrays for separation of signal from multiple slices simultaneously excited. J Magn Reson Imaging. 2001;13(2):313–317.
21 Moeller S, Yacoub E, Olman CA, Auerbach E, Strupp J, Harel N, Uğurbil K. Multiband multislice GE-EPI at 7 tesla, with 16-fold acceleration using partial parallel imaging with application to high spatial and temporal whole-brain fMRI. Magn Reson Med. 2010;63(5):1144–1153.

22 Feinberg DA, Moeller S, Smith SM, Auerbach E, Ramanna S, Gunther M, Glasser MF, Miller KL, Ugurbil K, Yacoub E. Multiplexed echo planar imaging for sub-second whole brain FMRI and fast diffusion imaging. PLoS One. 2010;5(12):e15710.
23 Stäb D, Ritter CO, Breuer FA, Weng AM, Hahn D, Köstler H. CAIPIRINHA accelerated SSFP imaging. Magn Reson Med. 2011;65(1):157–164.
24 Setsompop K, Cohen-Adad J, Gagoski BA, Raij T, Yendiki A, Keil B, et al. Improving diffusion MRI using simultaneous multi-slice echo planar imaging. Neuroimage. 2012;63(1):569–580.
25 Barth M, Breuer F, Koopmans PJ, Norris DG, Poser BA. Simultaneous multislice (SMS) imaging techniques. Magn Reson Med. 2016;75(1):63-81.
26 Conolly SM, Nishimura DG, Macovski A, Glover GH. Variable-rate selective excitation. J Magn Reson.1969;78(3):440–458.
27 Porter DA, Heidemann RM. High resolution diffusion-weighted imaging using readout-segmented echo-planar imaging, parallel imaging and a two-dimensional navigator-based reacquisition. Magn Reson Med 2009;62(2):468–475.
28 Runge VM. Simultaneous Multi-Slice (Slice Accelerated) Diffusion EPI: Early Experience for Brain Ischemia and Cervical Lymphadenopathy. ↗ MAGNETOM Flash 2015;63(3):92–95.
29 Gagoski BA, Bilgic B, Eichner C, Bhat H, Grant PE, Wald LL, Setsompop K. RARE/turbo spin echo imaging with Simultaneous Multislice Wave-CAIPI. Magn Reson Med. 2015;73(3):929–938.
30 Wang D. Multiband Slice Accelerated TSE: Application in Brain Imaging. Proc Int Soc Mag Reson Med. 2014;22, 4317.
31 Keil B, Blau JN, Biber S, Hoecht P, Tountcheva V, Setsompop K, et al. A 64-channel 3T array coil for accelerated brain MRI. Magn Reson Med. 2013;70(1):248–258.
32 Schmitt F. An attempt to reconstruct the history of Gradient-System technology at Siemens. MAGNETOM Flash 2020;76(1). Available online from https://marketing.webassets.siemens-healthineers.com/f3ba149b97c25738/939f80bd2cc4/siemens-healthineers_magnetom-world_case-studiesSchmitt_Gradient_Development_ISMRM_2020.pdf
33 Lustig M, Donoho DL, Santos JM, Pauly JM. Compressed sensing MRI. IEEE Signal Processing Magazine. 2008;25(2):72–82.
34 Lustig M, Donoho D, Pauly JM. Sparse MRI: The application of compressed sensing for rapid MR imaging. Magn Reson Med. 2007;58(6):1182–1195.
35 Yang AC, Kretzler M, Sudarski S, Gulani V, Seiberlich N. Sparse Reconstruction Techniques in Magnetic Resonance Imaging: Methods, Applications, and Challenges to Clinical Adoption. Invest Radiol. 2016;51(6):349–364.
36 Hollingsworth KG. Reducing acquisition time in clinical MRI by data undersampling and compressed sensing reconstruction. Phys Med Biol. 2015;60(21):R297–322.
37 Forman C. Compressed Sensing: a Paradigm Shift in MRI. ↗ Compressed Sensing Supplement to MAGNETOM Flash 2016;66(3) 8–13.
38 Natsuaki Y, Bi X, Zenge MO, Speier P, Schmitt P, Laub G. Time-Of-Flight with Sparse undersampling (TOFu): towards practical MR applications of the Compressed Sensing. Proc. ISMRM. 2014;#660.
39 Stalder AF, Natsuaki Y, Schmidt M, Bi X, Zenge MO, Nadar M, et al. Accelerating TOF MRA in Clinical Practice using Sparse MRI with Variable Poisson Density Sampling. Proc. ISMRM 2015;#3606.
40 Yanamoto T, Togashi K, Fujimoto K, Fushimi Y, Yamamoto A, Togashi K. Compressed Sensing: Application to Time-of-Flight MR Angiography. ↗ Compressed Sensing Supplement to MAGNETOM Flash. 2016;66(3):36–39.
41 Toledano-Massiah S, Sayadi A, de Boer R, Gelderblom J, Mahdjoub R, Gerber S, et al. Accuracy of the Compressed Sensing Accelerated 3D-FLAIR Sequence for the Detection of MS Plaques at 3T. AJNR Am J Neuroradiol. 2018;39(3):454–458.
42 Eliezer M, Vaussy A, Toupin S, Barbe R, Kannengiesser S, Stemmer A, et al. Iterative denoising accelerated 3D SPACE FLAIR sequence for brain MR imaging at 3T. Diagn Interv Imaging. 2022;103(1):13–20.
43 Benjamin AJV, Bano W, Mair G, Thompson G, Casado A, Di Perri C, et al. Diagnostic quality assessment of IR-prepared 3D magnetic resonance neuroimaging accelerated using compressed sensing and k-space sampling order optimization. Magn Reson Imaging. 2020;74:31–45.
44 Meister RL, Groth M, Jürgens JHW, Zhang S, Buhk JH, Herrmann J. Compressed SENSE in Pediatric Brain Tumor MR Imaging: Assessment of Image Quality, Examination Time and Energy Release. Clin Neuroradiol. 2022. doi: 10.1007/s00062-021-01112-3. Epub ahead of print.
45 Sartoretti T, Reischauer C, Sartoretti E, Binkert C, Najafi A, Sartoretti-Schefer S. Common artefacts encountered on images acquired with combined compressed sensing and SENSE. Insights Imaging. 2018;9(6):1107–1115.
46 Kayvanrad M, Lin A, Joshi R, Chiu J, Peters T. Diagnostic quality assessment of compressed sensing accelerated magnetic resonance neuroimaging. J Magn Reson Imaging. 2016;44(2):433–444.
47 Takatsu Y, Nakamura M, Yamashiro T, Ikemoto A, Sawa S, Nakamura M, et al. Evaluation of contrast and denoising effects related to imaging parameters of compressed sensitivity encoding in contrast-enhanced magnetic resonance imaging. Radiol Phys Technol. 2021;14(2):193–202.
48 Vranic JE, Cross NM, Wang Y, Hippe DS, de Weerdt E, Mossa-Basha M. Compressed Sensing-Sensitivity Encoding (CS-SENSE) Accelerated Brain Imaging: Reduced Scan Time without Reduced Image Quality. AJNR Am J Neuroradiol. 2019;40(1):92–98.
49 Polak D, Cauley S, Bilgic B, Wald L. Setsompop K. Ultrafast Multi-contrast High-resolution 3D Brain MRI: a Technical Description of Wave-CAIPI. ↗ MAGNETOM Flash 2020;76(1):21–27.
50 Polak D, Setsompop K, Cauley SF, Gagoski BA, Bhat H, Maier F, et al. Wave-CAIPI for highly accelerated MP-RAGE imaging. Magn Reson Med. 2018;79(1):401–406.
51 Chung MS, Lee EJ, Kim S, Kim SO, Byun JS. Wave-CAIPI susceptibility-weighted imaging achieves diagnostic performance comparable to conventional susceptibility-weighted imaging in half the scan time. Eur Radiol. 2020;30(4):2182–2190.
52 Filho ALG, Conklin J, Rapalino O, Schaefer P, Huang S. Ultrafast Multi-Contrast High-Resolution 3D Brain MRI: Clinical Evaluation of Wave-CAIPI Acceleration in SWI, MPRAGE, FLAIR, SPACE. ↗ MAGNETOM Flash 2020;76(1):21–27.
53 Conklin J, Longo MGF, Cauley SF, Setsompop K, González RG, Schaefer PW, Kirsch JE, Rapalino O, Huang SY. Validation of Highly Accelerated Wave-CAIPI SWI Compared with Conventional SWI and T2*-Weighted Gradient Recalled-Echo for Routine Clinical Brain MRI at 3T. AJNR Am J Neuroradiol. 2019;40(12):2073–2080.
54 Conklin J, Tabari A, Longo MGF, Cobos CJ, Setsompop K, Cauley SF, et al. Evaluation of highly accelerated wave controlled aliasing in parallel imaging (Wave-CAIPI) susceptibility-weighted imaging in the non-sedated pediatric setting: a pilot study. Pediatr Radiol. 2022;52(6):1115–1124.
55 Lin DJ, Johnson PM, Knoll F, Lui YW. Artificial Intelligence for MR Image Reconstruction: An Overview for Clinicians. J Magn Reson Imaging. 2021;53(4):1015–1028.
56 Baek HJ, Heo YJ, Kim D, Yun SY, Baek JW, Jeong HW et al. Usefulness of Wave-CAIPI for Postcontrast 3D T1-SPACE in the Evaluation of Brain Metastases. AJNR Am J Neuroradiol. 2022;43(6):857–863.
57 Behl N. Deep Resolve – Mobilizing the Power of Networks. ↗ MAGNETOM Flash 2021;78(1):29–35.

58 Hammernik K, Knoll F, Rueckert D. Deep Learning for Parallel MRI Reconstruction: Overview, Challenges, and Opportunities. ↗ MAGNETOM Flash 2019;75(4):10–15.
59 Hammernik K, Schlemper J, Qin C, Duan J, Summers RM, Rueckert D. Systematic evaluation of iterative deep neural networks for fast parallel MRI reconstruction with sensitivity-weighted coil combination. Magn Reson Med. 2021;86(4):1859–1872.
60 Knoll F, Hammernik K, Zhang C, Moeller S, Pock T, Sodickson DK, et al. Deep-Learning Methods for Parallel Magnetic Resonance Imaging Reconstruction: A Survey of the Current Approaches, Trends, and Issues. IEEE Signal Process Mag. 2020;37(1):128–140.
61 Koonjoo N, Zhu B, Bagnall GC, Bhutto D, Rosen MS. Boosting the signal-to-noise of low-field MRI with deep learning image reconstruction. Sci Rep. 2021;11(1):8248.
62 Chandra SS, Bran Lorenzana M, Liu X, Liu S, Bollmann S, Crozier S. Deep learning in magnetic resonance image reconstruction. J Med Imaging Radiat Oncol. 2021 Aug;65(5):564–577.
63 Eliezer M, Vaussy A, Toupin S, Barbe R, Kannengiesser S, Stemmer A, et al. Iterative denoising accelerated 3D SPACE FLAIR sequence for brain MR imaging at 3T. Diagn Interv Imaging. 2022 Jan;103(1):13–20.

## Contact

Michael Kean, FISMRT, Chief MR Technologist
Children's MRI and PET Centre, Department of Medical Imaging
Honorary Fellow, Developmental Imaging, Murdoch Children's Research Institute
Honorary Senior Research Fellow, Department of Paediatrics, The University of Melbourne
Royal Children's Hospital
Flemington Road
Parkville, Australia
Tel.: +61 411681198
Michael.Kean@rch.org.au

# Abbreviated Turbo Spin Echo T2- and FLAIR-weighted Sequences to Complement Multiplanar HASTE Images in "Quick MRI" Pediatric Brain Imaging at 3 Tesla: A child-tailored approach

**Andrea Righini, M.D.; Filippo Arrigoni, M.D.; Giana Izzo, M.D.; Cecilia Parazzini, M.D.; Chiara Doneda, M.D.; Giovanni Palumbo, M.D.**

Pediatric Radiology and Neuroradiology Department, Children's Hospital V. Buzzi, Milan, Italy

## Introduction

The "Quick MRI" approach is rapidly gaining popularity in pediatric neuro imaging to reduce the need for sedation in several conditions including hydrocephalus monitoring, ventricular shunting follow-up, intracranial cysts, minor to moderate head trauma, headaches, and prior to spinal tap procedures.

Single-shot half Fourier (HASTE) T2-weighted sequences are currently the mainstay of "Quick MRI" neuro imaging protocols. Such sequences have clear advantages in allowing brain depiction with minimal or even no motion artifacts. However, certain aspects such as low contrast resolution and a limited sensitivity to intraparenchymal hemorrhage can still present significant drawbacks to further "Quick MRI" applications.

To overcome such limitations and to explore the full potential of new-generation 3-tesla MR scanners (e.g., higher signal-to noise ratio, improved fast shimming, higher density receiver-unit head coils, 20–64 channels, and higher parallel imaging factors), we started testing an abbreviated version of the conventional turbo spin echo (TSE) 2D T2 and FLAIR (DarkFluid) weighted sequence in uncooperative children and all patients under 6 years of age[1].

These sequences were added to the usual HASTE T2-weighted based "Quick-MRI" protocol on our MAGNETOM Vida equipped with XQ gradients and the *syngo* MR XA31 software version. A 20-channel head/neck receiver coil was used. Since each sequence lasts less than a minute (40–55 seconds), the general strategy for each child is to acquire a sufficient number of motion-free images by repeated acquisition of the same sequence if necessary, according to the judgment of the pediatric neuroradiologist. This results in some redundancy in image acquisition, yet images are acquired in a few minutes and contain sufficient diagnostic information.

A tailored individual exam in pediatric neuro imaging is based on the threshold for motion artifacts determined to be acceptable depending on the clinical work-up and the particular diagnostic question.

| | HASTE-T2 | abbreviated TSE-T2 | abbreviated TSE-FLAIR |
|---|---|---|---|
| Acquisition time | 46 sec. | 52 sec. | 51 sec. |
| TR/TI/TE | 2000/90 msec | 7300/88 msec | 8500/2438/ 97 msec |
| Concatenations | 2 | 1 | 2 |
| FOV | 230 mm | 230 mm | 230 mm |
| phase FOV | 75% | 75% | 75% |
| In-plane res. acquisition | 1.0 × 0.9 mm | 1.14 × 0.8 mm | 1.73 × 1.44 mm |
| In-plane res. reconstruction | 0.9 × 0.9 mm | 0.8 × 0.8 mm | 0.7 × 0.7 mm |
| Slice thickness | 4 mm | 4 mm | 4 mm |
| Gap | 10% | 10% | 10% |
| Slice number | 23 | 23 | 23 |
| GRAPPA | 0 | 2 | 3 |
| Gradient set mode | fast | fast | fast |
| Turbo factor | 173 | 16 | 29 |
| Echo spacing bandwidth | 930 Hz/px | 126 Hz/px | 286 Hz/px |
| Slice order | ascending | interleaved | interleaved |

**Table 1**: Main parameters of the tested HASTE and abbreviated TSE sequences.

[1] *MR scanning has not been established as safe for imaging fetuses and infants less than two years of age. The responsible physician must evaluate the benefits of the MR examination compared to those of other imaging procedures.*

## Practical tips

- Position the child's head at the center of the coil and secure it using abundant foam padding. During the exam, a parent should maintain close physical contact with the child to reassure them and to prevent possible leg motion. Play music or fairy tales through the headphones at high volume or allow the child to wear goggles with cartoons to minimize scanner noise and distract the child.
- Start with three-plane HASTE T2 sequences and repeat if there is any significant motion. Then apply abbreviated axial and coronal TSE T2 and FLAIR sequences (Table 1) and repeat if necessary with no further pre-scan adjustment, until the motion artifacts are below the acceptable threshold.
- DWI, T1 VIBE sagittal and axial sections (< 30 sec acquisition time) can be added to the protocol and repeated if needed.

## Preliminary results

With respect to HASTE, abbreviated TSE images resulted in better contrast between gray and white matter and in sharper depiction of cerebral structures, for example in basal ganglia delineation (Fig. 1). Subcortical and cortical-white matter interface lesions were also better

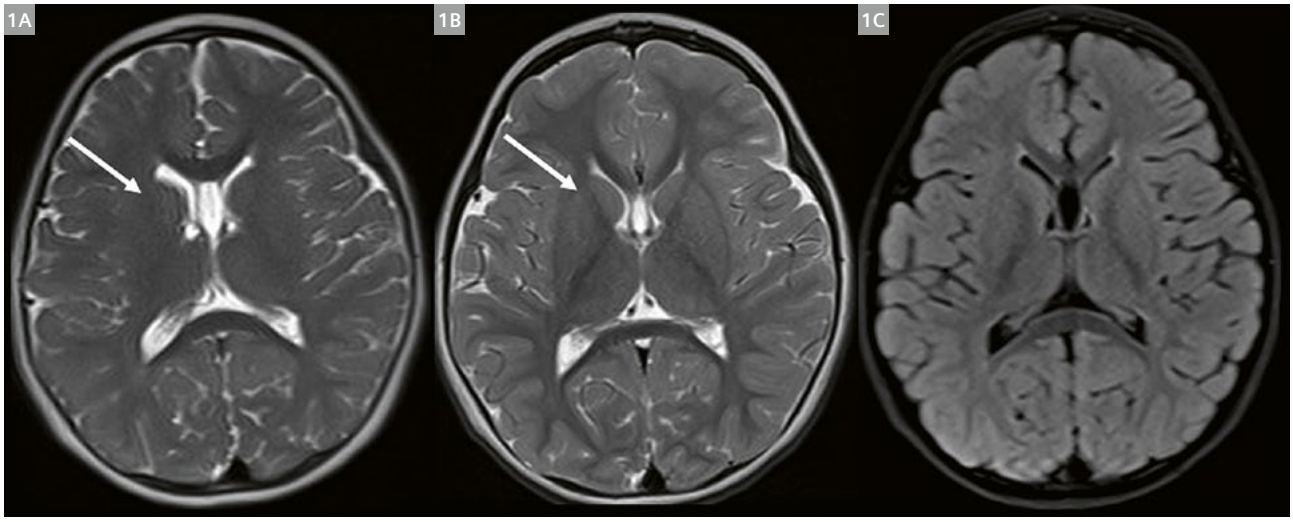


**1** Matched axial sections from a 21-month-old unsedated child[1]: **(1A)** HASTE, **(1B)** abbreviated TSE and **(1C)** FLAIR. Gray/white matter contrast and basal ganglia delineation is better on abbreviated TSE with respect to HASTE (arrows).

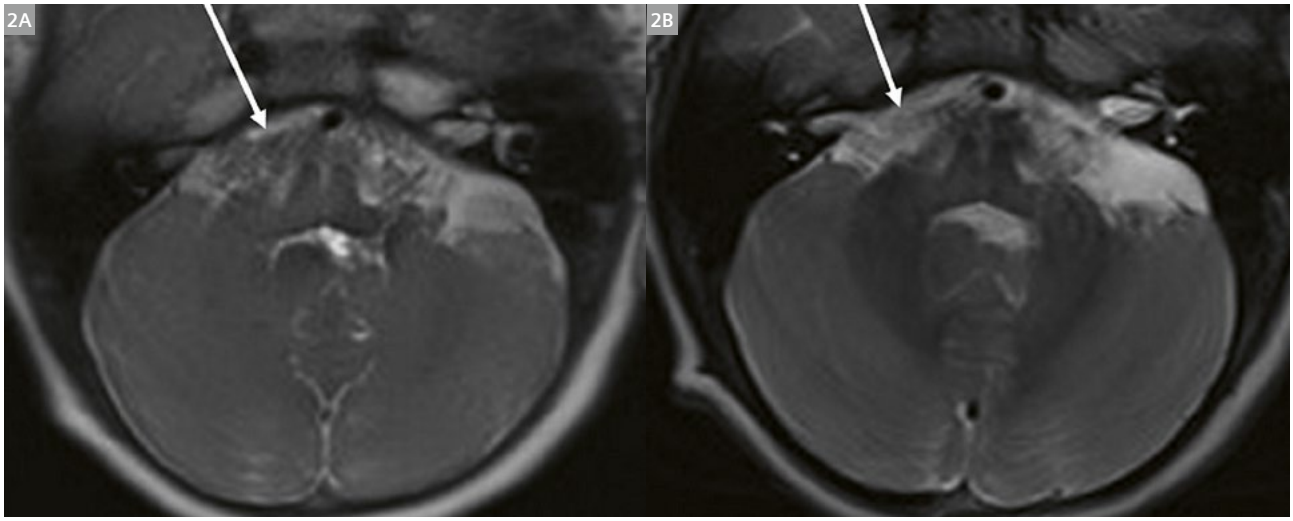


**2** Matched axial sections from a 20-month-old unsedated child[1]: **(2A)** HASTE and **(2B)** abbreviated TSE; CSF flow artifacts (arrows) are less evident in abbreviated TSE.

highlighted. They were less prone to CSF flow-related artifacts (Fig. 2), however, anomalies containing CSF (i.e., cysts) were better delineated by HASTE, probably due to the better fluid-parenchyma contrast as is commonly known. The FLAIR sequence provided additional confidence in judging focal parenchymal lesions and peri-cerebral/CSF-abnormal findings (Fig. 3).

In about half of the cases, either abbreviated T2- or-FLAIR-weighted sequences had to be repeated because there were deemed too heavily affected by motion. However, this only resulted in an increased global scanning time of 2–3 minutes. Moreover, we noticed that the repeated sequences were usually less or not at all affected by motion compared with the previous ones, probably due to a sort of "lullaby effect" from the rhythmic scanner noise (Fig. 4).

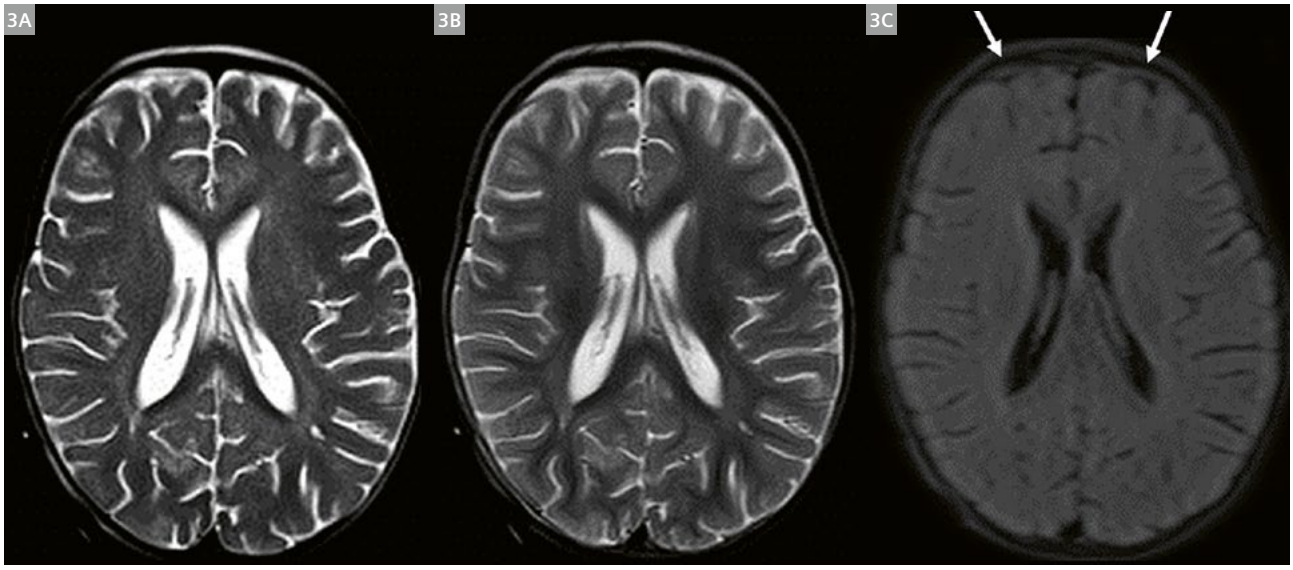


**3** Matched axial sections from a 12-month-old unsedated child[1]: **(3A)** HASTE, **(3B)** TSE, and **(3C)** FLAIR. Abnormal meningeal signal due to pneumococcal meningitis is noticeable in FLAIR (arrows).

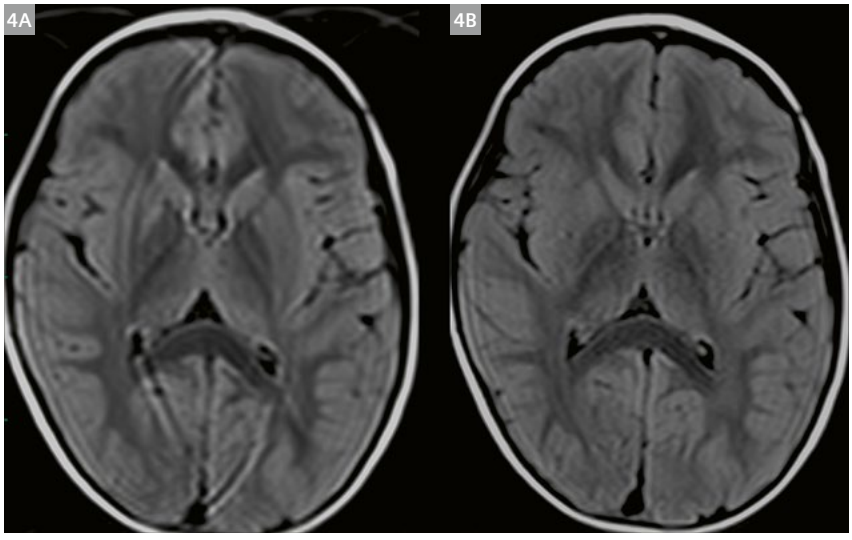


**4** Matched axial abbreviated FLAIR sections from a 6-year-old unsedated child with intellectual disability: **(4A)** shows marked motion artifacts, while on **(4B)** the consecutive repeated acquisition is not affected.

[1] *MR scanning has not been established as safe for imaging fetuses and infants less than two years of age. The responsible physician must evaluate the benefits of the MR examination compared to those of other imaging procedures.*

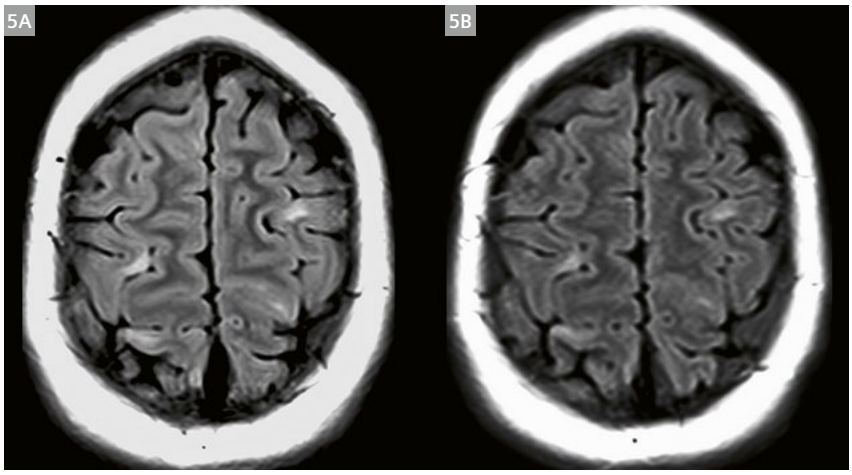


**5** Matched axial FLAIR sections from a 12-year-old patient with tuberous sclerosis. **(5A)** 3-minute long conventional sequence and, **(5B)** the abbreviated version. Cortical tuber identification is acceptable.

## Discussion

A similar approach was recently successfully tested by Jaimes et al. [6, 7]. They compared abbreviated versions of TSE sequences with conventional longer ones and found a good correspondence in diagnostic yield. Their sequence duration was longer than one minute, which might limit a strategy of potential iterative repetition of the sequence as used in our setting.

We believe that the addition of abbreviated FLAIR could expand the use of "Quick MRI" protocols to chronic conditions that require follow-up starting from pre-school age, such as cortical tubers and subependymal giant cell astrocytoma monitoring in tuberous sclerosis (Fig. 5).

Abbreviated TSE sequences would benefit from further improvement by using even higher density coil elements (i.e., 64-channel head/neck coil with a higher GRAPPA factor) or specially designed smaller coils carrying more elements (i.e., 32 channels) for children between 12 months and two years of age. In addition, using Simultaneous Multi-Slice (SMS) in TSE imaging could further reduce scan times. FLAIR- and T1-weighted 3D wave-CAIPI may also be helpful, although they are likely to be quite susceptible to motion artifacts.

In summary, we believe that the use of abbreviated versions of TSE sequences is feasible in uncooperative children or those under six years of age. It could provide some advantages in diagnostic pediatric work-up and complement HASTE techniques in current "Quick MRI" imaging, at least for some indications. Meanwhile, in conditions such as neuro oncology, complex brain malformations, or epilepsy such an approach is not suitable. Repetitive iterative sequence acquisitions of lower resolution TSE imaging may represent a valuable strategy to achieve a diagnostic target tailored to an individual child's condition.

**References**

1 Iskandar BJ, Sansone JM, Medow J, Rowley HA. The use of quick-brain magnetic resonance imaging in the evaluation of shunt-treated hydrocephalus. J Neurosurg. 2004 Nov;101(2 Suppl):147-51.
2 Vanderby SA, Babyn PS, Carter MW, Jewell SM, McKeever PD. Effect of anesthesia and sedation on pediatric MR imaging patient flow. Radiology. 2010 Jul;256(1):229-37.
3 Boyle TP, Paldino MJ, Kimia AA, Fitz BM, Madsen JR, Monuteaux MC, et al. Comparison of rapid cranial MRI to CT for ventricular shunt malfunction. Pediatrics. 2014 Jul;134(1):e47-54.
4 Jaimes C, Gee MS. Strategies to minimize sedation in pediatric body magnetic resonance imaging. Pediatr Radiol. 2016 May;46(6):916-27.
5 Trofimova A, Kadom N. Added value from abbreviated brain MRI in children with headache. AJR Am J Roentgenol. 2019 Mar 12;1-6.
6 Jaimes C, Yang E, Connaughton P, Robson CD, Robertson RL. Diagnostic equivalency of fast T2 and FLAIR sequences for pediatric brain MRI: a pilot study. Pediatr Radiol. 2020 Apr;50(4):550-559.
7 Jaimes C, Robson CD, Machado-Rivas F, Yang E, Mahan K, Bixby SD, et al. Success of non-sedated neuroradiological MRI in children 1 to 7 years old. AJR Am J Roentgenol. 2021 May;216(5):1370-1377.

## Contact

Andrea Righini, M.D.
Director of Pediatric Radiology and Neuroradiology
Children's Hospital V. Buzzi
Via Castelvetro 32
20154, Milan
Italy
andrea.righini@asst-fbf-sacco.it

The .exar1 protocol file is available for download at

**www.magnetomworld.siemens-healthineers.com**

# 2D BLADE Turbo Gradient- and Spin-Echo versus 2D Spin-Echo Echo-Planar Diffusion-Weighted Brain MRI in Children

**Aaron S McAllister, M.D.; Ramkumar Krishnamurthy, Ph.D.**

Department of Radiology, Nationwide Children's Hospital, Columbus, OH, USA

## Introduction

Diffusion-weighted imaging is a powerful technique for assessing brain pathologies and has become indispensable in pediatric brain MRI protocols [1–6]. It is commonly implemented as a 2D multislice single-shot spin-echo echo-planar-imaging (SE-EPI). Signal pile-ups and geometric distortions at areas of inhomogeneous magnetic field are well known as the limitations of the SE-EPI sequence [7]. For example, artifacts are often observed near air tissue interfaces such as the paranasal sinuses and petrous apices. Artifacts associated with surgical or dental implants[1] such as braces or shunt valves can obscure large portions of the brain yielding non-diagnostic images.

## BLADE DWI

The BLADE DWI sequence[2] mitigates the limitations of the SE-EPI DWI sequence. It utilizes turbo gradient- and spin-echo (TGSE) readouts and acquires *k*-space with a BLADE trajectory. The sequence is designed to minimize $B_0$ related artifacts, e.g., distortion and signal pile-ups. Motion related artifacts can be reduced by this sequence as well.

The MRI acquisition metrics for the BLADE sequence and the SE-EPI sequence as implemented at our institution are listed in Table 1.

| Parameter | Blade | SE-EPI |
|---|---|---|
| Matrix size | 192 × 192 | 192 × 192 |
| Acquired voxel dimension (mm) | 1.3 | 1.3 |
| Number of slices | 30 | 30 |
| Slice thickness (mm) | 4 | 4 |
| b-values (s/mm²) | 0, 1000 | 0, 1000 |
| TR (ms) | 5200 | 4100 |
| TE (ms) | 41 | 81 |
| EPI factor | 3 | 192 |
| Turbo factor | 11 | n/a |
| Parallel imaging (GRAPPA) | None | 2×, 40 reference lines |
| Scan time (min:sec) | 4:27 | 1:11 |

**Table 1**: Scan parameters utilized for BLADE DWI and SE-EPI.

[1] *The MRI restrictions (if any) of the metal implant must be considered prior to patient undergoing MRI exam. MR imaging of patients with metallic implants brings specific risks. However, certain implants are approved by the governing regulatory bodies to be MR conditionally safe. For such implants, the previously mentioned warning may not be applicable. Please contact the implant manufacturer for the specific conditional information. The conditions for MR safety are the responsibility of the implant manufacturer, not of Siemens Healthineers.*

[2] *BLADE Diffusion is a product with software version syngo MR XA 50 or later. The sequence used in the article was a prototype.*

## Discussion

In our previously published experience [8], the BLADE DWI sequence is a viable alternative to SE-EPI in pediatric[3] patients and effectively reduced signal pile-ups and geometric distortion in areas of high magnetic susceptibility changes from air-tissue interface or metallic implants[1] leading to compromised diagnostic image quality in SE-EPI DWI scans. For example, Figure 1 demonstrates the commonly observed signal pile-ups seen at the petrous apices in a 5-year-old male on SE-EPI and the marked reduction using the BLADE DWI sequence. Figure 2 demonstrates the improved visualization of the right cerebral hemisphere in a 28-year-old male with a right shunt valve and Figure 3 demonstrates a similar improvement in visualization in a 15-year-old patient with braces. It may be a first choice alternative in patients with known bulk susceptibility or where pathology is suspected near a susceptibility

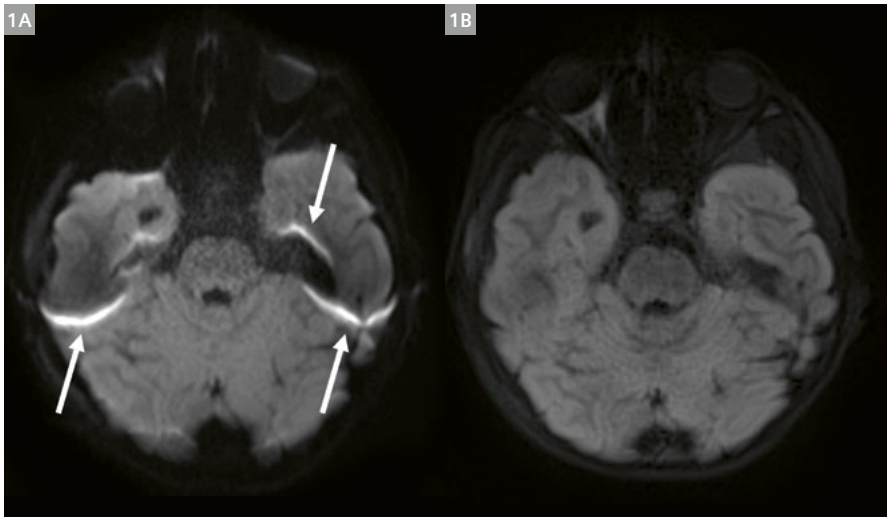


**1** 5-year-old male demonstrating common signal pile-ups and geometric distortion (white arrows) from the susceptibility interface at the petrous apices on the SE-EPI **(1A)**. Minimal on the BLADE DWI **(1B)**.

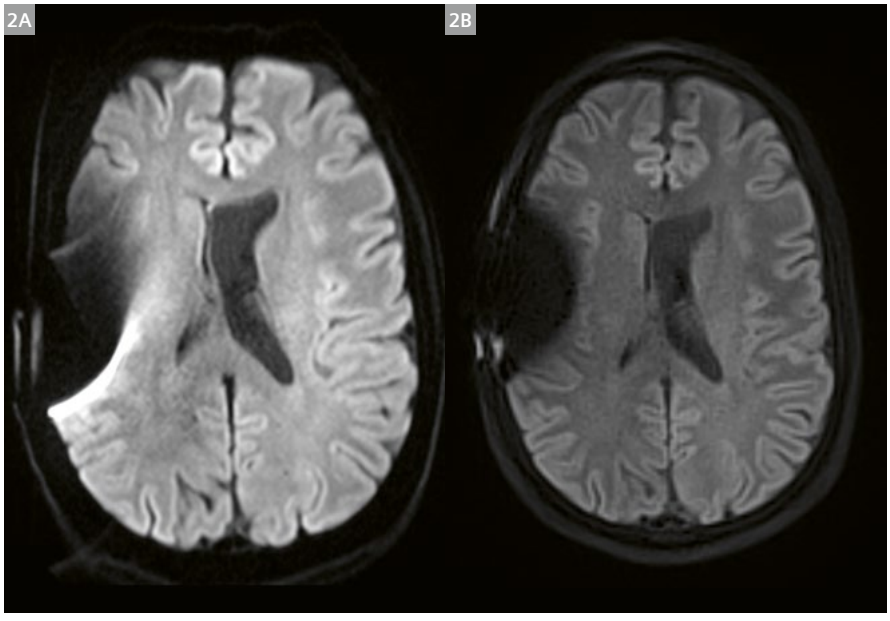


**2** 28-year-old male. Susceptibility artifact of the right frontal and parietal lobes from shunt valve. Notice the geometric distortion and signal pile-ups along the posterior margin of the artifact on the SE-EPI DWI image **(2A)**. Decreased on the BLADE DWI **(2B)**.

*[3]MR scanning has not been established as safe for imaging fetuses and infants less than two years of age. The responsible physician must evaluate the benefits of the MR examination compared to those of other imaging procedures. Note: This disclaimer does not represent the opinion of the authors.*

interface. BLADE DWI better demonstrated parietal dural extension of tumor laterally, which was obscured by signal pile-ups on the SE-EPI DWI, Figure 4. Image distortion and signal pile-ups from pneumocephalus complicates immediate post-operative diffusion imaging. For example, Figure 5 demonstrates improved visualization of the soft tissues at the resection margin of an immediate post-operative 5-year-old male who underwent partial frontal lobectomy for epileptogenic focus resection. The method of acquisition of BLADE DWI also makes the sequence less motion sensitive, but in our experience this relative motion insensitivity is offset by the increased likelihood of patient movement over the longer scan time: 4 minutes 27 seconds for BLADE DWI versus 1 minute 11 seconds for the SE-EPI.

## Conclusion

BLADE DWI demonstrates improvement in the geometric distortion and signal pile-ups commonly observed at regions of magnetic field inhomogeneity such as at air tissue interfaces and associated with metallic implants, but at a cost of increased scan time: 4 minutes 27 seconds versus 1 minute 11 seconds. The increased time may not justify its use for all patients, but has clear benefit in those patients with disease near the skull base or sinuses or those with known susceptibility artifact inducing dental or medical implants.

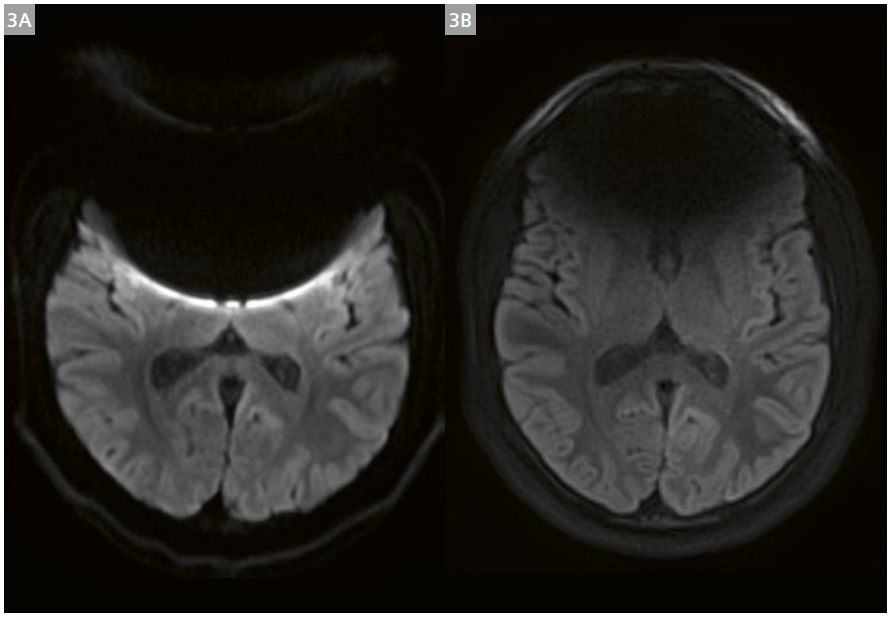


**3** 15-year-old male SE EPI DWI **(3A)** demonstrates architectural distortion and signal pile-ups from susceptibility artifact from braces. Both decreased on BLADE DWI **(3B)** with decreased size of the non-diagnostic area.

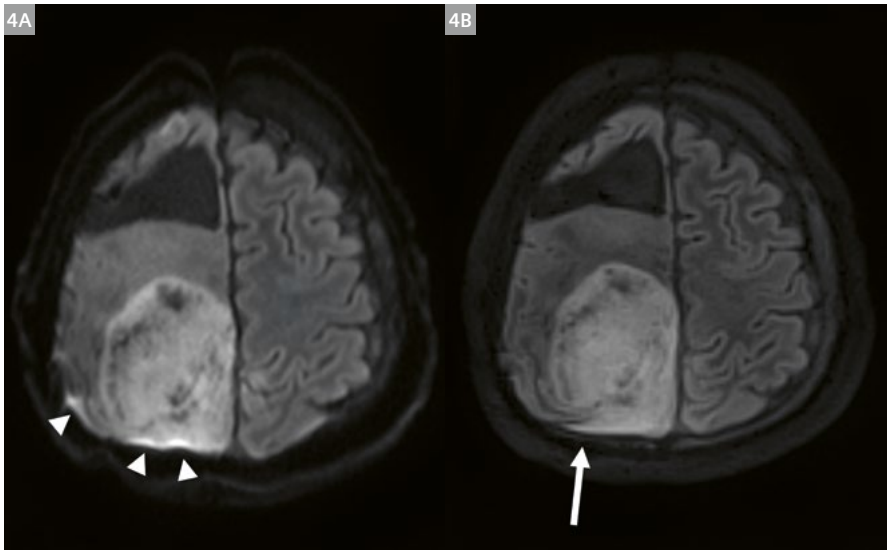


**4** 17-year-old male with large right parietal tumor, T-cell lymphoblastic lymphoma. Signal pile-ups at the skull/CSF susceptibility interface (white arrow heads) on SE-EPI **(4A)** obscures lateral tumor extension along the parietal dura that is clearly demonstrated (white arrow) on the BLADE DWI **(4B)**.

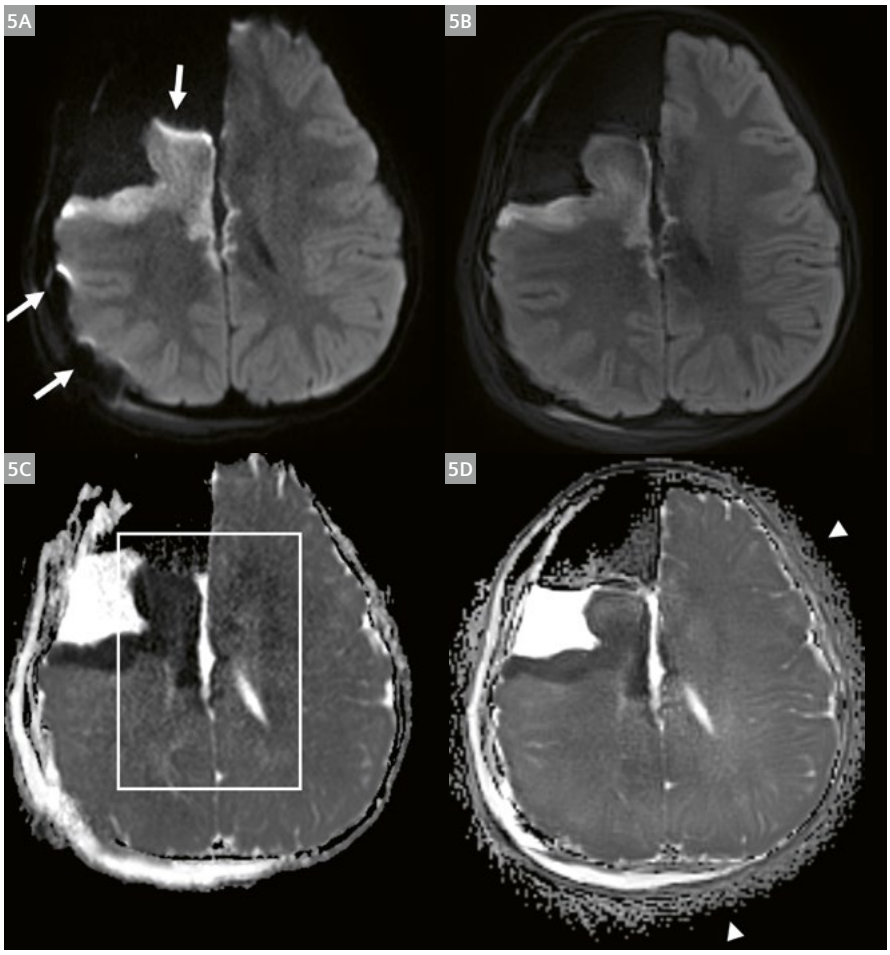


**5** 5-year-old male post-op from right frontal lobe epileptogenic focus resection. Note the geometric distortion and signal pile-ups at the resection margin and along the inner table of the right parietal bone (white arrows) on the SE-EPI sequence **(5A)** versus BLADE DWI **(5B)**. ADC map for SE-EPI **(5C)** demonstrates increased central granularity (white box), while the BLADE ADC map **(5D)** demonstrates extra-cranial noise (arrowheads).

**References**


1 Engelbrecht V, Scherer A, Rassek M, Witsack HJ, Modder U. Diffusion-weighted MR imaging in the brain in children: findings in the normal brain and in the brain with white matter diseases. Radiology. 2002;222(2):410-418.

2 Rutherford M, Counsell S, Allsop J, et al. Diffusion-weighted magnetic resonance imaging in term perinatal brain injury: a comparison with site of lesion and time from birth. Pediatrics. 2004;114(4):1004-1014.

3 Kan P, Liu JK, Hedlund G, Brockmeyer DL, Walker ML, Kestle JR. The role of diffusion-weighted magnetic resonance imaging in pediatric brain tumors. Childs Nerv Syst. 2006;22(11):1435-1439.

4 Jaremko JL, Jans LB, Coleman LT, Ditchfield MR. Value and limitations of diffusion-weighted imaging in grading and diagnosis of pediatric posterior fossa tumors. AJNR Am J Neuroradiol. 2010;31(9):1613-1616.

5 Utsunomiya H. Diffusion MRI abnormalities in pediatric neurological disorders. Brain Dev. 2011;33(3):235-242.

6 Drake-Perez M, Boto J, Fitsiori A, Lovblad K, Vargas MI. Clinical applications of diffusion weighted imaging in neuroradiology. Insights Imaging. 2018;9(4):535-547.

7 Morelli JN, Runge VM, Ai F, et al. An image-based approach to understanding the physics of MR artifacts. Radiographics. 2011;31(3):849-866.

8 Hu HH, McAllister AS, Jin N, et al. Comparison of 2D BLADE Turbo Gradient- and Spin-Echo and 2D Spin-Echo Echo-Planar Diffusion-Weighted Brain MRI at 3 T: Preliminary Experience in Children. Acad Radiol. 2019;26(12):1597-1604.


Ramkumar Krishnamurthy

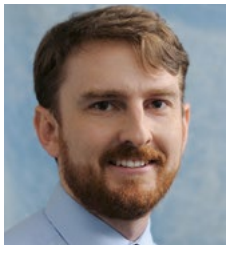

Aaron S McAllister

## Contact


Aaron S McAllister, M.D.
Department of Radiology
Nationwide Children's Hospital
700 Children's Dr E4A
Columbus, OH 43205
USA
Tel.: +1 (614) 355-4195
aaron.mcallister@nationwidechildrens.org

# MP2RAGE-based Inline Morphometric and Regional T1 Assessment in Pediatric Patients: Initial Clinical Experience and Potential Benefits

**Baptiste Morel[1]; Maximilien Périvier[2]; Pierre Thomas-Castelnau[1]; Tom Hilbert[3]; Gian Franco Piredda[3]; Kelvin Chow[4]; Till Huelnhagen[3]; Bénédicte Maréchal[3]; Tobias Kober[3]**

[1]University of Tours, Centre Hospitalier Régional Universitaire Tours, Department of Pediatric Radiology, Tours, France
[2]Pediatric Neurology Department, CHU Clocheville, Tours, France
[3]Advanced Clinical Imaging Technology, Siemens Healthineers, Lausanne, Switzerland
[4]MR R&D Collaborations, Siemens Medical Solutions USA, Inc., Chicago, IL, USA

## Introduction

The brain undergoes dramatic changes in the first years of life and continues to evolve during childhood. Two main processes occur simultaneously: growth with an increase in volume, and maturation with myelination [1, 2].

Normal brain development in children can be evaluated by measuring head circumference and examining neurological symptoms, allowing to reliably diagnose the majority of brain injuries. However, in case of diffuse or subtle brain volume abnormalities, it is difficult to assess brain regions objectively [3]. This is even more difficult when it comes to evaluating white matter signal intensity [4], as global changes in particular are hard to detect due to the lack of a reference intensity. Quantitative MRI (QMRI) enables absolute characterization of MR parameters that correspond to tissue properties in a reproducible and comparable way. QMRI thus has the potential to increase sensitivity to subtle tissue changes, and to be of use in cases where no good contrast reference is available, such as when the whole white matter parenchyma exhibits pathological changes (due to inflammation, for instance).

Another tool for objective brain measures is morphometry, i.e., brain segmentation and volumetry. In pediatric[1] radiology, brain segmentation is complicated by two children specific challenges:

i) an increased relative effect of partial volumes, which occurs because the voxel sizes can't usually be adapted to the smaller structures in a child's brain due to time or technical constraints – this is relevant for gray and white matter segmentation, and for distinguishing unmyelinated from myelinated white matter [5];
ii) ongoing myelination, which means that the contrast in the brain changes drastically, especially in the first year of life – effectively "inverting" the gray/white matter contrast.

While T1-weighted MPRAGE-based brain morphometry is readily available in clinical routine for adult patients, the abovementioned challenges have hindered clinical adoption for children; in particular, normative ranges (i.e., ranges for volumetric values of different brain regions considered healthy) have so far not been available for pediatric patients. Additionally, it would be desirable to have integrated processing that allows simultaneous assessment of morphometry and quantitative values. We pursued the idea to implement such a strategy based on a single MP2RAGE acquisition that provides both anatomical information (the MPRAGE-like "uniform" contrast) for morphometry, and quantitative T1 maps.

To this end, the existing research application MorphoBox[2] [6, 7] was extended to provide reference ranges for morphometric and regional T1 values of pediatric subjects from one year of age at 1.5T [8]. We have further integrated the solution into an inline processing workflow using the Framework for Image Reconstruction Environments (FIRE)[2] from Siemens Healthineers. This allows us to easily integrate prototype reconstruction and post-processing algorithms into the inline processing pipeline. Our prototype, dubbed QuantiFIRE[2], enables radiologists to obtain a comprehensive and quantitative analysis of children's brains as DICOM outputs, which makes it easy to integrate this information into daily routine. The imaging is based on an adapted and harmonized MP2RAGE protocol. To maximize the clinical value of this add-in, z-score maps of absolute brain volumes and

[1] *MR scanning has not been established as safe for imaging fetuses and infants less than two years of age. The responsible physician must evaluate the benefits of the MR examination compared to those of other imaging procedures.*
[2] *Work in progress. The application is currently under development and is not for sale in the U.S. and in other countries. Its future availability cannot be ensured.*

regional T1 relaxometry values compared to age-matched normal children are also provided. The results can be displayed either on 3D deviation maps, highlighting regions with abnormally high or low volumes and T1 values, or in a DICOM report directly at the scanner and in the PACS system.

The research application QuantiFIRE is currently being evaluated in a multicentric study.

## Methodology

**Image processing**

The MorphoBox research application was developed by the Advanced Clinical Imaging Technology group of Siemens Healthineers in Lausanne, Switzerland, and was primarily designed for adults. It underwent a major adaptation of its atlases to automatically measure brain volumes and regional T1 distributions in children. Age-appropriate T1-weighted templates were generated for three age groups: infants aged 1–2 years[1], children aged 2–7 years, and children aged 8–16 years. The templates were built using an iterative method. A voxel-wise average across subjects was used as an initial reference target volume. This target volume was updated after each iteration by a voxel-wise average across the registered volumes. A total of 38 anatomical regions (gray and white matter depending on lobes and lateralization; basal ganglia and thalami; cerebrospinal fluid; ventricles, etc.) were drawn by a pediatric neuroradiologist on the three resulting templates. Consensus was obtained with two other neuroradiologists according to the standard anatomical nomenclature [9].

Volumes of these structures are estimated using the MorphoBox pipeline in its original form, but substituting the adult template with the age-appropriate one. Mean T1 values are then calculated for all included anatomical regions using the corresponding segmentation masks.

**Reference range creation**

A prospective monocentric study was conducted with 70 children (35 boys and 35 girls) recruited from the University Hospital of Tours, France, between January 2017 and November 2019. All subjects underwent brain MRI with an original indication of an isolated headache without neurological symptoms that showed a spontaneously favorable evolution. Normal clinical follow-up was performed for at least one year. Clinical exclusion criteria were the following identified brain pathologies: intracranial surgery, developmental delay, autism spectrum disorder, chronic epilepsy, significant prematurity, macrocephaly, microcephaly hydrocephalus, and genetic abnormalities.

All patients were scanned at 1.5T using a MAGNETOM Aera scanner (Siemens Healthcare, Erlangen, Germany) and a 20-channel head coil without general anesthesia. Intrarectal pentobarbital was administrated to young children requiring sedation. Whole-brain simultaneous T1-weighted imaging and T1 mapping was achieved with the MP2RAGE sequence using acquisition parameters tailored to pediatric applications (spatial resolution = $1.33 \times 1.33 \times 1.25$ mm$^3$, FOV = $256 \times 240$ mm$^2$, TI1/TI2 = 600/2000 ms, flip angles = 5/6°, TR = 5000 ms, TA = 6:36 min).

Using the age-appropriate templates, the volumes and average T1 relaxation values of the 38 anatomical regions were automatically estimated on all 70 patients. Reference brain volume ranges were established for each region using a logarithmic model, while a modified Gompertz growth model was used for regional T1 values. A Shapiro-Wilk test was used in both cases to investigate whether the fitting residuals were normally distributed. Resulting p-values smaller than 0.05 were considered to reject normality after Bonferroni's correction for multiple comparisons.

**Workflow integration with QuantiFIRE: report and deviation map creation**

To enable inline image processing on the scanner, the MorphoBox MP2RAGE processing pipeline was integrated with the standard image reconstruction using FIRE to form the QuantiFIRE research package. With QuantiFIRE, processing can be conveniently linked to the MP2RAGE acquisition as a sequence add-in without requiring any user interaction. The results are available directly at the scanner console and can be transferred to the PACS like any other DICOM series.

Automated volumetric and T1 relaxometry brain results were compared to the reference ranges and displayed on a deviation color map, which allows rapid identification of atrophic/hypertrophic regions or of structures with abnormally high or low T1 values (Fig. 1).

Z-score values from -1.3 to +1.3 are green. Values above a z-score of +1.3 or below -1.3 are considered pathological. Results are also available in a tabulated DICOM report (Fig. 1). Structures with a volume or regional T1 value deviating from the reference range ($1.3 < \text{z-score} < -1.3$) are highlighted with an asterisk.

The results are available within one minute after the end of the MP2RAGE acquisition, allowing the radiologists to have quantitative information at the time of the MR interpretation. QuantiFIRE's highlighting of some volumetric or T1 relaxometry values may be helpful to guide the radiologist to evaluate the corresponding brain regions with extra caution; depending on the patient's neurological symptoms, it may even lead to a dedicated examination. The presentation of the results against normal reference ranges can also be helpful in detecting subtle abnormalities or symmetric pathologies, particularly for junior radiologists.

Preferences for different presentations of the results are currently being evaluated in a multicentric study – as are the levels of confidence and reproducibility of MR image interpretation by radiologists.

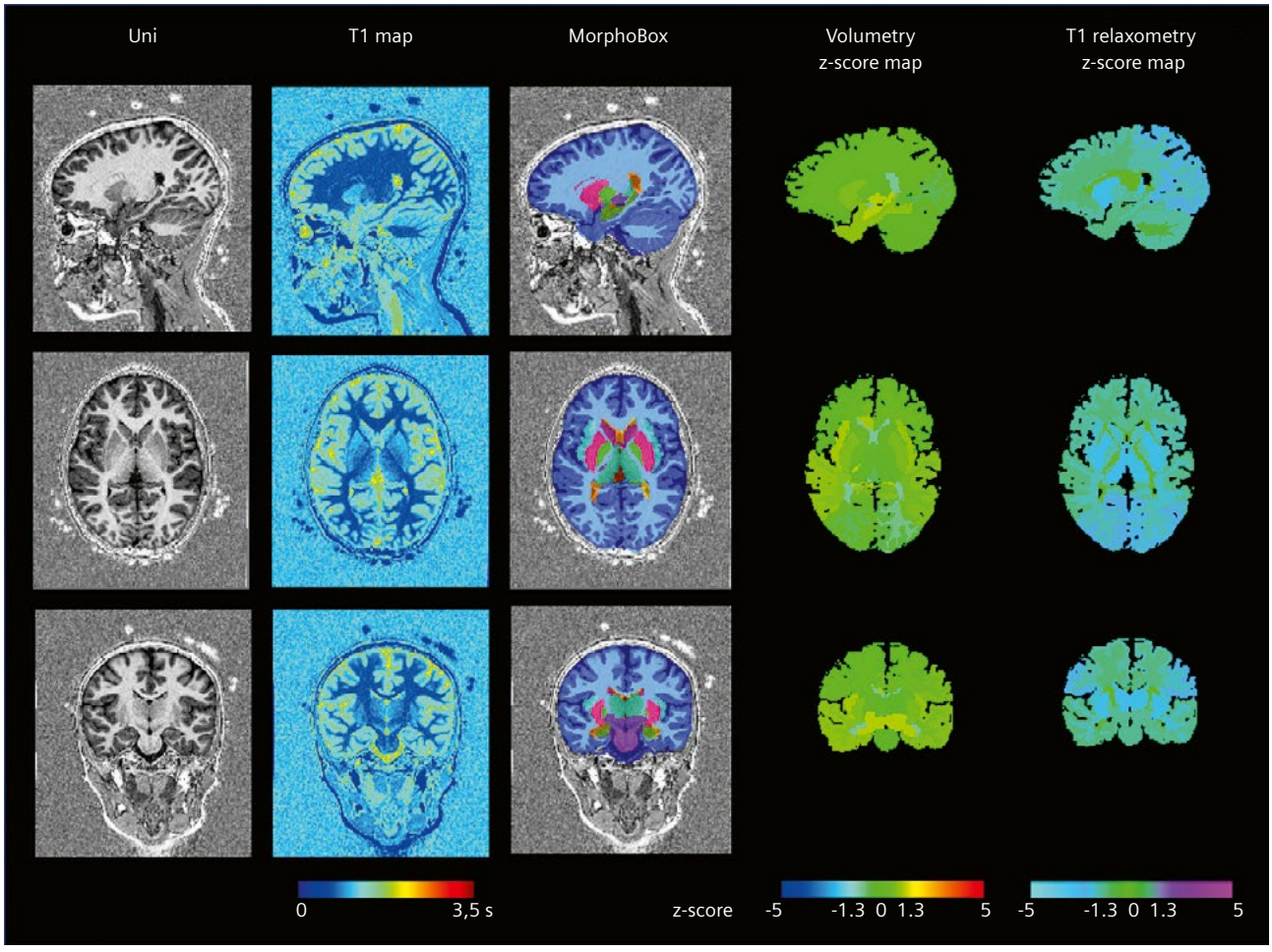


**1** Sagittal, transversal and coronal views of the different QuantiFIRE outputs in an example case. The first two columns show the "uniform" MPRAGE-like anatomical contrast of the MP2RAGE sequence as well as the T1 map. The third column shows the segmentation result of MorphoBox, visualizing the morphometric assessment. The last two columns show the deviation maps, i.e. the difference from the sex- and gender-matched healthy normal values in unit "standard deviation" (z-scores), for both the volumetric and T1 assessment.

RESEARCH ONLY. NOT FOR CLINICAL USE

Brain Morphometry Report - 6/7

| Lobar WM | Absolute[ml] | Normative Range**[ml] | Z-scor |
|---|---|---|---|
| Frontal lobe | * 147.7 | [89.9 - 137.0] | 1.86 |
| WM left | 59.0 | [45.2 - 68.3] | 0.25 |
| WM right | * 88.6 | [44.6 - 69.8] | 3.39 |
| Parietal lobe | * 106.4 | [64.5 - 99.8] | 1.76 |
| WM left | 42.6 | [32.8 - 51.4] | 0.06 |
| WM right | * 63.8 | [31.4 - 48.7] | 3.54 |
| Occipital lobe | 33.4 | [22.8 - 34.9] | 0.97 |
| WM left | 11.7 | [10.6 - 16.9] | -0.83 |
| WM right | * 21.7 | [12.0 - 18.2] | 2.76 |
| Temporal lobe | * 66.0 | [38.2 - 59.4] | 2.07 |
| WM left | 24.3 | [18.2 - 28.4] | 0.24 |
| WM right | * 41.7 | [19.8 - 31.1] | 3.69 |

RESEARCH ONLY. NOT FOR CLINICAL USE

Brain Morphometry Report - 7/7

| Stucture | Absolute[ml] | Normative Range**[ml] | Z-score |
|---|---|---|---|
| Cerebellum (WM + GM) | 132.3 | [94.9 - 132.8] | 1.25 |
| Cerebellum left | 62.8 | [46.6 - 65.2] | 0.94 |
| Cerebellum right | * 69.5 | [48.2 - 67.7] | 1.52 |
| GM left | 51.5 | [38.8 - 54.4] | 0.81 |
| GM right | 56.5 | [40.4 - 56.8] | 1.23 |
| WM left | * 11.2 | [7.4 - 11.2] | 1.31 |
| WM right | * 13.0 | [7.6 - 11.2] | 2.58 |
| Brainstem | 28.7 | [21.7 - 29.9] | 0.90 |
| Mesencephalon | 9.7 | [8.0 - 10.6] | 0.43 |
| Pons | 14.0 | [9.8 - 14.7] | 0.95 |
| Medulla Oblongata | 5.0 | [3.6 - 5.2] | 1.03 |
| | Midsagittal area [cm^2] | Normative Range**[cm^2] | Z-score |
| Corpus Callosum | * 2.7 | [1.4 - 2.1] | 3.54 |

**2** DICOM report of a 3-year-old boy with hemimegalencephaly. Abnormal asymmetric volumes of the white matter are marked with an asterisk.

## Highlights from the initial clinical experience

In the following, we review some example cases of children from our institution, for whom the MP2RAGE sequence and QuantiFIRE output provided interesting insights. We present only the radiological findings.

## Case 1: White-matter volume increase

In a 2-year-old child with a clinical increase of head circumference without any prior medical pathology, we observed an increase of volume of the parenchyma, mainly in the sus-tentorial white matter. This was detected in the volumetric deviation map with a z-score above 4 (Fig. 3).

The T1 relaxometry values were abnormal only in the white matter, which might indicate WM microstructural alterations that need to be further explored. We also noticed that the corpus callosum had a particular morphology, with an increased volume at +2 z-scores.

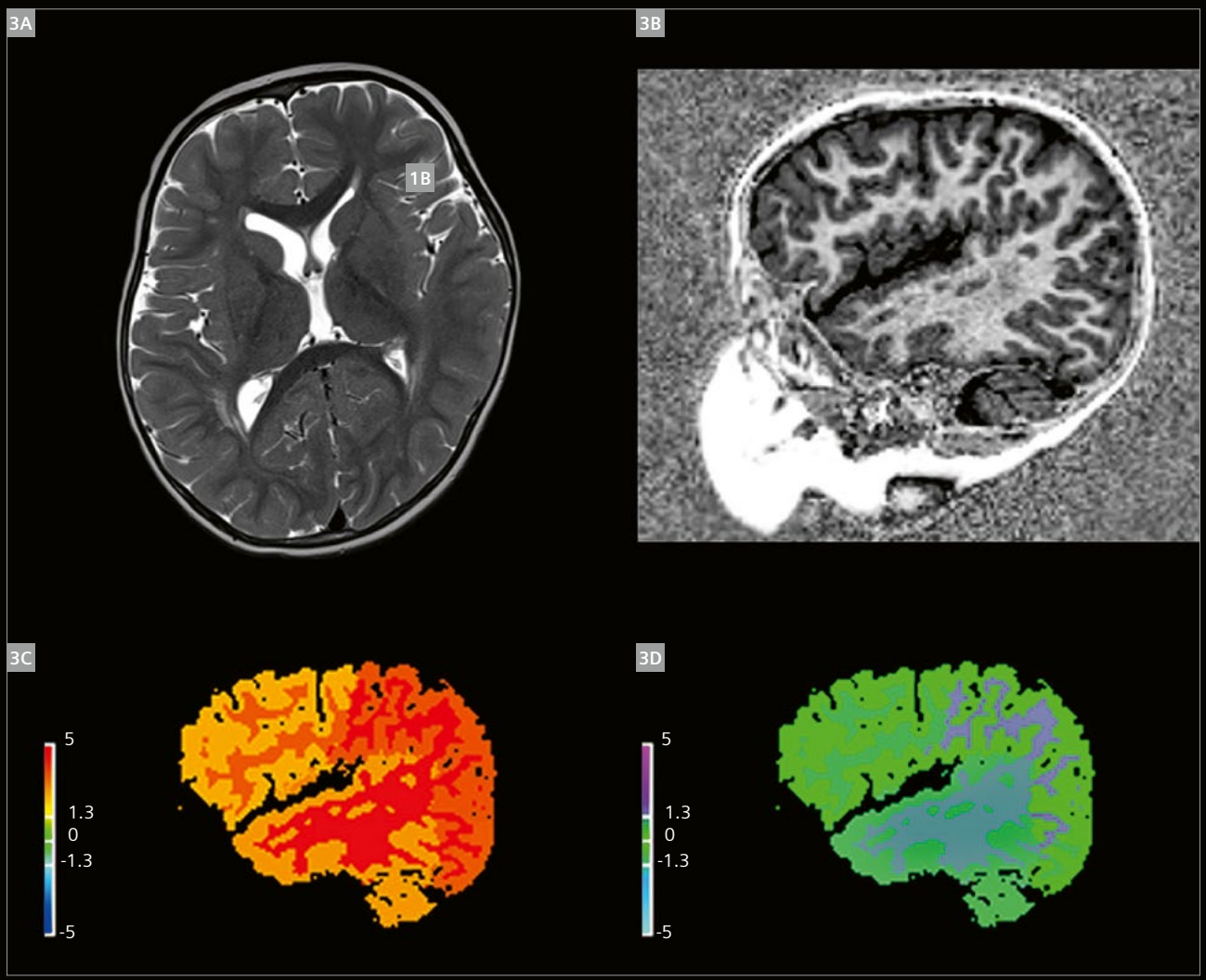


3 **(3A)** Axial TSE T2 slice of a 2-year-old child. **(3B)** Sagittal T1 view of the brain. **(3C)** Volumetric z-score deviation map of the right hemisphere. **(3D)** T1 relaxometry z-score deviation map of the previous view.

## Case 2: Global brain atrophy

The second case is a 12-year-old boy who had a developmental acquisition delay (Fig. 4). The neurological examination described fine motor troubles and attention disorder. No obvious brain abnormality was depicted on the morphological anatomical sequence. However, the deviation maps indicated global brain atrophy, while the T1 relaxometry values where in the normal range across the whole brain. This is also interesting in relation to the prior case, where suspected tissue loss and T1 deviation were symmetrical, and should be investigated further.

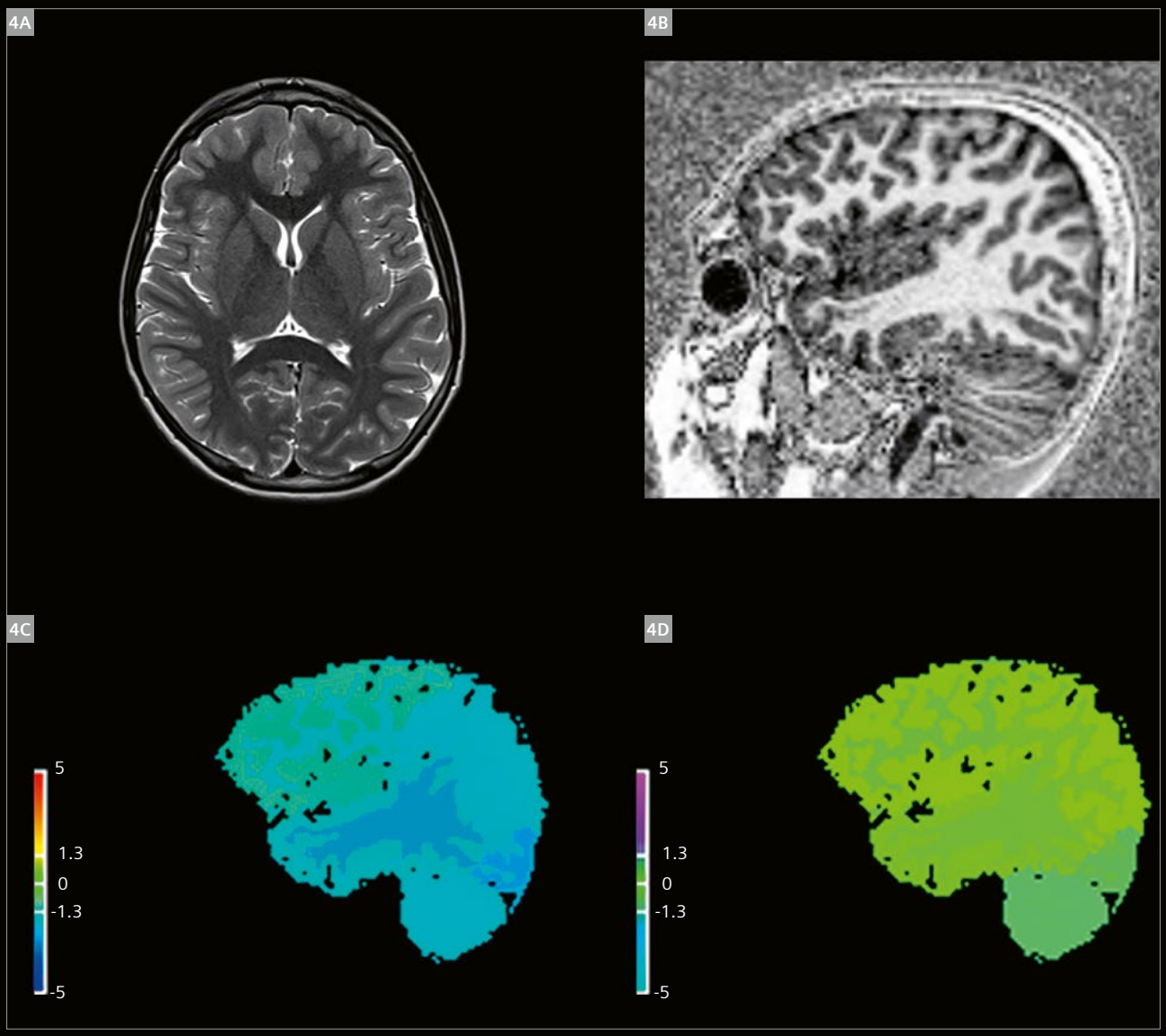


**4** **(4A)** Axial TSE T2 slice of a 12-year-old child. **(4B)** Sagittal T1 view of the brain. **(4C)** Volumetric z-score deviation map of the right hemisphere. **(4D)** T1 relaxometry z-score deviation map of the previous view.

## Case 3: Spatially distributed T1 increase without atrophy

The third example case is a brain MRI reading of a 2.5-year-old boy who had suspected microcephaly and a significant acquisition delay. We observed no morphological malformation and no significant decrease in brain volume.

We did, however, observe a significant increase in the T1 relaxometry values (Fig. 5), particularly in the basal ganglia, brain stem, and cortical gray matter. This might suggest an unknown genetic or metabolic pathology.

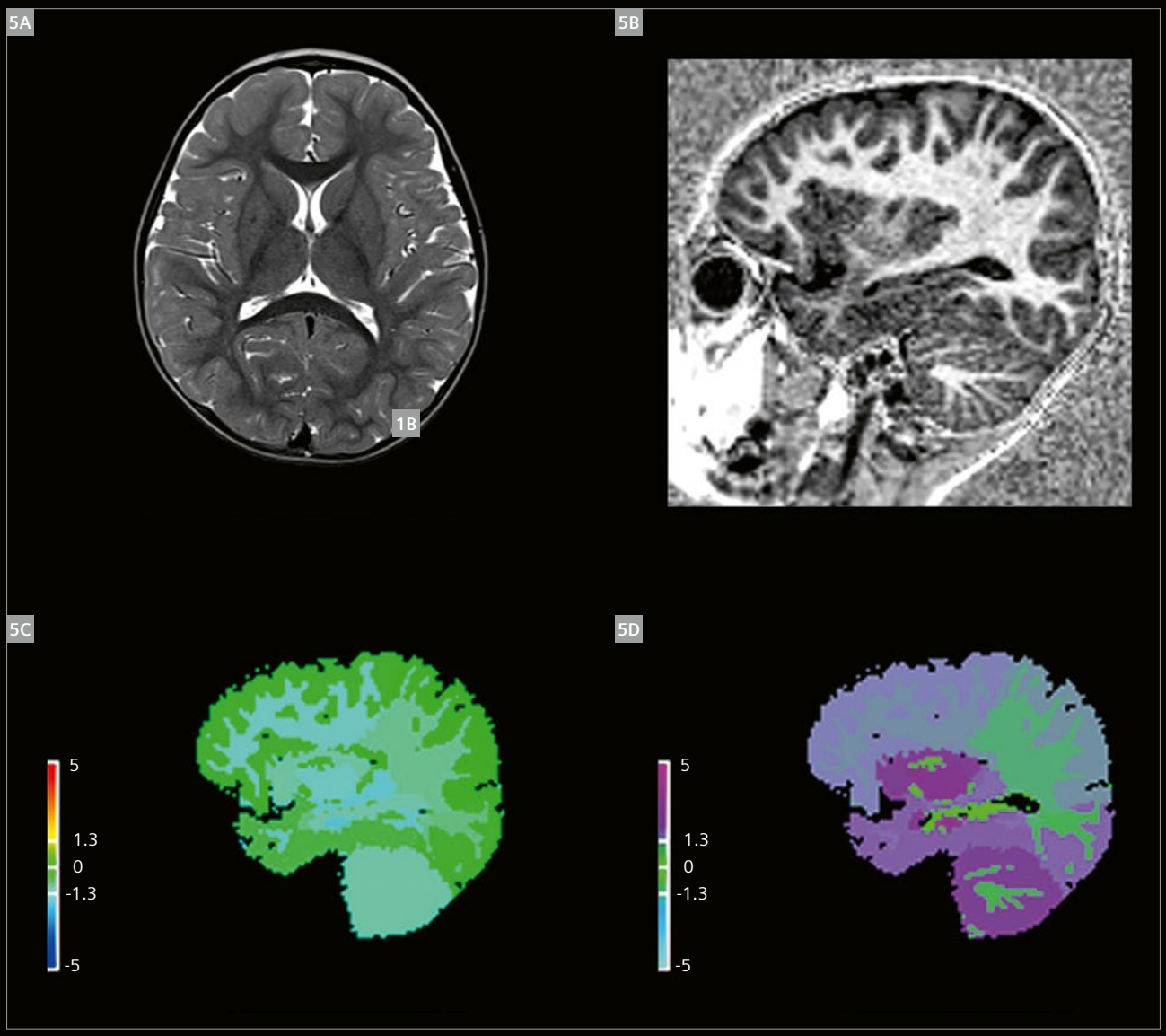


**5** **(5A)** Axial TSE T2 slice of a 2.5-year-old child. **(5B)** Sagittal T1 view of the brain. **(5C)** Volumetric z-score deviation map of the right hemisphere. **(5D)** T1 relaxometry z-score deviation map of the previous view.

## Discussion

Our first experiences suggest that the direct availability of quantitative brain volume and T1 relaxometry values in 38 segmented regions, contextualized by reference ranges of healthy controls of the same age, might indeed improve the quality of the radiological interpretation. As we have shown in the examples above, some pathological effects are subtle and not easily observed on morphological MRI scans, so the automated detection of morphometry or relaxometry abnormalities can help to explain some neurological conditions in children. However, further research is needed to better understand how this additional information could support diagnosis or clinical decisions. Our initial assessment suggests that some brain pathology might be distinguished by specific abnormality patterns that could help to identify and describe the pathology more accurately. The increase in sensitivity and the combined information from volumetry and a microstructural tissue parameter might also, as some of the cases above suggest, allow to find new disease patterns.

Besides an improved T1 contrast, the advantage of the MP2RAGE sequence over conventional T1-weighted MPRAGE acquisitions is that it provides T1 relaxation time measurements that have been reported as useful for assessing myelination in infants and young children [2]. In addition, MP2RAGE-based T1 relaxometry values in the cortex and thalamus at 3T were shown to be correlated with information processing speed in adult patients with multiple sclerosis [10]. MP2RAGE acquisitions have also been reported to be helpful in epileptic patients and for detecting focal cortical dysplasia at 3T [11, 12]. An even more precise anatomy of the deep gray nuclei would be available at 7T [13], probably with more precise delineation. The use of advanced acceleration techniques like compressed sensing could also decrease the acquisition time while maintaining high repeatability in volumetry and relaxation times [14]. This would help encourage wider application of MP2RAGE acquisitions in children at 1.5T or 3T, regardless of their age at the time of the exam.

## Conclusion

The MP2RAGE QuantiFIRE technique is promising for children and adults at 1.5T, and probably even more so at 3T and 7T. The quantitative description of brain volumes and T1 relaxometry may help in some pathologies such as epilepsy and congenital or acquired abnormalities of brain development. Combining a dedicated MP2RAGE protocol with the QuantiFIRE research application may provide quantitative results potentially useful in radiological practice. We believe that, complementary to volumetry, the availability of T1 relaxometry can play an important role in helping radiologists better describe, understand, and characterize congenital or acquired brain pathology.

## Acknowledgments

The authors would like to thank Professor Dominique Sirinelli who provided an invaluable input to kick-off this longstanding collaboration project as well as their collaborators (particularly the MR technologist team) or colleagues at Siemens Healthineers, in particular Matthieu Lepetit-Coiffé, Marc Lapert, Thomas Troalen, Laurent Arnould and Aurélien Monnet for their precious contributions to the development and testing of the QuantiFIRE research application.

**References**

1 Girard N, Raybaud C, du Lac P. MRI study of brain myelination. J Neuroradiol. 1991;18(4):291–307.
2 Kühne F, Neumann WJ, Hofmann P, Marques J, Kaindl AM, Tietze A. Assessment of myelination in infants and young children by T1 relaxation time measurements using the magnetization-prepared 2 rapid acquisition gradient echoes sequence. Pediatr Radiol. 2021 Oct;51(11):2058–2068.
3 Serru M, Marechal B, Kober T, Ribier L, Sembely Taveau C, Sirinelli D, et al. Improving diagnosis accuracy of brain volume abnormalities during childhood with an automated MP2RAGE-based MRI brain segmentation. J Neuroradiol. 2021 Jun;48(4):259–265.
4 Morel B, Antoni G, Teglas JP, Bloch I, Adamsbaum C. Neonatal brain MRI: how reliable is the radiologist's eye? Neuroradiology. 2016;58(2):189–93.
5 McAllister A, Leach J, West H, Jones B, Zhang B, Serai S. Quantitative Synthetic MRI in Children: Normative Intracranial Tissue Segmentation Values during Development. AJNR Am J Neuroradiol. 2017 Dec;38(12):2364–2372.
6 Schmitter D, Roche A, Maréchal B, Ribes D, Abdulkadir A, Bach-Cuadra M, et al. An evaluation of volume-based morphometry for prediction of mild cognitive impairment and Alzheimer's disease. Neuroimage Clin. 2014;7:7–17.
7 Boto J, Gkinis G, Roche A, Kober T, Maréchal B, Ortiz N, et al. Evaluating anorexia-related brain atrophy using MP2RAGE-based morphometry. Eur Radiol. 2017;27(12):5064–5072.
8 Morel B, Piredda GF, Cottier JP, Tauber C, Destrieux C, Hilbert T, et al. Normal volumetric and T1 relaxation time values at 1.5 T in segmented pediatric brain MRI using a MP2RAGE acquisition. Eur Radiol. 2021;31(3):1505–1516. Epub 2020 Sep 3.
9 Destrieux C, Fischl B, Dale A, Halgren E. Automatic parcellation of human cortical gyri and sulci using standard anatomical nomenclature. Neuroimage. 2010;53(1):1–15.
10 Thaler C, Hartramph I, Stellmann JP, Heesen C, Bester M, Fiehler J, et al. T1 Relaxation Times in the Cortex and Thalamus Are Associated With Working Memory and Information Processing Speed in Patients With Multiple Sclerosis. Front Neurol. 2021;12:789812.
11 Demerath T, Rubensdörfer L, Schwarzwald R, Schulze-Bonhage A, Altenmüller DM, Kaller C, et al. Morphometric MRI Analysis: Improved Detection of Focal Cortical Dysplasia Using the MP2RAGE Sequence. AJNR Am J Neuroradiol. 2020;41(6):1009–1014.
12 Demerath T, Kaller CP, Heers M, Staack A, Schwarzwald R, Kober T, et al. Fully automated detection of focal cortical dysplasia: Comparison of MPRAGE and MP2RAGE sequences. Epilepsia. 2022;63(1):75–85.

13 Brun G, Testud B, Girard OM, Lehmann P, de Rochefort L, Besson P, et al. Automatic segmentation of deep grey nuclei using a high-resolution 7T magnetic resonance imaging atlas-Quantification of T1 values in healthy volunteers. Eur J Neurosci. 2022;55(2):438–460.
14 Trotier AJ, Dilharreguy B, Anandra S, Corbin N, Lefrançois W, Ozenne V, et al. The Compressed Sensing MP2RAGE as a Surrogate to the MPRAGE for Neuroimaging at 3 T. Invest Radiol. 2022;57(6):366–378. Epub 2022 Jan 14.

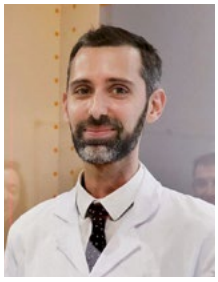

## Contact

Baptiste Morel, M.D., Ph.D.
Associate Professor of Pediatric Radiology
Université de Tours and
Centre Hospitalier Régional Universitaire de Tours
10 Boulevard Tonnellé
37032 Tours CEDEX 1
France
baptiste.morel@univ-tours.fr



## Learn more

Listen to

### "Measuring Brain Maturation with Quantitative MRI in Pediatrics"

**Baptiste Morel, M.D., Ph.D.**
(Université de Tours, CHRU de Tours, France)

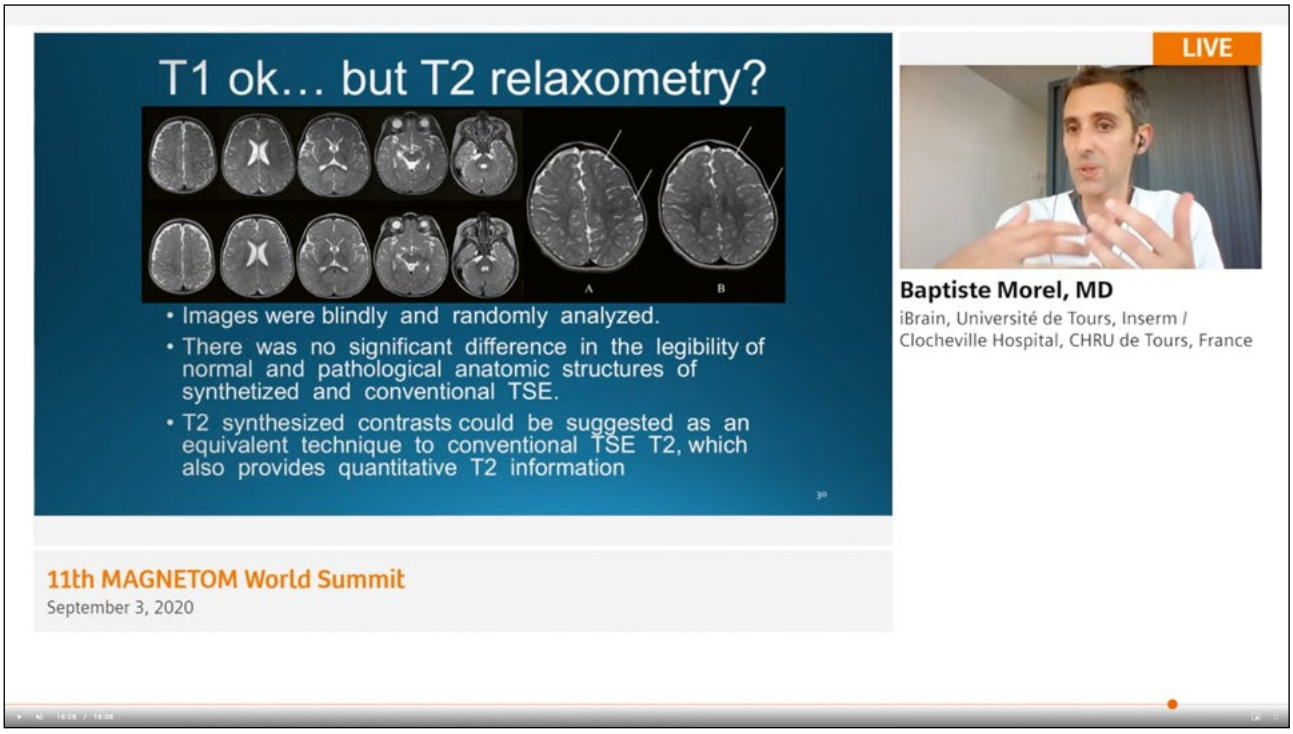


The talk is online at
www.siemens-healthineers.com/MWS2020-recordings

# Deep Resolve in Pediatric MRI

**Johan Dehem, M.D.**

Jan Yperman Ziekenhuis, Ieper, Belgium

Why pediatric[1] MRI? Well MRI is a completely radiation-free technique making it an excellent "primum non nocere" tool and it also comes with high resolution and high soft-tissue contrast. Actually, it offers excellent diagnostic information at no radiation cost. However, there is always a catch! With MRI, image quality can decline quickly if the patient moves. Having a toddler lie still in the bore during the scan can be tricky or rather "pedia-tricky". In fact, there's our challenge! The first approach is to bring in our friends from the anesthesia department. Using an inhalation anesthetic (sevoflurane) delivered through a larynx mask, they can induce light sedation, with the child still breathing autonomously. Knowing that the patient is securely ventilated and monitored throughout the exam is reassuring and the only right approach. Seeing how parents trust us with the life of their little one is a strong appeal to one's sense of duty and responsibility.

For really young children[1] with a smaller head size, we use a dedicated pediatric head coil. It comes with a cradle to secure the patient immediately after the anesthesia has been induced.

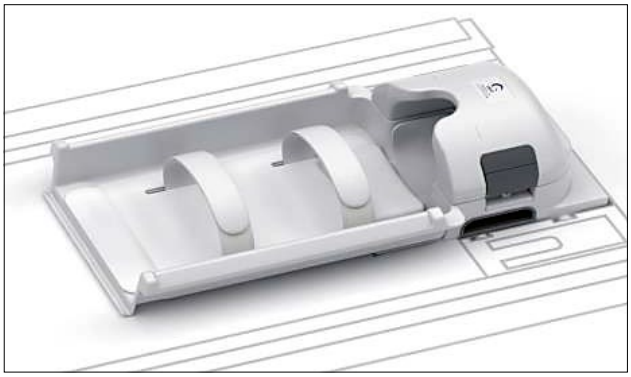

**2** Pediatric head coil

**1** Anesthetized, ventilated (larynx mask) two-year-old child in the preparation room. Notice the (fluo) ear protection plug, nametag on the wrist, and the comforter just to the left of the child.

**3** Our very first patient in this cradle.

[1] *MR scanning has not been established as safe for imaging fetuses and infants less than two years of age. The responsible physician must evaluate the benefits of the MR examination compared to those of other imaging procedures. Note: This disclaimer does not represent the opinion of the author.*

Bringing the little one to the magnet is so much more reassuring with the baby safe in the cradle instead of toneless (sedated) in your arms.

Since children have smaller brains, we need higher resolution images and thinner slices compared with adults so scanning times typically are longer. However, anesthesia should never take longer than necessary and scan times should be kept as short as possible! Using examples from our clinical practice, we show how the image reconstruction technology Deep Resolve really helps to achieve high resolution images in low acquisition times so that we can reduce the time the child spends under anesthesia. To illustrate the possibilities, in Figures 5 and 6 we compare the Deep Resolve (top image) and classic reconstruction of the same raw data using retro reconstruction at the scanner.

During our test phase with Deep Resolve, this 13-month-old girl[1] (Fig. 5) presented with a swelling in the left parotid gland. Clinical examination and ultrasound suggest a hemangioma. An MRI of the parotid gland is ordered to confirm a hemangioma or to rule out another type of tumor. An MRI of the brain is performed in the same session to exclude intracranial locations.
Sagittal T2 sequence with Deep Resolve reconstruction

Upper row: Same dataset retro reconstructed with the same parameters but using a standard reconstruction algorithm.

Lower row: Since all the images are reconstructed from the same dataset, they are comparable pixel for pixel. In the Deep Resolve images (upper row), you can see more detail in the parotid hemangioma, small veins in the subcutaneous fat, as well as better delineation of the cortical gray matter and sulci.

The same improvement in detail can be seen in a more median sagittal image from the same series: Deep Resolve (top), same dataset with standard reconstruction (bottom).

**4** Technical note: In the cradle, UltraFlex coils can be easily wrapped and fixed via straps for abdominal or pelvic examinations.

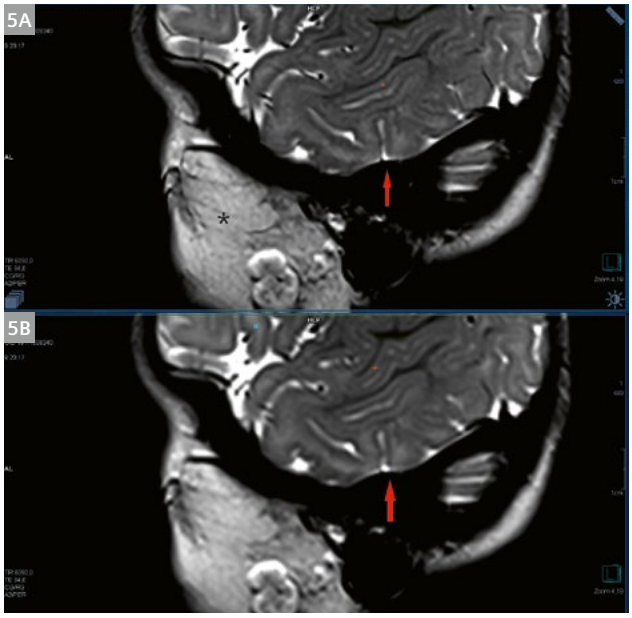


**5** In the Deep Resolve images (5A), you can see more detail in the parotid hemangioma and clearer delineation of small veins in the subcutaneous fat (black*), better delineation of the cortical gray matter (red*) and cortical sulcus adjacent to the petrosal bone (red arrow).

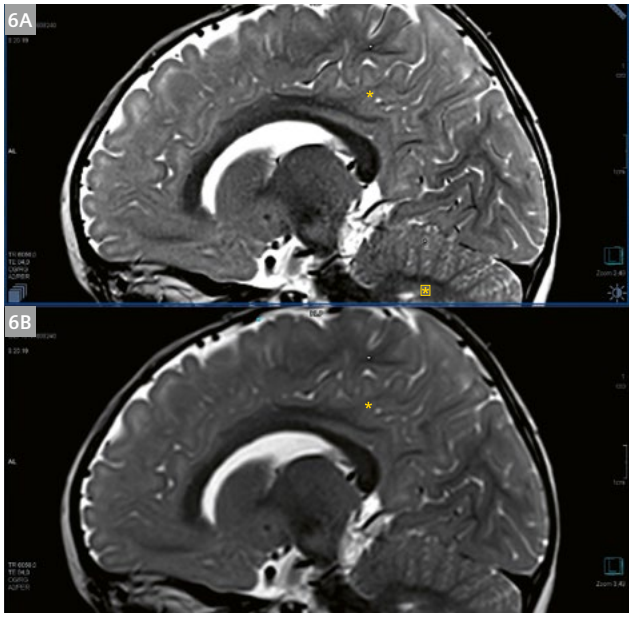


**6** The branching cortical vein (yellow*) can only be sharply delineated in the Deep Resolve images (6A). The detailed cortical delineation of the foliae vermis are only clear in the images with Deep Resolve (small square box in top 6A).

*All images have been acquired using a 1.5T MAGNETOM Sola.*

Figures 7 and 8 demonstrate the improvement in image detail we have with Deep Resolve. This is more than just eye candy, you actually have more anatomic detail!

As a side note: The Deep Resolve image (7A, 7C, 8A) can be "harder windowed" than the classic image (bottom). The reason is that you have so much more resolution in the fine image details and also, for example, in the high-intensity CSF. (Compare the ambient cisterns in Figure 8). Hence you can apply a more narrow window setting without "drowning out" smaller structures such as the peri pontine vessels in the surrounding high-intensity CSF.

So one thing is clear: With Deep Resolve comes deep resolution! Our initial kneejerk reaction when we hear high resolution is: Doesn't high resolution come at the expense of image noise? Actually, quite the opposite is true: The first step in Deep Resolve reconstruction is intelligent optimizing of the signal-to-noise ratio. The results are quite impressive as you can see in Figure 9.

This signal enhancement is achieved by generating noise maps which are then used to take the noise but not the details out of the image in an iterative process. To me, this resembles very much the iterative reconstruction approach used in low-dose CT images.

This three-month-old baby[1] in Figure 9 presented with paroxysmal tonic upgaze (PTU) and abducens paresis on the left side. The pediatrician wanted to rule out an underlying tumor or malformation. The examination was performed after feeding and wrapping the baby in a blanket. No anesthesia was needed; we just exercised some patience and waited for sleep to come. Congenital abducens paresis turned out to be the final diagnosis.

Really small babies up to three or four months or so sometimes do lend themselves to be being lulled to sleep by the friendly vibrations of an MRI, especially after a good meal and when snuggly wrapped up resting on the lap of an adult. Babies often also fall asleep when they are in a car. Here again Deep Resolve is a formidable tool: Since we have an enhanced signal at a high resolution, we can trade some of this signal for faster scan time. You can also decide to leave out an average, for example, or apply an extra PAT factor, or less oversampling. Take your pick!

With shorter sequences, you can really apply the first sequence several times until you notice that the baby has been lulled to sleep. In Figure 11, you see just such an example: The pediatrician asked us to scan this hypotone rather passive 4-month-old baby[1] to determine the myelinization status and exclude anomalies, but without anesthesia if possible since it would be difficult to persuade the parents of the need for an MRI under sedation. Well, with some patience, good timing shortly (15 min) after feeding, and the short Deep Resolve sequences, this worked perfectly. By simply repeating the first sequence twice, the baby fell asleep and the baby's scan was completed in just 22 minutes (including the repeats). Such a short examination time is very much appreciated by the pediatric nurse who accompanies the baby in the bore during the exam.

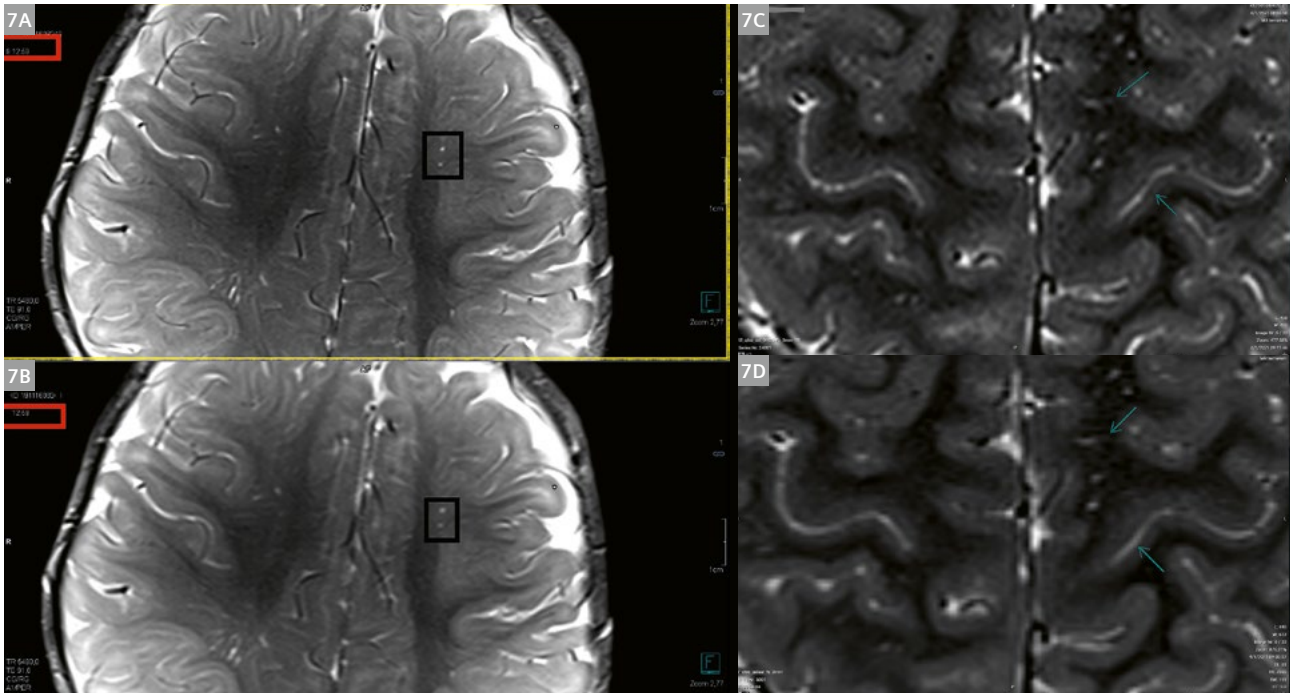


**7** **(7A, B)** Deep Resolve (7A) and standard reconstruction (7B) of same raw data, T2 TSE axial. Deep Resolve images (7A) better detail the white matter and perivascular spaces including better delineation of the cortical gyri.
**(7C, D)** Follow-up of cerebellar hamartoma. (7C) Deep Resolve sequence; (7D) Standard sequence. The arrows point to anatomical details in the Deep Resolve image (7C) that are obscured, blurred, or pixeled-out in the standard sequence (7D).

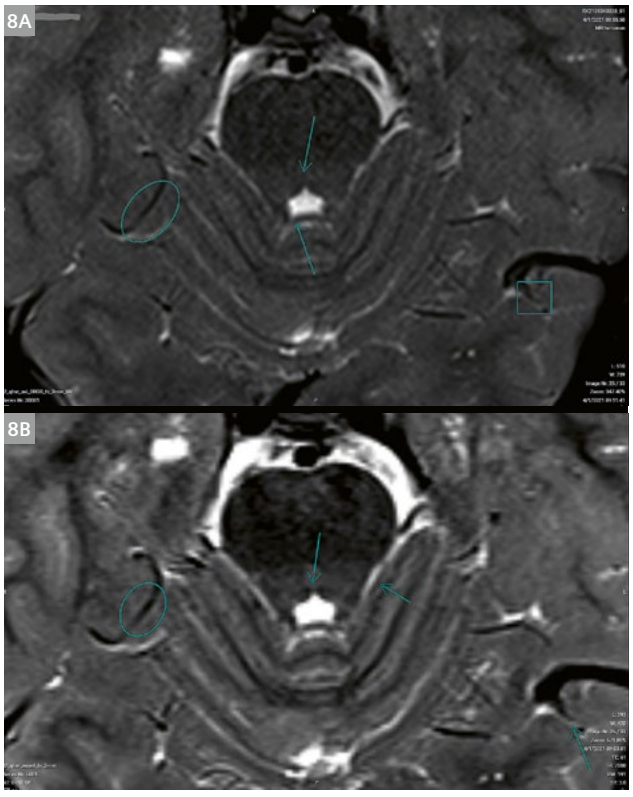


**8** The same sequences as in Figures 7C, D at the level of the cerebellum. Note the cortical vein delineation (oval) or the demarcation of the 4th ventricle (arrows). In fact, delineation of the 4th ventricle is not only sharper with Deep Resolve, it is actually more anatomically correct **(8A)**!

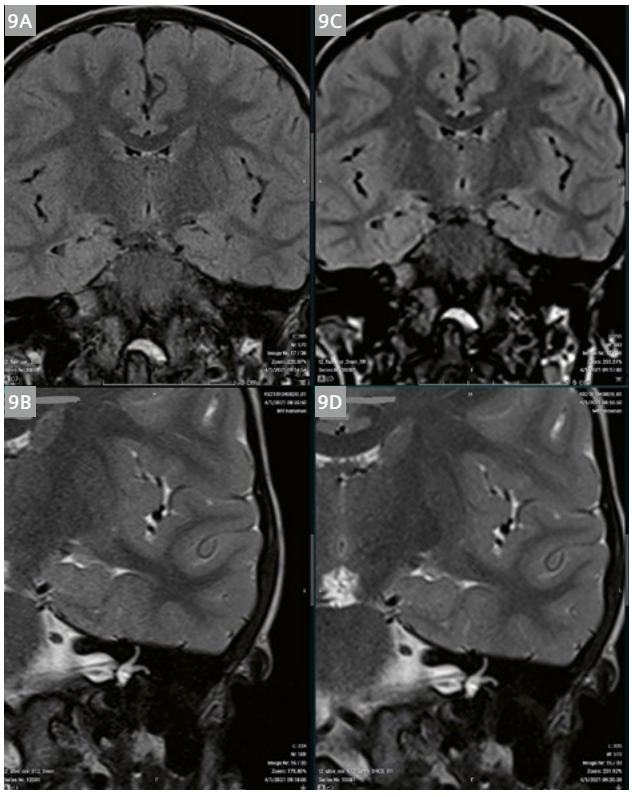


**9** Noise extraction is clearly visible when comparing the standard images with image noise in the center **(9A, B)** with the Deep Resolve reconstruction images **(9C, D)**.

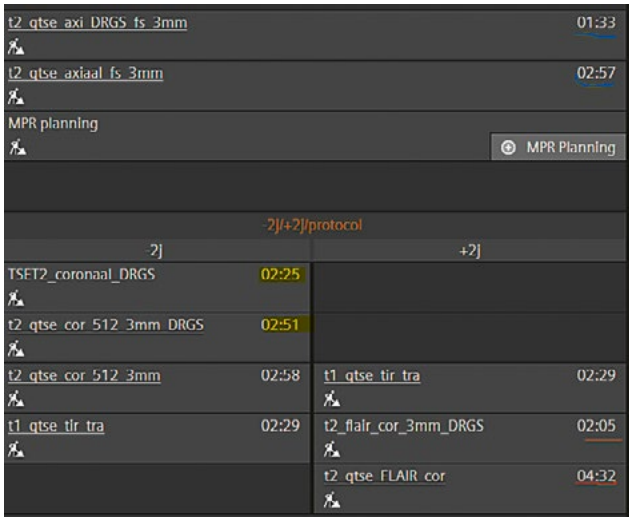


**10** Screenshot from a standard head exam: T2 axial at TA 1:33 min with Deep Resolve (DR) versus conventional TA 2:57 min; T2 FLAIR cor at TA 2:05 min DR versus conventional TA 4:32 min.

[1] *MR scanning has not been established as safe for imaging fetuses and infants less than two years of age. The responsible physician must evaluate the benefits of the MR examination compared to those of other imaging procedures. Note: This disclaimer does not represent the opinion of the author.*

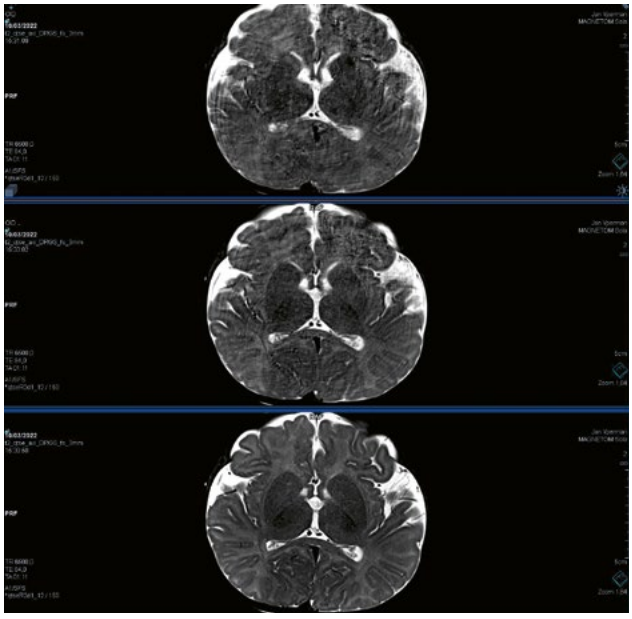

**11** Quiet T2 TSE Deep Resolve axial sequence in 1:11 mins or 71 seconds! Performing this T2 FatSat sequence 2 times (spending 2:22 minutes) lulls the baby to sleep and results in crisp image quality.

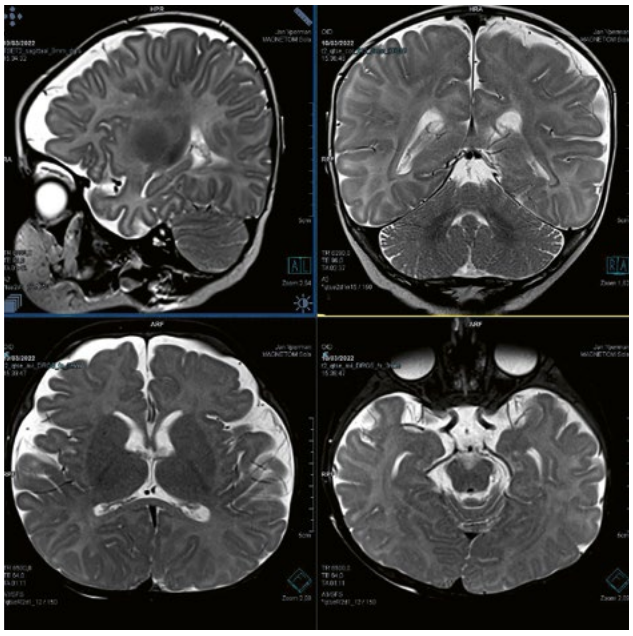

**12** Once the baby is asleep, the sagittal and coronal Deep Resolve quiet T2 TSE images are also acquired along with the axial hemosiderine and 3-plane T1 images. Total exam time: 22 minutes including localizer, planning, shimming and repeating initial sequences until the baby is asleep.

Short acquisition times are also convenient in older children as with this 6-year-old girl with left-sided perceptive hearing loss. Although she was very brave, we needed a rerun of the axial T2. With an acquisition time of just 1:25 minutes, it does no harm to speak some words of comfort to her and repeat the sequence (see Fig. 13).

The signal gain that comes with Deep Resolve can also be used to scan at a higher resolution. You can scan with thinner slices, smaller field of view, higher matrix, or a combination.

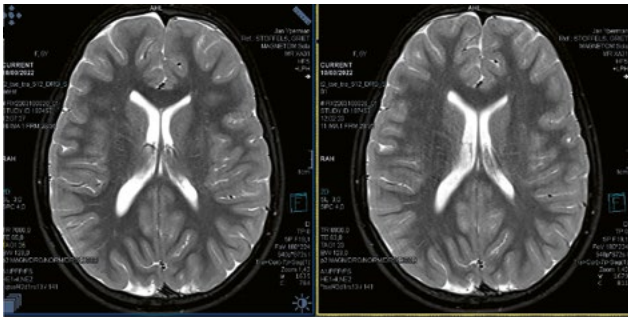

**13** Six-year-old girl with left-sided perceptive hearing loss. Axial T2 with an acquisition time of just 1:25 minutes.

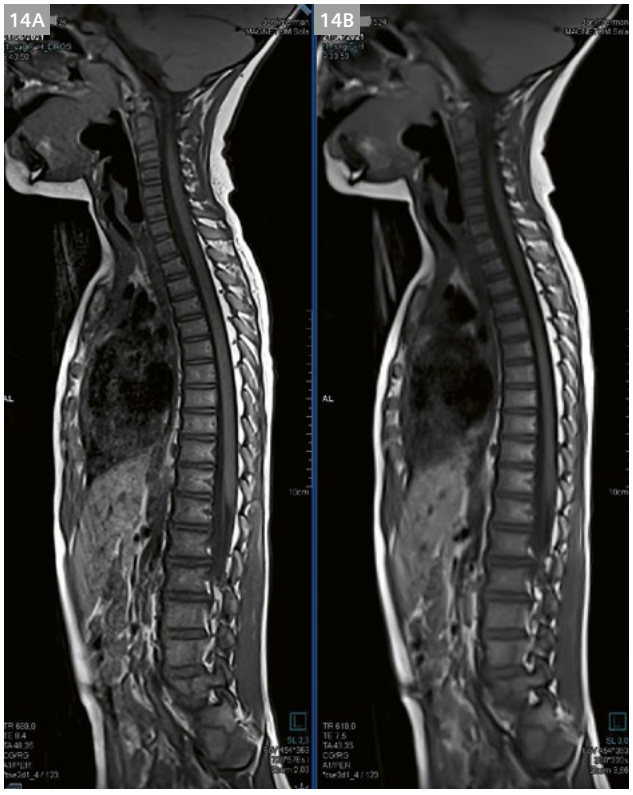


**14** T1 TSE Deep Resolve **(14A)** full spine images in a 4-year-old child with double matrix size (all other parameters kept similar), compared with the original **(14B)** with an SNR that is even better than in the original – lower resolution full spine image.

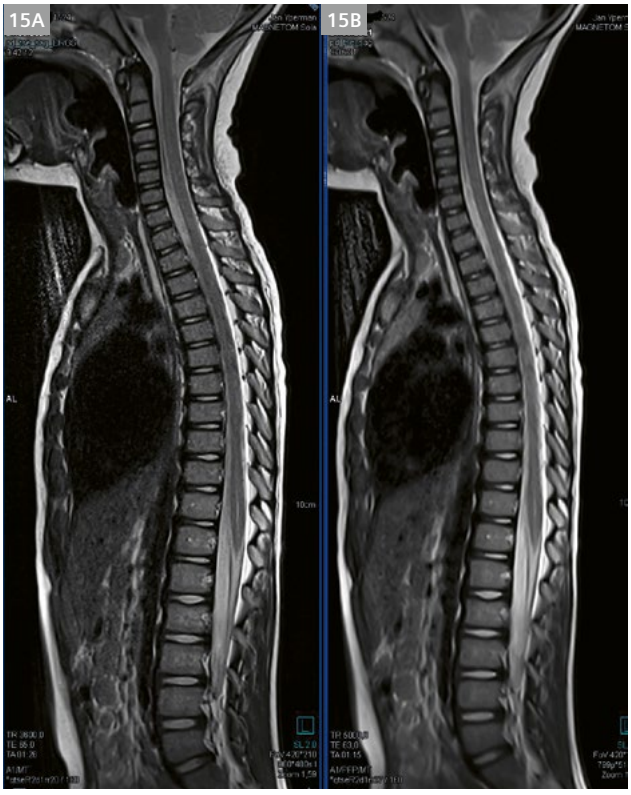


**15** PD TSE Deep Resolve **(15A)** full spine images in a 4-year-old child with double matrix size and thinner slice thickness (2.4 mm instead of 3 mm in the original) with a resolution but also an SNR that is better than the original – lower resolution full spine image.

In conclusion, what Deep Resolve brought to our pediatric imaging was shorter imaging times making exams shorter with less sedation time needed for toddlers. It also makes it easier to repeat sequences in really small babies just to lull them to sleep. Also if a patient does move, it is not as painful any more to repeat a sequence with these short acquisition times.

Even more importantly, you need high resolution in pediatric imaging and Deep Resolve delivers this high resolution without the penalty of longer scanning times; in fact our high-resolution images are acquired faster than previously with standard resolution images.

Just to give you a concrete idea of how far the technique has evolved: Take a look at this two-and-a-half-year-old girl who presented with a limp since two weeks. The hip was "dry" on ultrasound and there was no indication of transient synovitis or septic arthritis. His X-ray was unremarkable. There were no clinical signs of infection. The orthopedic surgeon wanted to rule out LCP disease and also rule out malignancy (see Fig. 16). MRI findings were unexpected and remarkable: There was partial avulsion trochanter major apophysis with some chip avulsion and periosteal stripping and hematoma. For me this nicely sums up the benefits of Deep Resolve: Pristine image quality thanks to unprecedented signal in high-resolution images. An equally important contribution from Deep Resolve is the short examination time, so that the anesthesia can be short! In fact, sometimes you "lose" more time installing the patient ventilation tube, perfusion, and especially patient monitoring than needed for the scan itself!

And yes, pediatric MRI, especially when anesthesia is required can be cumbersome. You need time for the pediatric crew to arrive, comfort the patient, and mostly the parents! Time for induction, time for perfusion (not so easy in these young children). You also you need time to carefully install the patient and make sure that ventilation and monitoring (capnography, ECG, saturation) are working properly. We have scheduled dedicated pediatric timeslots for MRI under sedation, every third Monday. What we tend to do is schedule normal adult examinations between the examinations under sedation so that we can keep scanning while the pediatric patient is being prepared. This lets us keep pace with our workflow. Here, Deep Resolve helps us to stay on schedule. Take a look at this screenshot of our pediatric session two weeks ago (Fig. 17, including the hip exam supra):

One 13-year-old girl without sedation, two toddlers 2 and 3 years old, both underwent a brain MRI under sedation, and our pelvic MRI trochantic avulsion case in a two-year-old child with sedation together with 10 adult patients, all before noon 😊 That's how you do it!

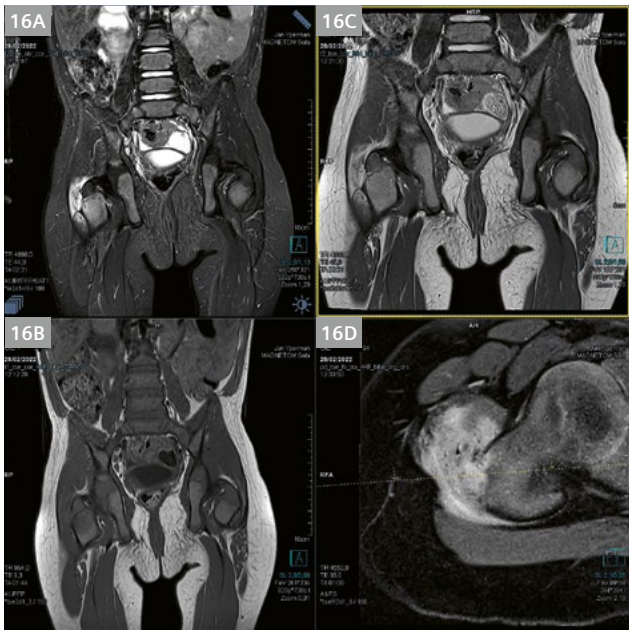


**16** Two-and-a-half-year-old girl. Coronal STIR **(16A)** 0.3 mm in-plane resolution, 2.5 mm slice thickness, and acquisition time of 2:21 min. Coronal T1 **(16B)** 0.3 mm in-plane resolution, slice thickness 2 mm, and acquisition time of 1:44 min. Coronal T2 **(16C)** 0.2 mm in-plane resolution, slice thickness 2 mm, and acquisition time of 2:21 min. Axial T2 FS **(16D)** 0.2 mm in-plane resolution, slice thickness 2.1 mm, and acquisition time of just 68 seconds!

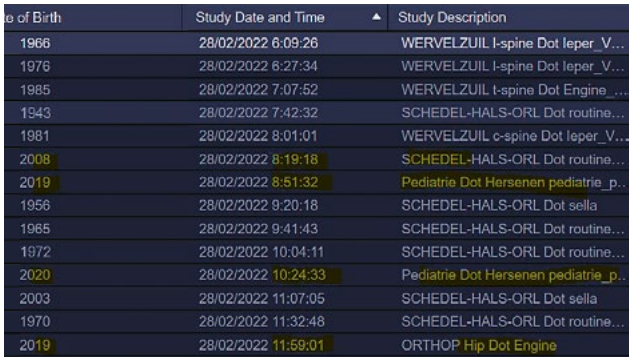

| e of Birth | Study Date and Time | Study Description |
|---|---|---|
| 1966 | 28/02/2022 6:09:26 | WERVELZUIL l-spine Dot Ieper_V... |
| 1976 | 28/02/2022 6:27:34 | WERVELZUIL l-spine Dot Ieper_V... |
| 1985 | 28/02/2022 7:07:52 | WERVELZUIL t-spine Dot Engine_... |
| 1943 | 28/02/2022 7:42:32 | SCHEDEL-HALS-ORL Dot routine... |
| 1981 | 28/02/2022 8:01:01 | WERVELZUIL c-spine Dot Ieper_V... |
| 2008 | 28/02/2022 8:19:18 | SCHEDEL-HALS-ORL Dot routine... |
| 2019 | 28/02/2022 8:51:32 | Pediatrie Dot Hersenen pediatrie_p... |
| 1956 | 28/02/2022 9:20:18 | SCHEDEL-HALS-ORL Dot sella |
| 1965 | 28/02/2022 9:41:43 | SCHEDEL-HALS-ORL Dot routine... |
| 1972 | 28/02/2022 10:04:11 | SCHEDEL-HALS-ORL Dot routine... |
| 2020 | 28/02/2022 10:24:33 | Pediatrie Dot Hersenen pediatrie_p... |
| 2003 | 28/02/2022 11:07:05 | SCHEDEL-HALS-ORL Dot sella |
| 1970 | 28/02/2022 11:32:48 | SCHEDEL-HALS-ORL Dot routine... |
| 2019 | 28/02/2022 11:59:01 | ORTHOP Hip Dot Engine |

**17** Screenshot of a pediatric session. We schedule normal adult examinations between the examinations under sedation so that we can keep scanning while the pediatric patient is being prepared.

## Contact

Johan Dehem, M.D.
Jan Yperman Ziekenhuis
Briekestraat 12
8900 Ypres
Belgium
Phone: +32 57 35 74 00
johan.dehem@yperman.net

### What happens when you have an MRI scan?

# Help your little patients lose their fear – with Lottie

Lottie is an adventurous little lamb that loves to skateboard. But poor Lottie had an accident and may have broken her ankle. Now instead of leaping, she can only limp. Lottie is off to the hospital for an MRI scan. This engaging story by Professor Rolf Vosshenrich and Sylvia Graupner explains to children what it's like to have an MRI scan in a way they can understand.

We offer Lotti's story as a children's book in 15 languages (PDF) and as video in 5 languages. You can also order hard copies of the book in German, English, and Spanish.

The material is available at
**www.siemens-healthineers.com/magnetom-world**

Go to **> Publications > MR Basics**

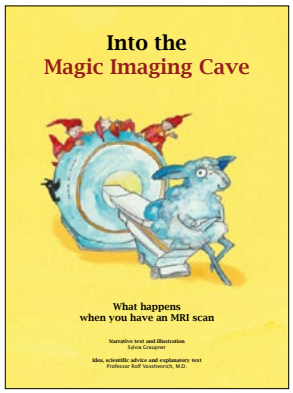


Children's book


Animated video


Pixi book

# Liver Magnetic Resonance Elastography in Children

**Jędrzej Sarnecki[1], Piotr Pawliszak[1], Paulina Opyrchał[1], Cepuch Kamil[2], Elżbieta Jurkiewicz[1]**

[1]Department of Diagnostic Imaging, The Children's Memorial Health Institute, Warszawa, Poland
[2]Siemens Healthineers, Warszawa, Poland

Magnetic resonance elastography (MRE) was introduced in the mid-90s by researchers at Mayo Clinic in Rochester, MN, USA. It is a dynamic imaging technique that assesses the elasticity of tissues [1]. The basic principle of this diagnostic technique relies on the evaluation of the mechanical properties, often referred to as stiffness or elasticity, of tissues. This is possible by measuring the tissue's distortion in response to a mechanical stimulus in the form of vibrations [2]. Some authors refer to MRE as "virtual palpation", as this approach to tissue evaluation somewhat resembles palpation. Similar to the observations made during a physical examination, normal and abnormal tissues differ in elasticity, mostly due to fibrosis and to cellular proliferation and infiltration in pathologically altered regions.

In order to assess a tissue's stiffness using MRE, an external force needs to be applied to the evaluated organ. The force is provided by an external device referred to as a "driver", which generates vibrations at a single, specified frequency within the lower part of the audio frequency range [2]. The motion induced by the mechanical stress is then imaged using a standard phase-contrast imaging sequence with motion-encoding gradients (MEG) synchronized with the driver's function. The imaging time itself is short and does not significantly extend the duration of a standard abdominal MRI study. Typically, MRE of the liver consists of four cross-sectional scans of the liver, each obtained in less than one minute on a MAGNETOM Avanto$^{fit}$ scanner (Siemens Healthcare, Erlangen, Germany). The study is normally well tolerated, and patients describe the sensations caused by the vibrations as "tingling". The data acquired in the process of wave propagation are used to generate elastograms (Fig. 1D and 2D). Image analysis using selected regions of interest (ROIs) enables measurement of the target tissue's stiffness, typically expressed in kilopascals (kPa). Aside from typical MRI contraindications, there are no absolute contraindications for MRE. However, study postponement should be considered for patients directly after liver biopsy or with skin lesions at the typical driver location.

Over the years, many potential fields of MRE application have emerged. However, it is currently most widely used in liver assessment for both adults and children. As the prevalence of chronic liver disease increases – mainly due to the rising number of patients with nonalcoholic fatty liver disease (NAFLD) – there is a need for noninvasive methods of assessing the liver parenchyma. Hepatic fibrosis is a dynamic and potentially (in the early stages) reversible condition that precedes cirrhosis. Currently, core liver biopsy is regarded as the gold standard in liver disease diagnosis and hepatic disease staging. Nevertheless, it has several disadvantages: It is invasive, costly, and only assesses a minute sample of the liver [3]. There is also a non-negligible risk of obtaining nondiagnostic material, for example due to fragmentation or lack of liver tissue [4, 5]. Low sampling volume may affect the sensitivity of diagnosing liver disease that is heterogeneously distributed across the parenchyma.

Therefore, there is increasing interest in using MRI or ultrasound elastographic techniques to assess and monitor liver fibrosis. In contrast to liver biopsy, MRE is a noninvasive diagnostic procedure that enables a much larger sampling volume of liver parenchyma. Its other advantages are the short scanning time, relatively low cost, and high interobserver and intraobserver agreement [6]. It is currently the most accurate noninvasive method of detecting and grading liver fibrosis [7, 8]. In some cases, simultane-

ous calculation of spleen elasticity can provide additional value, especially in patients with portal hypertension and esophageal varices.

To date, numerous studies have proven MRE to be a feasible tool for evaluating liver fibrosis. Some authors even suggest that, owing to its high negative predictive value for advanced fibrosis, MRE could replace core liver biopsy for surveilling patients who have undergone the invasive diagnostic procedure in the past [9, 10]. Noninvasive assessment of the liver may also be useful in patients with chronic diseases that predispose them to liver fibrosis, such as cystic fibrosis, multicystic kidney disease, biliary atresia, inflammatory bowel disease, and alpha-1 antitrypsin deficiency. In patients after liver transplantation, MRE could possibly substitute some protocolary liver biopsies, which are performed every 5 to 10 years, or identify patients who would benefit from a biopsy. In combination with the LiverLab tool (Siemens Healthcare, Erlangen, Germany), MRE could also be used for noninvasive liver assessment in living donors to prevent or anticipate possible complications of the procedure.

Moreover, MRE can detect increased liver stiffness even in the absence of histologically detectable fibrosis. The results possibly reflect the increased volume of extracellular fluid in the early stages of liver disease preceding fibrosis [11]. This can occur in steatohepatitis – the mechanical properties of extracellular fluid lead to perisinusoidal cell activation (Ito cells) with consecutive development of fibrosis due to dedifferentiation of these cells to myofibroblasts [12]. Nevertheless, simple steatosis does not alter the mechanical properties of the liver, so it is undetectable using elastography. Given current growing trends in the epidemiology of NAFLD and nonalcoholic steatohepatitis (NASH), grading steatosis in all patients with liver disease should be considered. Parametric imaging of the liver and assessing it using the LiverLab tool, which evaluates liver steatosis and liver iron load, can easily be incorporated into the abdominal MRI study.

Proper positioning of the driver allows us to simultaneously evaluate both liver and spleen [13]. This is particularly useful in liver disease that leads to portal hypertension and increased hepatic venous pressure gradient (HVPG), which correlates with the risk of esophageal varices development, ascites, and splenomegaly. Currently, HVPG can only be evaluated invasively [14, 15]. However, there is data suggesting that MRE is a feasible tool for estimating this parameter and has prognostic value. Liver and spleen elasticity increases with the degree of esophageal varices on endoscopy. Additionally, spleen stiffness measured using MRE in children was shown to have good diagnostic performance in predicting the presence of gastroesophageal varices [16].

## MRE in pediatric liver disease

Pediatric patients can suffer from a variety of chronic liver diseases, both of hereditary and sporadic origin. Some conditions may lead to liver fibrosis and, when untreated, to cirrhosis.

NALFD is currently the most common chronic liver disease in children and its prevalence is rising. The condition constitutes a significant public health issue, as its sequalae include cirrhosis and hepatocellular carcinoma. In the United States, NAFLD is currently the second most common cause of liver transplantation in adults [17]. Between 40% and 90% of patients with NAFLD develop liver fibrosis, so MRE and LiverLab assessment might be increasingly employed in pediatric patients [18]. In a prospective multicenter observational study (MRI Assessment Guiding NAFLD Evaluation and Treatment, MAGNET) Schwimmer et al. compared hepatic stiffness assessed in MRE and histologic fibrosis staging in children aged 8–17 with known or suspected NAFLD [18]. The study showed good correlation between the histologically established degree of liver fibrosis and MRE liver stiffness measurements in the 90 patients with reliable imaging data. Importantly, the inter-reader agreement of liver stiffness evaluation was strong. The study also showed potential problems with conducting MRE in children, as the percentage of unreliable imaging studies was relatively high, at 16% [18]. However, a large retrospective analysis of 468 MRE studies in children and young adults demonstrated successful MRE data acquisition in the vast majority (96%) of attempts [19].

In a study which included 35 children with chronic liver disease – of whom 27 had NAFLD, and of those 22 had NASH – Xanthakos et al. showed very good accuracy of MRE in diagnosing significant liver fibrosis (stage ≥ 2), with a sensitivity of 88%, a specificity of 85%, and an AUC of 0.92 [20]. Another study analyzed 86 children and adults under 21 years of age with clinical indications for liver biopsy (most commonly fatty liver disease, followed by autoimmune hepatitis and primary sclerosing cholangitis) who also underwent MRE [21]. The analysis of the collected data showed a good correlation between hepatic stiffness and severity of liver fibrosis. Additionally, the study demonstrated moderate predictive performance of MRE for identification of Ludwig stage ≥ 2 fibrosis (AUC = 0.70). However, the accuracy was significantly higher for diagnosis of stage 3 or higher fibrosis (AUC = 0.92) [21].

MRE was also compared with other quantitative MRI markers and clinical variables in a study of 58 children and young adults with autoimmune hepatitis (AIH), primary sclerosing cholangitis (PSC), or autoimmune sclerosing

cholangitis (ASC) [22]. Mahalingam et al. demonstrated significant associations between liver stiffness measured in MRE and magnetic resonance cholangiopancreatography (MRCP) metrics, T1 relaxation times, and the levels of laboratory markers of liver disease [22]. Additionally, McCary et al. showed that the above quantitative parameters, including hepatic stiffness, are independently associated with worse Mayo risk scores and SCOPE index in children and young adults with autoimmune liver disease [23]. MRE can also be used to assess liver parenchyma in children after a Fontan operation, as liver injury is a well-known complication of the procedure [24].

The results of the studies show potential for diagnosing and monitoring liver fibrosis in pediatric patients with NAFLD and other chronic liver diseases. A number of authors also believe that some typically pediatric conditions may become clinically significant indications for MRE. It is debated whether MRE can help differentiate biliary atresia from neonatal[1] hepatitis or provide early diagnoses of liver disease in patients on total parenteral nutrition or with short bowel syndrome [3]. Nevertheless, more studies are needed to expand the clinical indications for liver MRE in pediatric patients.

Importantly, Trout et al. recently published normative liver stiffness values measured with MRE in a prospective, multicenter study with 71 participants who were aged 7 to 17 and had no personal or family history of liver disease [25]. The mean liver stiffness in the study group was 2.1 kPa, with the 95$^{th}$ percentile equal to 2.8 kPa [25]. Crucially, the investigators did not observe significant differences in liver stiffness measured on different MRI scanners, which suggests that the established normative data can be uniformly applied across different MRI platforms [25]. The study also did not show significant differences between MRE imaging on 1.5T and 3T scanners. In our experience a similar cutoff value of 2.86 kPa, which is significantly lower than in adults, is associated with very good diagnostic accuracy of biopsy-confirmed significant liver fibrosis corresponding to an Ishak score of ≥ 3 in patients with AIH and Wilson's disease (Pawliszak et al., unpublished data).

## How we do it

Patient preparation for liver MRE does not differ significantly from preparation for a standard abdominal MRI, except for the recommended fasting period of 4 to 6 hours [2, 25]. This is due to the fact that, in patients with chronic liver disease and liver fibrosis, liver stiffness may increase following a meal. Therefore, fasting is advised to increase measurement reproducibility [2].

As previously described, liver MRE requires reproducible vibrations with a predefined frequency. This is achieved by using a driver, which should be placed over the right liver lobe. The standard driver position is usually in the right midclavicular line, at the level of the xiphoid process of the sternum. In some cases, such as in patients post right hemihepatectomy or post liver transplant, the driver placement might need to be modified and should cover the approximate location of the largest portion of the liver [2]. The driver position can be adjusted after the localizer sequence.

For standard liver MRE, the driver's frequency should be set to 60 Hz. Performing test stimuli from the driver prior to proper acquisition can increase the patient's compliance.

Liver MRE is usually part of an abdominal MR examination, or it is performed together with MRCP. Breath-holding is useful, but not vital for successful image acquisition during liver MRE. If the patient is cooperating, image acquisition should preferably be performed at end-expiration.

Imaging starts with two T2-weighted HASTE sequences in transverse and coronal planes for precise liver localization. The standard imaging protocol consists of imaging at four levels of the liver, including an acquisition at the level of the liver hilum. A GRE MRE sequence is acquired with a voxel size of 1.4 × 1.4 × 5.0 mm, with one slice positioned transversally in the scanner coordinate system and with TR/TE = 50/23.75 ms. The acquisition lasts 19 seconds, which corresponds to one breath-hold. Each elastography is followed by a low-resolution T1-weighted FLASH sequence for position confirmation and spatial localization. After the elastography, patients undergo examination for their specific clinical questions.

The causes of poor or nondiagnostic elastographic imaging include poor shear-wave delivery to the liver, improper driver power, other technical issues with the driver, paramagnetic or motion artifacts, or liver iron overload. Each of the acquired scans undergoes automatic quantitative analysis, and all areas with a confidence threshold below 95% are marked as unsuitable for evaluation.

Liver stiffness is measured by placing an ROI in the liver parenchyma with good imaging quality. The ROI should not include the subcapsular portions of the liver (approx. 1 cm thick), the hilum, the great vessels, the gall bladder (if applicable), or any apparent artifacts. Mean liver stiffness values calculated for each area should be added and divided by the number of scans (usually four) [26]. In cases of a smaller liver, due to area differences, mean liver stiffness can be adjusted for this parameter.

[1] *MR scanning has not been established as safe for imaging fetuses and infants less than two years of age. The responsible physician must evaluate the benefits of the MR examination compared to those of other imaging procedures.*

## Case 1

A 17-year-old boy with ulcerative colitis, AIH, and PSC diagnosed five years prior was referred for a check-up by MRCP. At the time of the imaging study, the patient had no clinical signs or symptoms. However, laboratory tests revealed elevated transaminases, GGTP, bilirubin, bile acids, and IgG4, and thrombocytopenia.

Figure 1A shows a volume-rendered reconstruction of the biliary ducts. Peripheral biliary ducts were significantly dilated, with a diameter of up to 6 mm, and had irregular contours. MRE revealed significantly increased liver stiffness, with a mean value of 5.5 kPa. The spleen was significantly enlarged at 27 cm and had stiffness of 7.0 kPa. Figures 1B, 1C, and 1D show magnitude, wave, and color elastogram with 95% confidence masks. Biopsy performed the day after MRI confirmed significant liver fibrosis, corresponding to an Ishak score of 6. Gastroscopy performed during the same hospitalization period revealed esophageal varices, which were endoscopically ligated.

## Case 2

A 14-year-old girl with biliary atresia, five years after liver transplantation (LTx), was admitted due to fever and elevated inflammatory markers. She received antibiotic therapy, which relieved her clinical signs and normalized her laboratory markers. Afterwards, she was referred for MRCP to assess the biliary ducts. In addition, MRE was performed to assess the stiffness of the transplanted liver.

The study revealed a heterogeneous, polycystic liver. In segment III of the liver, a fluid collection measuring

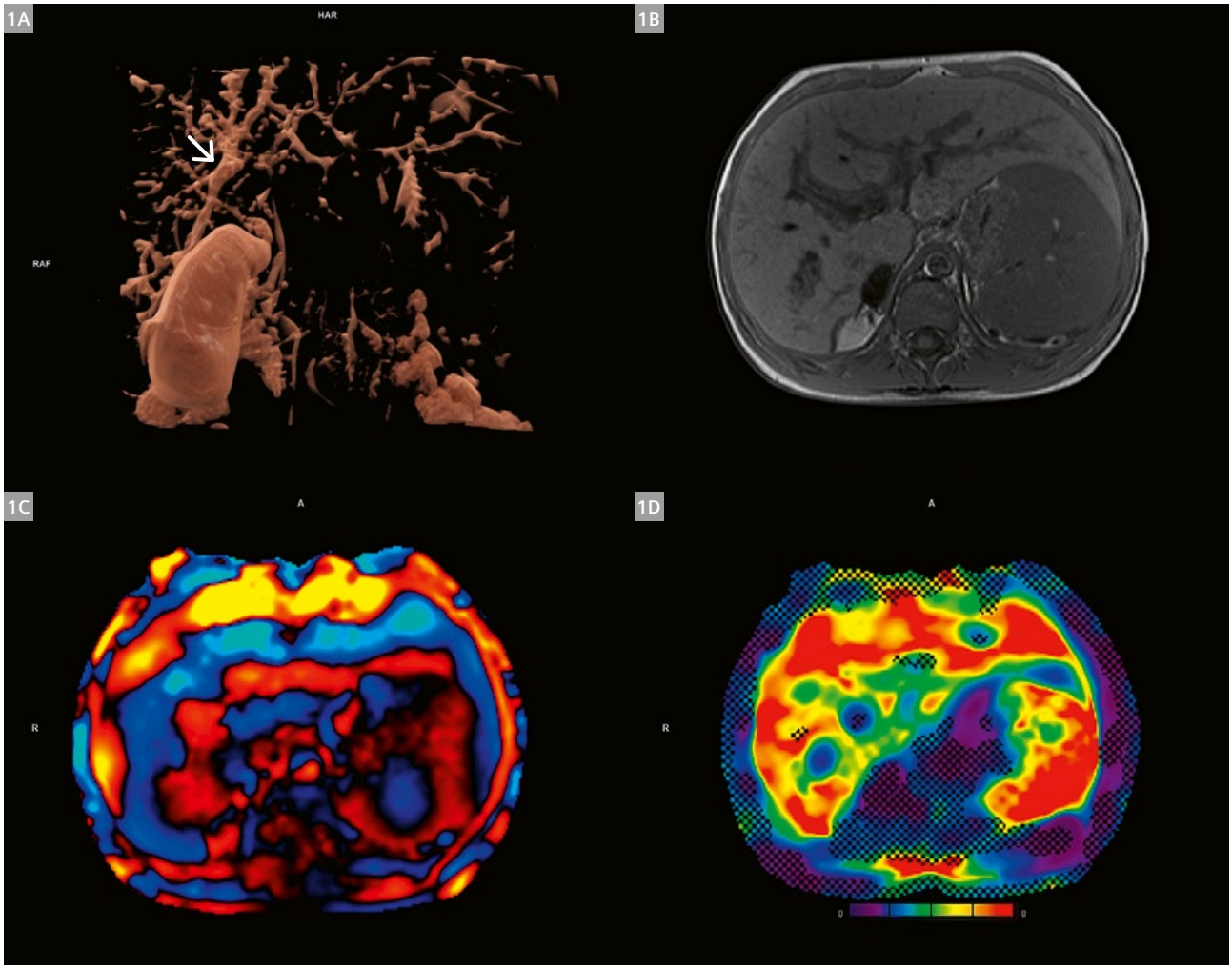

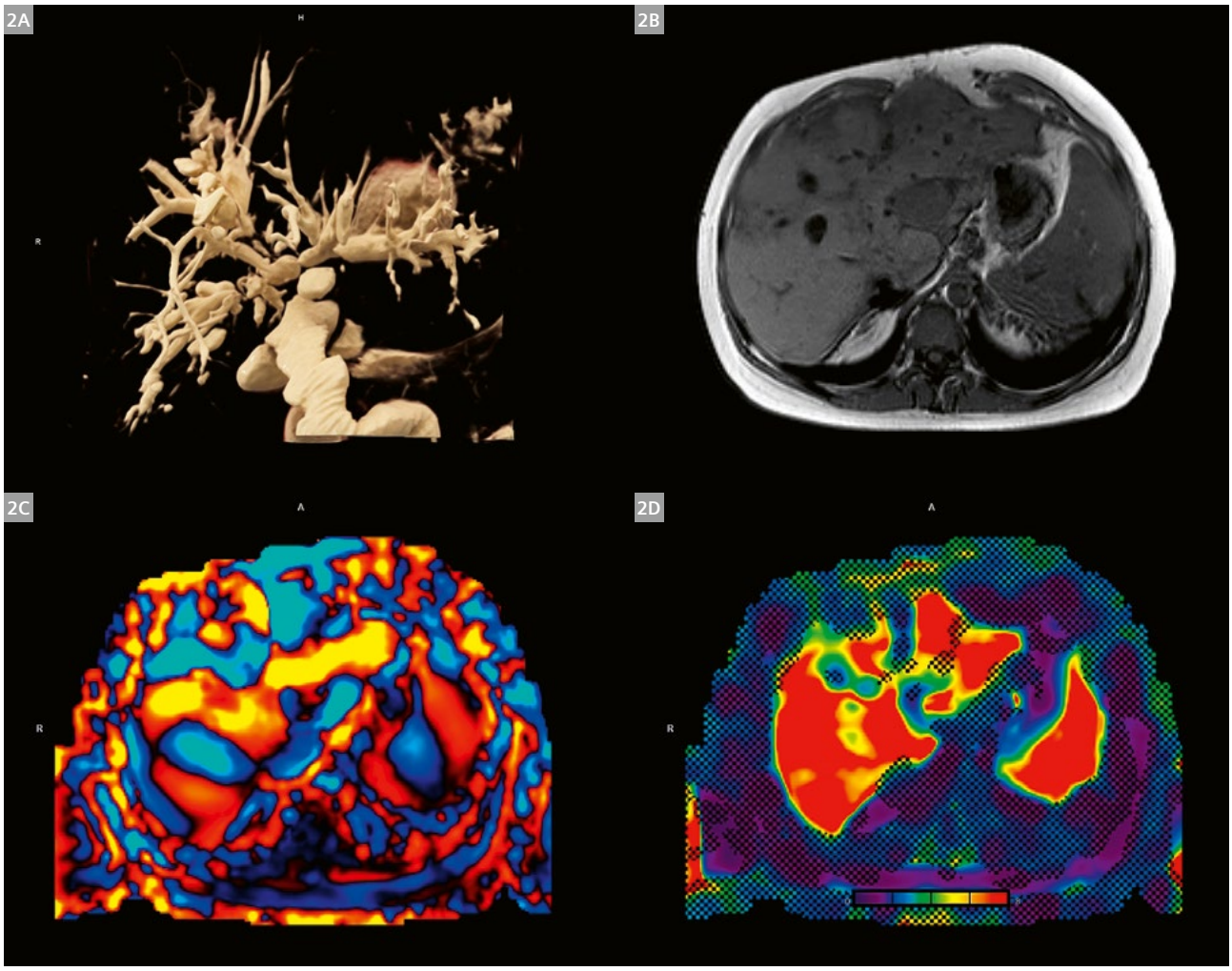


3.5 × 3 × 3.5 cm was observed, without diffusion restriction. Bile ducts were significantly and irregularly dilated by up to 10 mm. The stiffness of the transplanted liver was markedly elevated, with a global mean value of 7.5 kPa. Spleen stiffness was 7.8 kPa. Figures 2A–D show magnitude, wave, and color elastogram with 95% confidence masks and a volume rendering of the liver bile ducts.

During the same hospitalization period, the patient underwent liver biopsy, which confirmed significant liver fibrosis with an Ishak score of 6. Grade I esophageal varices and a single gastric varix were diagnosed. The patient was discharged in a good state with cyclic antibiotic therapy.

**References**

1 Muthupillai R, Lomas DJ, Rossman PJ, Greenleaf JF, Manduca A, Ehman RL. Magnetic resonance elastography by direct visualization of propagating acoustic strain waves. Science. 1995;269(5232):1854–7.
2 Guglielmo FF, Venkatesh SK, Mitchell DG. Liver MR Elastography Technique and Image Interpretation: Pearls and Pitfalls. RadioGraphics. 2019;39(7):1983–2002.
3 Binkovitz LA, El-Youssef M, Glaser KJ, Yin M, Binkovitz AK, Ehman RL. Pediatric MR elastography of hepatic fibrosis: principles, technique and early clinical experience. Pediatr Radiol. 2012;42(4):402–9.
4 Talwalkar JA. Elastography for detecting hepatic fibrosis: options and considerations. Gastroenterology. 2008;135(1):299–302.
5 Mehta SH, Lau B, Afdhal NH, Thomas DL. Exceeding the limits of liver histology markers. J Hepatol. 2009;50(1):36–41.
6 Shire NJ, Yin M, Chen J, Railkar RA, Fox-Bosetti S, Johnson SM, et al. Test-retest repeatability of MR elastography for noninvasive liver fibrosis assessment in hepatitis C. J Magn Reson Imaging. 2011;34(4):947–55.
7 Venkatesh SK, Yin M, Takahashi N, Glockner JF, Talwalkar JA, Ehman RL. Non-invasive detection of liver fibrosis: MR imaging features vs. MR elastography. Abdom Imaging. 2015;40(4):766–75.
8 Singh S, Venkatesh SK, Wang Z, Miller FH, Motosugi U, Low RN, et al. Diagnostic performance of magnetic resonance elastography in staging liver fibrosis: a systematic review and meta-analysis of individual participant data. Clin Gastroenterol Hepatol. 2015;13(3):440–451.e6.
9 Venkatesh SK, Yin M, Ehman RL. Magnetic resonance elastography of liver: technique, analysis, and clinical applications. J Magn Reson Imaging. 2013;37(3):544–55.

10 Park HS, Kim YJ, Yu MH, Choe WH, Jung SI, Jeon HJ. Three-Tesla magnetic resonance elastography for hepatic fibrosis: comparison with diffusion-weighted imaging and gadoxetic acid-enhanced magnetic resonance imaging.
World J Gastroenterol. 2014;20(46):17558–67.
11 Simonetto DA, Yang H, Yin M, de Assuncao TM, Kwon JH, Hilscher M, et al. Chronic passive venous congestion drives hepatic fibrogenesis via sinusoidal thrombosis and mechanical forces.
Hepatology. 2015;61(2):648–59.
12 Chen J, Talwalkar JA, Yin M, Glaser KJ, Sanderson SO, Ehman RL. Early detection of nonalcoholic steatohepatitis in patients with nonalcoholic fatty liver disease by using MR elastography.
Radiology. 2011;259(3):749–56.
13 Dyvorne HA, Jajamovich GH, Besa C, Cooper N, Taouli B. Simultaneous measurement of hepatic and splenic stiffness using MR elastography: preliminary experience.
Abdom Imaging. 2015;40(4):803–9.
14 Escorsell A, Garcia-Pagán JC, Bosch J. Assessment of portal hypertension in humans. Clin Liver Dis. 2001;5(3):575–89.
15 Ripoll C, Groszmann R, Garcia-Tsao G, Grace N, Burroughs A, Planas R, et al. Hepatic venous pressure gradient predicts clinical decompensation in patients with compensated cirrhosis.
Gastroenterology. 2007;133(2):481–8.
16 Yoon H, Shin HJ, Kim M-J, Han SJ, Koh H, Kim S, et al. Predicting gastroesophageal varices through spleen magnetic resonance elastography in pediatric liver fibrosis.
World J Gastroenterol. 2019;25(3):367–377.
17 Wong RJ, Aguilar M, Cheung R, Perumpail RB, Harrison SA, Younossi ZM, et al. Nonalcoholic steatohepatitis is the second leading etiology of liver disease among adults awaiting liver transplantation in the United States.
Gastroenterology. 2015;148(3):547–55.
18 Schwimmer JB, Behling C, Angeles JE, Paiz M, Durelle J, Africa J, et al. Magnetic resonance elastography measured shear stiffness as a biomarker of fibrosis in pediatric nonalcoholic fatty liver disease.
Hepatology. 2017;66(5):1474–1485.
19 Joshi M, Dillman JR, Towbin AJ, Serai SD, Trout AT. MR elastography: high rate of technical success in pediatric and young adult patients.
Pediatr Radiol. 2017;47(7):838–843.
20 Xanthakos SA, Podberesky DJ, Serai SD, Miles L, King EC, Balistreri WF, et al. Use of magnetic resonance elastography to assess hepatic fibrosis in children with chronic liver disease.
J Pediatr. 2014;164(1):186–8.
21 Trout AT, Sheridan RM, Serai SD, Xanthakos SA, Su W, Zhang B, et al. Diagnostic Performance of MR Elastography for Liver Fibrosis in Children and Young Adults with a Spectrum of Liver Diseases.
Radiology. 2018;287(3):824–832.
22 Mahalingam N, Trout AT, Gandhi DB, Sahay RD, Singh R, Miethke AG, et al. Associations between MRI T1 mapping, liver stiffness, quantitative MRCP, and laboratory biomarkers in children and young adults with autoimmune liver disease.
Abdom Radiol (NY). 2022;47(2):672–683.
23 McCrary J, Trout AT, Mahalingam N, Singh R, Rojas CC, Miethke AG, et al. Associations Between Quantitative MRI Metrics and Clinical Risk Scores in Children and Young Adults With Autoimmune Liver Disease. AJR Am J Roentgenol. 2022;1–9.
24 DiPaola FW, Schumacher KR, Goldberg CS, et al. Effect of Fontan operation on liver stiffness in children with single ventricle physiology. Eur Radiol. 2017;27(6)2434–2442.
25 Trout AT, Anupindi SA, Gee MS, Khanna G, Xanthakos SA, Serai SD, et al. Normal Liver Stiffness Measured with MR Elastography in Children. Radiology. 2020;297(3):663–669.
26 QIBA Profile, Magnetic resonance elastography of the liver.
Stage 2: consensus profile. Radiological Society of North America
https://qibawiki.rsna.org/images/a/a5/MRE-QIBAProfile-2018-05-02 CONSENSUS.pdf (2018).

## Contact

Professor Elżbieta Jurkiewicz, M.D., Ph.D.
Department of Diagnostic Imaging
The Children's Memorial Health Institute
aleja Dzieci Polskich 20
04-736 Warszawa
Poland
e.jurkiewicz@ipczd.pl

# PET-MRI Patterns in Pediatric Patients with Neurofibromatosis Type 1 (NF1) and NF1-associated Malignant Peripheral Nerve Sheath Tumors (MPNSTs)

**Valentina Bodanza[1]; Chiara Giraudo[2]; Eva Trevisson[3]; Chiara Mozzato[3]; Pietro Zucchetta[1]; Diego Cecchin[1,4]**

[1]Nuclear Medicine Unit, Department of Medicine – DIMED, University Hospital of Padova, Italy
[2]Unit of Advanced Clinical and Translational Imaging, Department of Medicine – DIMED, University Hospital of Padova, Italy
[3]Department of Women's and Children's Health, University Hospital of Padova, Italy
[4]Padova Neuroscience Center, University of Padova, Italy

## Abstract

Neurofibromatosis type 1 (NF1) is an autosomal dominant monogenic condition with increased risk of developing tumors, particularly soft tissue sarcomas. The malignant neoplasms most frequently associated with NF1 are malignant peripheral nerve sheath tumors (MPNSTs), which often arise from plexiform neurofibromas. Imaging methods play a key role in monitoring these neurofibromas to allow early detection of MPNSTs. Moreover, patients with NF1 often present with masses of the central nervous system that require instrumental monitoring. PET-MRI is a multimodal imaging method that combines detailed morphological information with metabolic data and reduces exposure to radiation compared to conventional methods (CT, PET-CT imaging). It is therefore promising for monitoring NF1. We present a case series of three NF1 patients monitored using $^{18}$F-FDG PET-MRI.

## Introduction

Neurofibromatosis type 1 (NF1) is a multisystem neurocutaneous disease. It has an autosomal dominant origin in approximately 50% of cases, and is due to a *de novo* mutation in the remaining cases [1]. According to the recent article of Legius et al. [2], the diagnostic criteria for NF1 are met in an individual who does not have a parent diagnosed with NF1 if two or more of the following are present:

- Six or more café-au-lait macules over 5 mm in greatest diameter in prepubertal individuals and over 15 mm in greatest diameter in postpubertal individuals
- Freckling in the axillary or inguinal region
- Two or more neurofibromas of any type or one plexiform neurofibroma
- Optic pathway glioma
- Two or more iris Lisch nodules identified by slit lamp examination or two or more choroidal abnormalities (CAs) – defined as bright, patchy nodules imaged by optical coherence tomography (OCT)/near-infrared reflectance (NIR) imaging
- A distinctive osseous lesion such as sphenoid dysplasia, anterolateral bowing of the tibia, or pseudarthrosis of a long bone
- A heterozygous pathogenic NF1 variant with a variant allele fraction of 50% in apparently normal tissue such as white blood cells

A child of a parent who meets the diagnostic criteria merits a diagnosis of NF1 if one or more of the criteria are present.

Given the abovementioned criteria, it is clear that imaging plays a key role in diagnosing and monitoring NF1. In fact, signs of various organ involvement can be easily detected by different techniques. For example, MRI allows to identify cerebral anomalies (e.g., focal areas of signal intensity in the deep white matter, basal ganglia, or corpus callosum) and cutaneous and/or subcutaneous neurofibromas [3].

It is important to note that NF1 is associated with an increased risk of developing tumors, with malignant peripheral nerve sheath tumors (MPNSTs) being the most frequent (prevalence range: 8%–13%). While anatomical imaging can contribute to the early detection of malignant transformation using MRI signs such as ill-defined margins, irregular enhancement, intratumoral lobulation, and perilesional edema, hybrid imaging also has a crucial role to play [4]. In fact, it was recently demonstrated that $^{18}$F-FDG PET-MRI (PET-MRI) is a valuable tool for differentiating between benign lesions and MPNSTs in NF1 patients. It has been shown that MPNSTs usually have higher FDG uptake [5] than benign NF1 lesions. The range of $SUV_{max}$ values associated with malignant tumors is 1.8 to 7.0, but to the best of our knowledge the most widely used cutoff is 3.5 [6].

Although this evidence is encouraging, PET-CT is associated with relatively high radiation exposure (on average ~8–17 mSv), which is a drawback when children[1] with NF1 have to be evaluated [7].

PET-MRI is a multimodal hybrid technique that combines the high soft-tissue contrast and functional information of MRI with metabolic data acquired by the PET component. It is an innovative and sensitive way of diagnosing and monitoring patients with NF1, and it significantly reduces the radiation exposure (on average ~3–5 mSv) [7].

Another significant benefit of using integrated PET-MRI instead of two separate examinations (PET-CT and MRI) is that it reduces the number of sedations required in patients younger than six [8].

Reinert et al. examined 28 patients with NF1 and demonstrated that, as well as reducing exposure, PET-MRI also guarantees a good diagnostic performance for this disease [9].

In this short report, we would like to share our PET-MRI protocol for imaging children with NF1 using a Biograph mMR scanner from Siemens Healthcare. It includes diffusion-weighted imaging (RESOLVE), since it can provide crucial information for the diagnostic assessment of this group of patients, especially if combined with PET data (Table 1). We also highlight the diagnostic value of PET-MRI for NF1 in children by presenting three of the pediatric cases examined in the last six years at the tertiary center of the University Hospital Padova, Italy.

[1] *MR scanning has not been established as safe for imaging fetuses and infants less than two years of age. The responsible physician must evaluate the benefits of the MR examination compared to those of other imaging procedures. Note: This Siemens Healthineers disclaimer does not represent the opinion of the authors.*

| MR sequence | TR/TE (ms) | FA | Slice thickness (mm) | Duration |
|---|---|---|---|---|
| Axial WB T2 HASTE | 1600/95 | 160 | 5 | 2 minutes |
| T2 TIRM | 6320/51 | 120 | 4 | 2 minutes |
| WB axial CAIPIRINHA | 3.9/1.2–2.5 | 10 | 3 | 13 seconds |
| DWI b 50-800 | 4900/53 | 90 | 5 | 2 minutes |

**Table 1**: **PET-MRI protocol for children with NF1**
MR = magnetic resonance;
FA = flip angle;
HASTE: half-fourier acquisition single-shot turbo spin echo imaging;
WB = whole body;
CAIPI = controlled aliasing in parallel imaging results in higher acceleration;
DWI = diffusion-weighted imaging;
STIR = short tau inversion recovery

## Case 1

$^{18}$F-FDG-PET-MRI of a 16-year-old boy with NF1 examined for follow-up (top row) of a lesion in the right deep cervical space (arrow in 1C, and 1D). Compared to the PET-MRI (bottom row) performed one year earlier, the upper cranial portion of the abovementioned lesion appeared enlarged (18 × 14 mm vs. 14 × 11 mm) and demonstrated restricted diffusion as well as higher tracer uptake ($SUV_{max}$ 5.6 vs. 3.6). Given the progression of the disease, a biopsy was scheduled that revealed an MPNST.

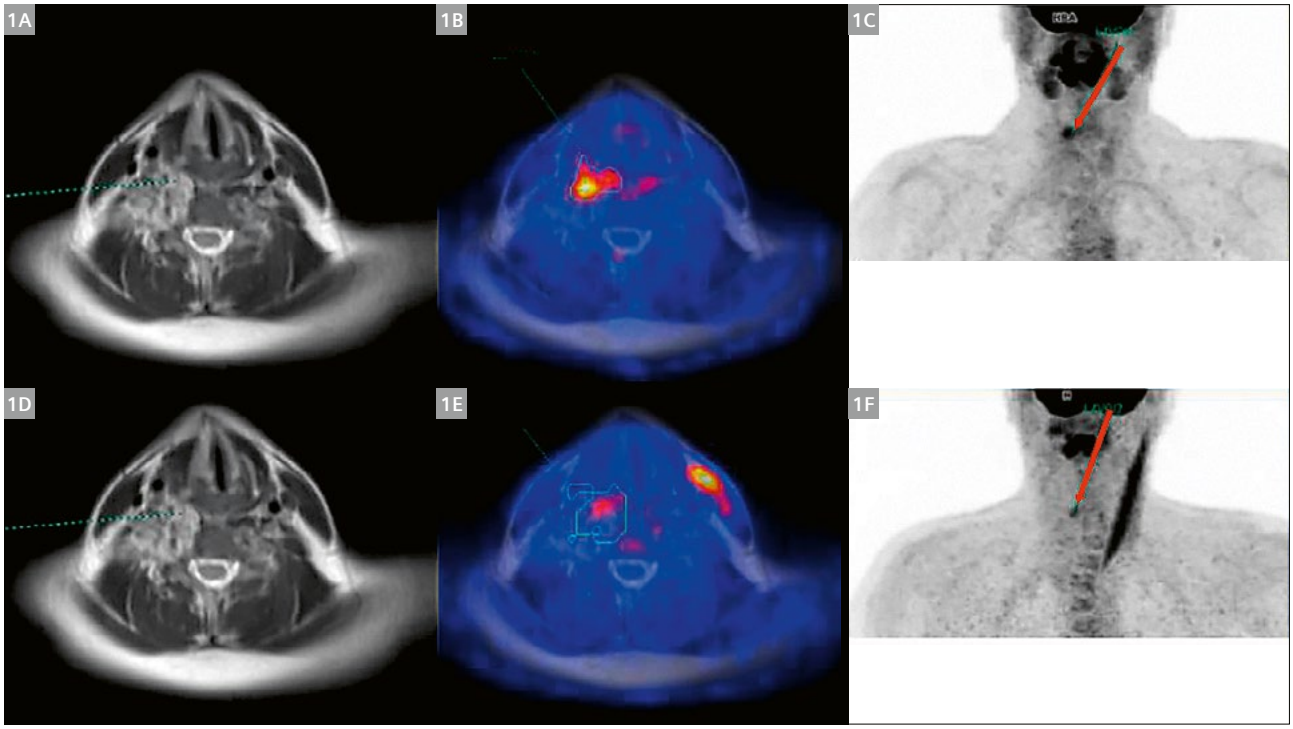


## Case 2

$^{18}$F-FDG-PET-MRI of a 14-year-old girl with a final diagnosis of MPNST. The PET-MRI demonstrated a skeletal metastatic hypermetabolic lesion ($SUV_{max}$ 5.9) that was clearly depicted on the axial fused images (left). DWI with a b-value of 800 s/mm$^2$ (center) and the ADC map (right) show that the skeletal lesion in the right sacrum is characterized by restricted diffusion.

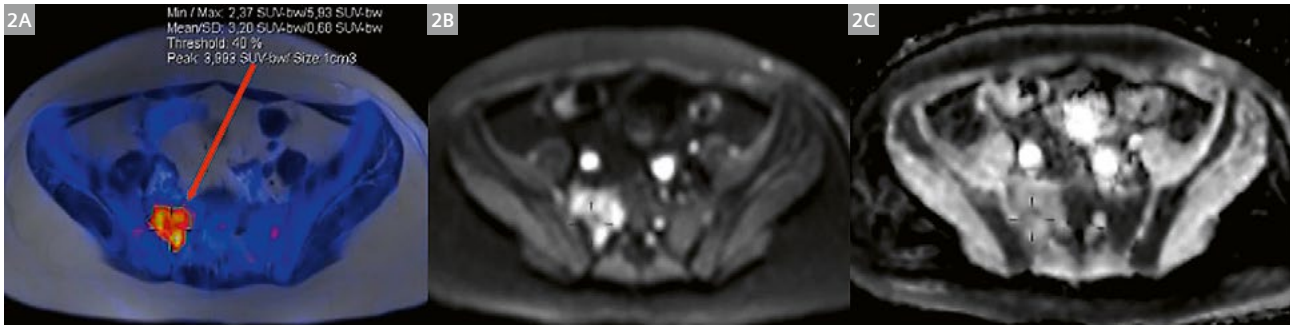

## Case 3

Monitoring of multiple neurofibromas (with volume increasing over time) of the right leg using $^{18}$F-FDG PET-MRI in a 17-year-old girl. No significant FDG uptake (3A shows fused T2 and PET images) or significant restriction of diffusivity (bottom row: ADC b-value 800 s/mm$^2$) was detected, which confirmed the benign nature of the lesion.

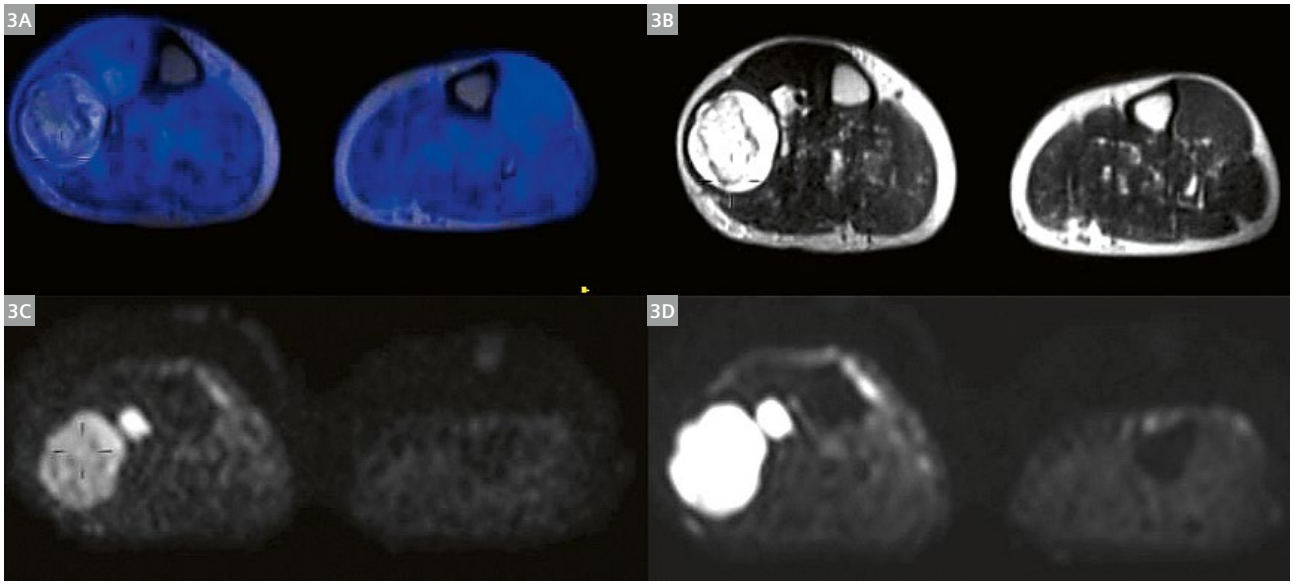


**References**

1 Fortman BJ, Kuszyk BS, Urban BA, Fishman EK. Neurofibromatosis type 1: a diagnostic mimicker at CT. Radiographics. 2001;21(3):601–12.
2 Legius E, Messiaen L, Wolkenstein P, Pancza P, Avery RA, Berman Y, et al. Revised diagnostic criteria for neurofibromatosis type 1 and Legius syndrome: an international consensus recommendation. Genet Med. 2021;23(8):1506-1513.
3 Mautner VF, Asuagbor FA, Dombi E, Fünsterer C, Kluwe L, Wenzel R, et al. Assessment of benign tumor burden by whole-body MRI in patients with neurofibromatosis 1. Neuro Oncol. 2008;10(4):593–8.
4 Yu YH, Wu JT, Ye J, Chen MX. Radiological findings of malignant peripheral nerve sheath tumor: reports of six cases and review of literature. World J Surg Oncol. 2016;14:142.
5 Salamon J, Veldhoen S, Apostolova I, Bannas P, Yamamura J, Herrmann J, et al. 18F-FDG PET/CT for detection of malignant peripheral nerve sheath tumours in neurofibromatosis type 1: tumour-to-liver ratio is superior to an SUVmax cut-off. Eur Radiol. 2014;24(2):405–12.
6 Martin E, Geitenbeek RTJ, Coert JH, Hanff DF, Graven LH, Grünhagen DJ, et al. A Bayesian approach for diagnostic accuracy of malignant peripheral nerve sheath tumors: a systematic review and meta-analysis. Neuro Oncol. 2021;23(4):557–571.
7 Martin O, Schaarschmidt BM, Kirchner J, Suntharalingam S, Grueneisen J, Demircioglu A, et al. PET/MRI Versus PET/CT for Whole-Body Staging: Results from a Single-Center Observational Study on 1,003 Sequential Examinations. J Nucl Med. 2020;61(8):1131–1136.
8 Vanderby SA, Babyn PS, Carter MW, Jewell SM, McKeever PD. Effect of anesthesia and sedation on pediatric MR imaging patient flow. Radiology. 2010;256(1):229–37.
9 Reinert CP, Schuhmann MU, Bender B, Gugel I, la Fougère C, Schäfer J, et al. Comprehensive anatomical and functional imaging in patients with type I neurofibromatosis using simultaneous FDG-PET/MRI. Eur J Nucl Med Mol Imaging. 2019;46(3):776–787.

## Contact

Professor Diego Cecchin
University Hospital of Padova
Nuclear Medicine Unit
Department of Medicine – DIMED
Via Giustiniani 2
35128 Padova
Italy
diego.cecchin@unipd.it

# Pediatric Whole-Body MRI: How I Do It

**Bac Nguyen, BSc; Lil-Sofie Muller, M.D., Ph.D.**

Oslo University Hospital, Rikshospitalet, Oslo, Norway

## Introduction

At Oslo University Hospital we have a high rate of pediatric patients, which can often pose a technical and diagnostic challenge. Indications for MRI in children at our institution include brain, spine, heart, abdomen, pelvis, MSK, and whole body. In non-cooperative children or children under 5 or 6 years of age[1], the examinations are most often performed under general anesthesia. For the older children, entertainment on a TV screen is offered and the examination is then generally well tolerated. In infants under 3 months of age, the feed and wrap technique is used, sometimes in combination with light sedation.

As the name indicates, whole-body MRI (WB-MRI) can image the entire body in one scan. It gives a full overview of multifocality, and favors detection of disease over characterization, sometimes even before symptoms develop. Although the entire body is not always imaged, the term whole-body MRI is normally used when three or more anatomical areas are included in one scan. There are numerous indications for WB-MRI [1]. In our institution, it is most often used for cancer staging, for early detection of cancer in children with genetic predisposition syndromes, or in cases of relapse in children with treated malignancy. It is also widely used in inflammatory disorders like chronic non-bacterial osteomyelitis and in children with juvenile idiopathic arthritis (JIA). Sometimes WB-MRI is used in children with non-specific symptoms and unknown underlying pathology.

[1] *MR scanning has not been established as safe for imaging fetuses and infants less than two years of age. The responsible physician must evaluate the benefits of the MR examination compared to those of other imaging procedures.*

## Equipment

Modern high-end systems like the 3T MAGNETOM Vida and 1.5T MAGNETOM Sola (Siemens Healthcare, Erlangen, Germany) are equipped with BioMatrix technology, which facilitates WB-MRI with exquisit image quality within a short scan time. At our hospital, we mostly perform WB-MRI on our 1.5T systems. We currently only have one 3T scanner, which is prioritized for other uses. Our 1.5T scanners are a MAGNETOM Aera and a MAGNETOM Avanto$^{fit}$ (Siemens Healthcare, Erlangen, Germany). The protocols are highly optimized regarding image quality and total scan time. The coils available for these scanners are designed for WB-MRI and consist of a Head/Neck 20, a Spine 32, two Body 18, and a peripheral angiography coil


**1** The TV screen is behind the bore. A mirror (not shown here) allows the patient to see the screen while lying in the bore.

with 36 channels. These coils make our workflow faster, and we use the time saved to invest in the image quality.

TV entertainment is offered through our NordicNeuroLab solution (Fig. 1). The child can choose to watch a movie, YouTube, Netflix, etc. (Fig. 2). In our experience, being able to watch TV drastically reduces the need for sedation or anesthesia, and most patients manage to complete a WB-MRI examination with sufficient image quality.

## Protocols

With a team of 26 MRI radiographers, it is important to have robust protocols that are easy to set up and have minimal need for adjustment. For optimal and consistent image quality, we decided to make the protocols according to weight rather than age (Fig. 3). It is easier to tailor each

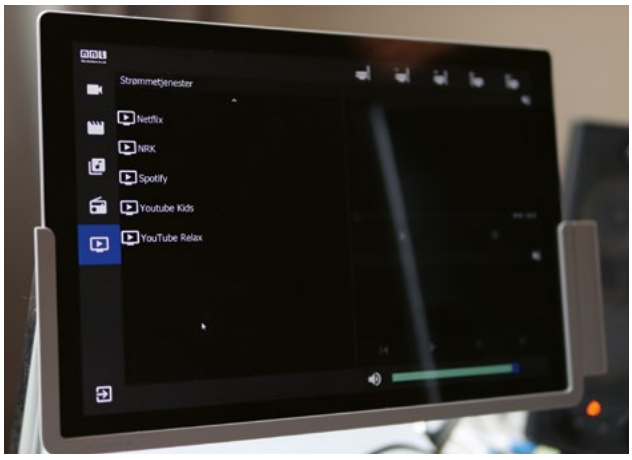


**2** Children can choose from various entertainment options.

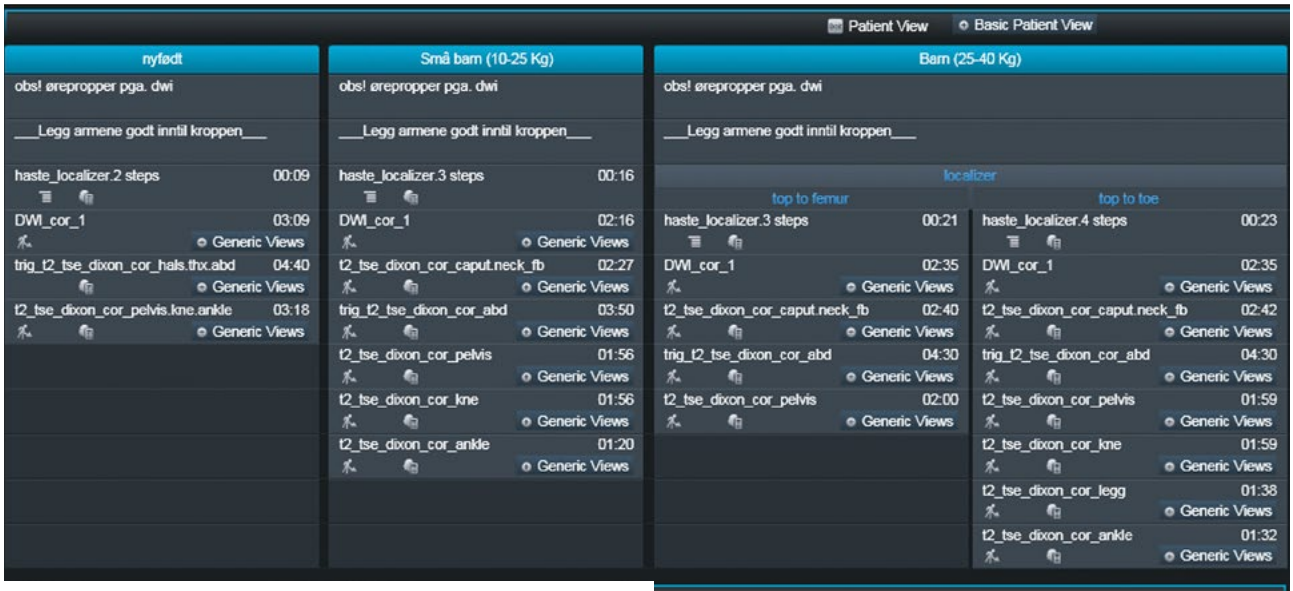


**3** Screenshots showing how our WB-MRI are set up. We sometimes perform head-to-femur scans, and sometimes head-to-toe. The protocols are optimized according to weight rather than age.

protocol according to weight, because children with the same age can vary considerably in size.

There is no unifying protocol for WB-MRI in children. The sequences and planes are chosen according to the clinical question. However, WB-MRI is most often used as a screening tool for detecting pathology or identifying multifocality. This means that almost all protocols include a water-sensitive sequence with fat suppression, most often performed in the coronal plane. Historically, the STIR sequence was used most frequently due to its homogenous fat suppression [1]. In recent years, the Dixon fat-suppression technique has become readily available and

| | 0–10 kg | | 10–25 kg | | 25–40 kg | | > 40 kg | |
|---|---|---|---|---|---|---|---|---|
| | T2w TSE Dixon | DWI | T2w TSE Dixon | DWI | T2w TSE Dixon | DWI | T2w TSE Dixon | DWI |
| Orientation | coronal | coronal | coronal | coronal | coronal | coronal | coronal | coronal |
| FOV read (mm) | 350 | 300 | 350 | 400 | 450 | 450 | 450 | 450 |
| FOV Phase (%) | 90.6 | 98.5 | 112.5 | 74.6 | 131.3 | 69.3 | 140.6 | 69.3 |
| FOV Phase Oversampling (%) | 0 | 50 | 0 | 50 | 0 | 50 | 0 | 50 |
| Phase direction | R-L | F-H | R-L | F-H | R-L | F-H | R-L | F-H |
| Base resolution | 384 | 130 | 384 | 134 | 384 | 150 | 384 | 150 |
| Phase resolution (%) | 100 | 100 | 100 | 100 | 100 | 100 | 100 | 100 |
| Slice thickness (mm) | 3 | 3.5 | 3.5 | 3.5 | 4 | 4 | 4 | 4 |
| Slices | 30* | 28* | 38* | 38* | 46* | 46* | 46* | 46* |
| Voxel size, interpolated (mm) | 0.5 × 0.5 | 1.2 × 1.2 | 0.5 × 0.5 | 1.5 × 1.5 | 0.5 × 0.5 | 1.5 × 1.5 | 0.5 × 0.5 | 1.5 × 1.5 |
| Scantime | 2.5 min – 3 min | 2.5 min – 3 min | 2 min – 2.5 min | 2 min – 2.5 min | 2 min – 2.5 min | 2.5 min – 3 min | 2 min – 2.5 min | 2.5 min – 3 min |
| TR (ms) | 3540* | 4560* | 4470* | 5320* | 5400* | 7290* | 5200* | 7290* |
| TE (ms) | 109* | 96* | 109* | 78* | 109* | 78* | 109* | 78* |
| Concatenations | 2 | 1 | 2 | 1 | 2 | 1 | 2 | 1 |
| Averages | 3 | 10 (b50) / 30 (b1000) | 1 | 2 (b50) / 15 (b1000) | 1 | 4 (b50) / 15 (b1000) | 1 | 4 (b50) / 15 (b1000) |
| Flip Angle (degree) | 150 | | 150 | | 150 | | 150 | |
| Restore magnetization | yes | no | yes | no | yes | no | yes | no |
| PAT (GRAPPA) | 2 | 2 | 2 | 2 | 2 | 2 | 2 | 2 |
| Bandwidth (Hz/Px) | 521 | 2024 | 512 | 2488 | 512 | 2380 | 512 | 2380 |
| Turbo Factor | 20 | | 20 | | 20 | | 20 | |
| b-values | | b50 / b1000 | | b50 / b1000 | | b50 / b1000 | | b50 / b1000 |
| TI | | 180 | | 180 | | 180 | | 180 |
| DWI mode | | 3D diagonal | | 3D diagonal | | 3D diagonal | | 3D diagonal |
| Diffusion scheme | | monopolar | | monopolar | | monopolar | | monopolar |

**Table 1**: An overview of our parameter settings on a 1.5T MAGNETOM Aera. Keep in mind these settings can be different depending on scanner model. Also, this table only shows one step, while WB-MRI uses multiple steps.
*varies due to coverage

enables the combination of robust Dixon fat suppression with the image quality from the T2-weighted TSE sequence. In addition, this produces in-phase, out-of-phase, water-sensitive and fat-sensitive images in one acquisition. Our WB-MRI protocol now consists of T2w coronal TSE Dixon and coronal DWI (b-values 0 and 1000 s/mm$^2$, and ADC map) because we mainly use WB-MRI for detection rather than characterizing lesions. Previously, we included T1w coronal TSE in our WB-MRI protocol, mainly for bone-marrow pathology, but this is now no longer included in the standard protocol because we get all the information we need from T2w coronal TSE Dixon fat-only images [2].

Leaving out T1 sequences saves time that we can then invest in other dedicated sequences depending on the region of interest. For instance, we can add a T1-weighted sequence for T1 characterization. The setup for our protocol parameters can be seen in Table 1.

WB-DWI is often performed in transverse plane because it results in fewer distortion artifacts and better image quality. We later reconstruct and compose the images in the coronal plane, often in inverted scale to resemble PET images (Fig. 4). The big drawback of transverse acquisition is the long scan time, especially if two or more b-values with an ADC map are required. We have worked on optimizing the DWI in order to obtain the sequence directly in the coronal plane with two b-values and an ADC map. The main benefit is that this is time-efficient, but the coronal images are also better quality than the ones reconstructed from the transversal acquisition. We have protocols for both 3T and 1.5T systems, but we mainly use 1.5T scanners because it results in less distortion and inhomogeneity on the DWI sequence. Another important reason for using 1.5T is that it allows us to cover more of each step in the coronal plane than we can with 3T.

Shorter scan times in coronal acquisition are possible due to less coverage in the A-P direction, which means fewer slices and shorter TR. Due to inhomogeneity and distortion when acquiring images in the coronal plane, you need to use a FOV phase of around 60–70% (scanner dependent). If you choose a larger FOV phase, it will cause distortion in the periphery of the images. Phase direction is F-H to cope with distortion, and a phase oversampling of up to 50% helps to avoid aliasing artifacts (Fig. 5).

A good tip is to start the protocol with coronal DWI. However, this comes with advantages and disadvantages. One advantage is that you get a fast overview with the help of DWI to draw your attention to the area of pathology. Then, subsequent sequences can be focused on the area of interest. Another point is that coronal DWI requires more post-processing time compared to other sequences in the protocol. This includes composing, multiplanar reconstruction, and maximum intensity projection. The post-processing can be performed during the acquisition of the morphological sequences to save time.

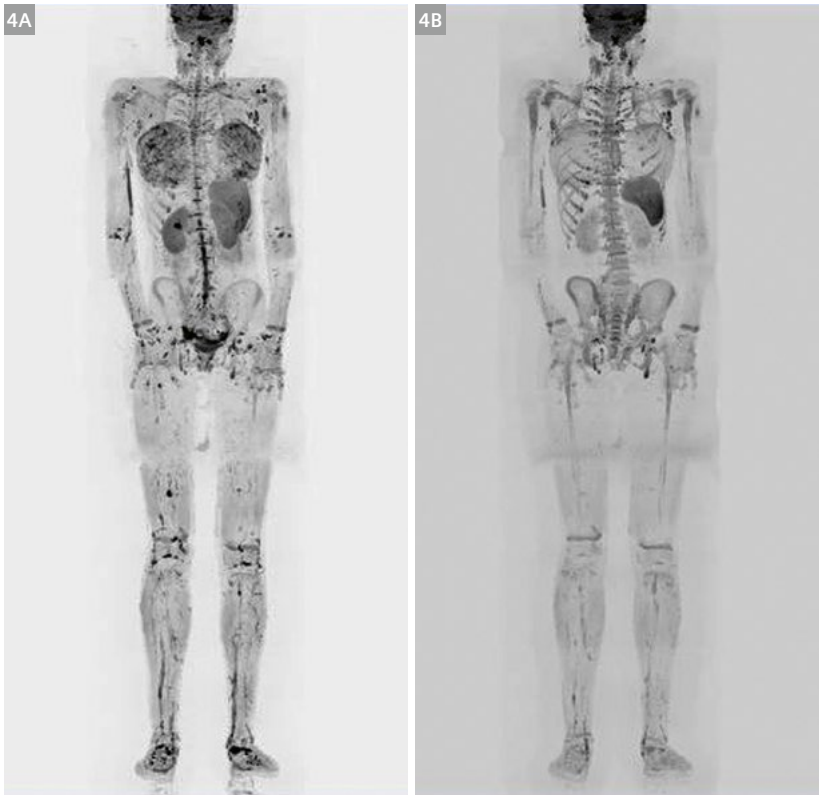


**4** WB-DWI with inverted scale to resemble PET images. **(4A)** b-value 50 s/mm$^2$ and **(4B)** b-value 1000 s/mm$^2$. Performed directly in the coronal plane with multiple steps and then composed.

The disadvantage of starting with DWI is that the intense noise from the sequence at the very beginning of the protocol can scare children. Therefore, we always talk to the children to prepare them for the noise and also stay open to the option of starting with morphological sequences such as T2w coronal TSE Dixon if needed. We give the children headphones and earplugs. For younger children, earplugs can be fitted by cutting them in half, but this is not something we do at our institution. Instead, we use "Putty Soft", which can be sized to fit any ear (Fig. 6).

## Conclusion

It is feasible to perform WB-MRI in children of all ages. The protocol must be robust and adjusted to patient weight. For specific indications, WB-MRI may give a good overview of disease burden in multifocal disease. It can also be useful in follow-ups for disease recurrence, and is occasionally used to look for disease focus in non-specific findings or symptoms.

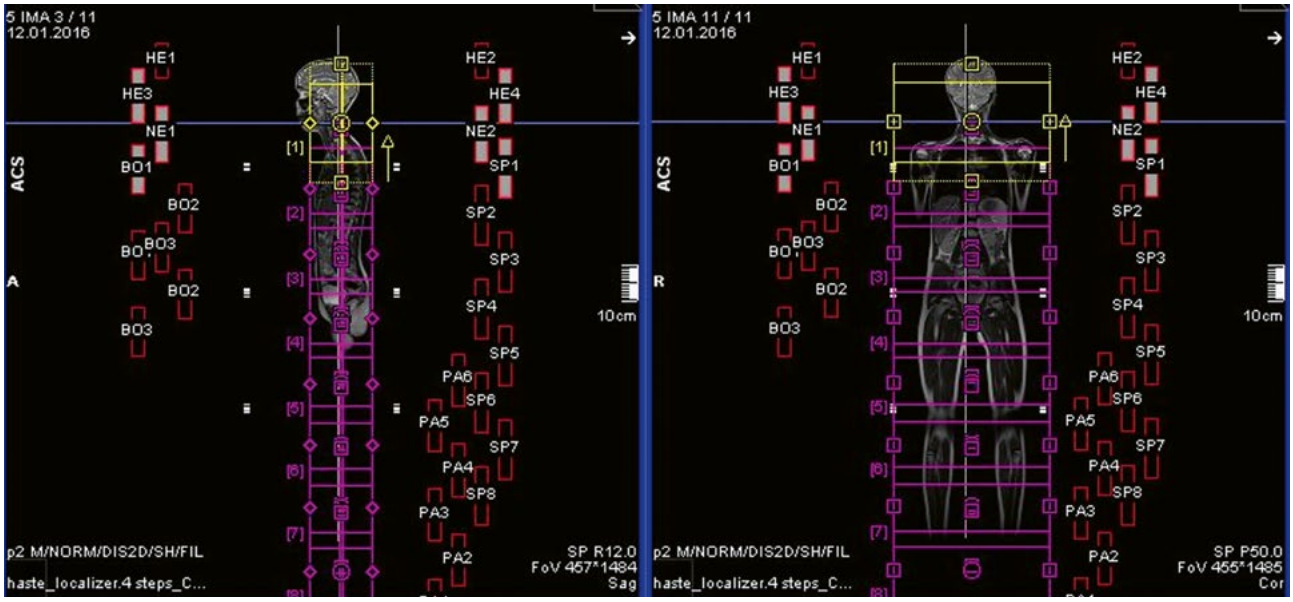


**5** Our setup of WB-DWI for direct coronal imaging. In this case, we had eight multiple steps and then composed later.

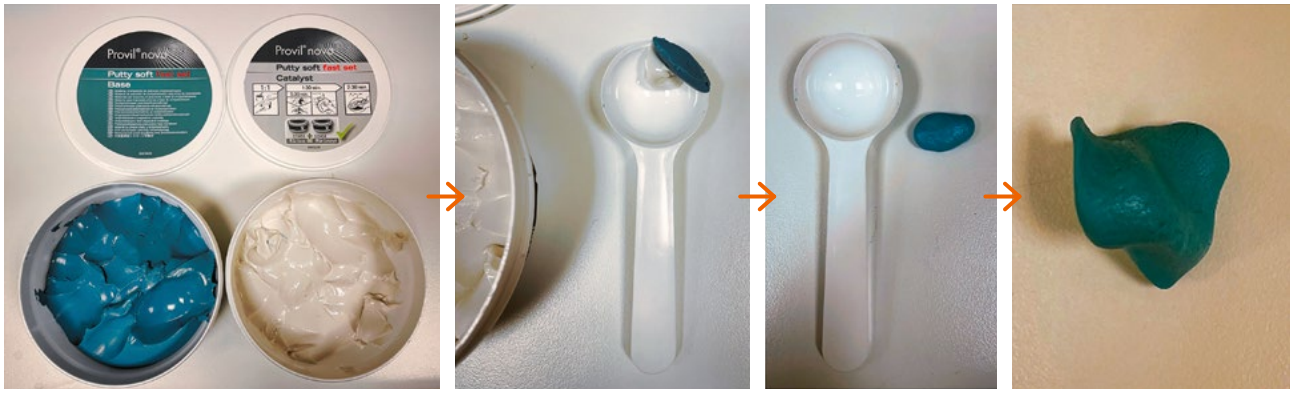


**6** We mix the Putty Soft to shape earplugs that fit any patient perfectly. It is easy and fast to use, and reduces noise in combination with the headphones.

## Case 1

A 5-month-old baby[1] with suspected multifocal Langerhans cells (LCH). WB-MRI was performed for disease staging with general anesthesia on a 1.5T MAGNETOM Avanto$^{Fit}$. The examination showed multiple lesions throughout the skeleton and lesions in the spleen, skin, and retroperitoneum.

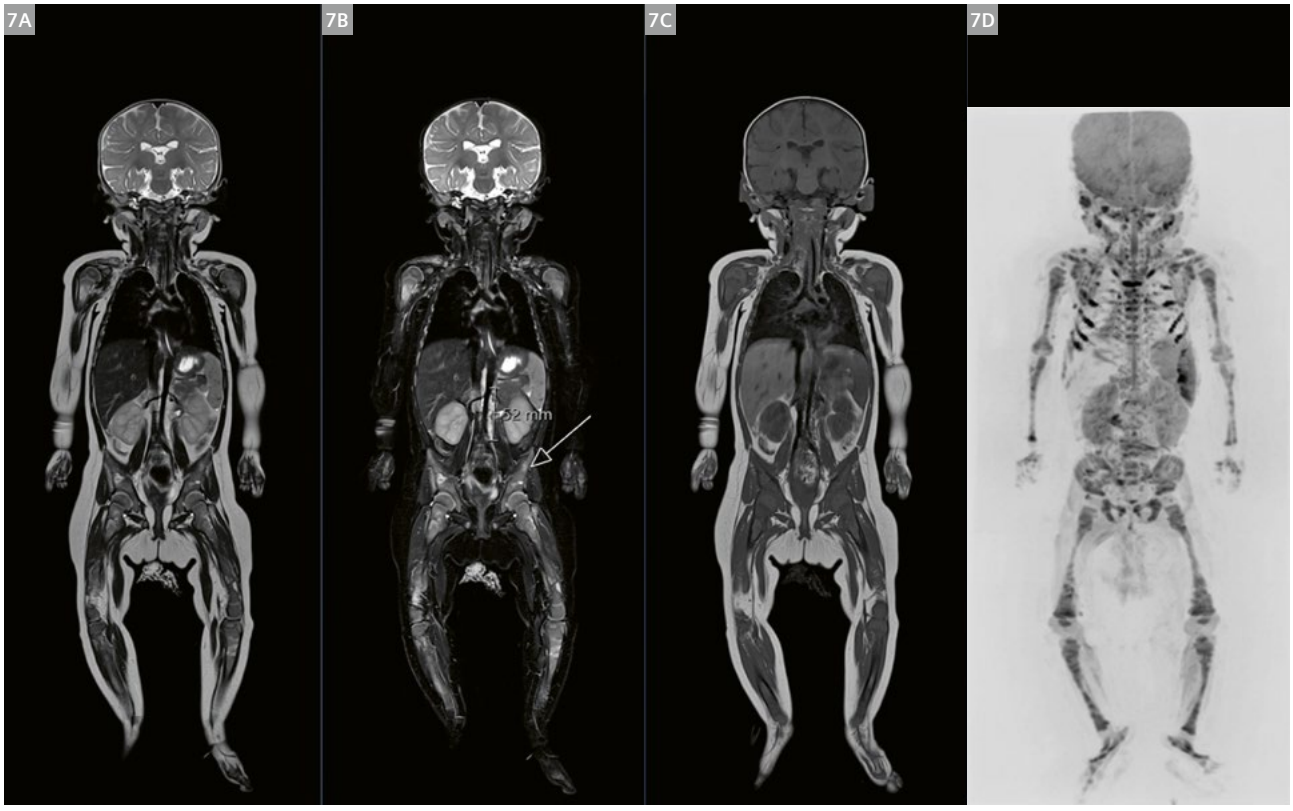


**7** **(7A)** T2w TSE Dixon in-phase coronal, 0.45 × 0.45 × 3.5 mm, TA 2–2.5 min. Multiple steps, composed.
**(7B)** T2w TSE Dixon water-only coronal.
**(7C)** T1w TSE coronal, 0.45 × 0.45 × 3.5 mm, TA 2–2.5 min. Multiple steps, composed.
**(7D)** EPI DWI STIR coronal, 1 × 1 × 3 mm, b-value 1000 s/mm², TA 3–3.5 min. Multiple steps, composed.

[1] *MR scanning has not been established as safe for imaging fetuses and infants less than two years of age. The responsible physician must evaluate the benefits of the MR examination compared to those of other imaging procedures.*

## Case 2

A 10-month-old baby[1] treated for neuroblastoma with an intra-abdominal tumor, and lymph-node and liver metastases. WB-MRI was performed three months post-treatment under general anesthesia on a 1.5T MAGNETOM Avanto$^{Fit}$.

The coronal WB-MRI images provide an overview of the total disease burden, with both the primary tumor and the metastasis. Dedicated sequences of the abdomen were performed as part of the pre-operative assessment.

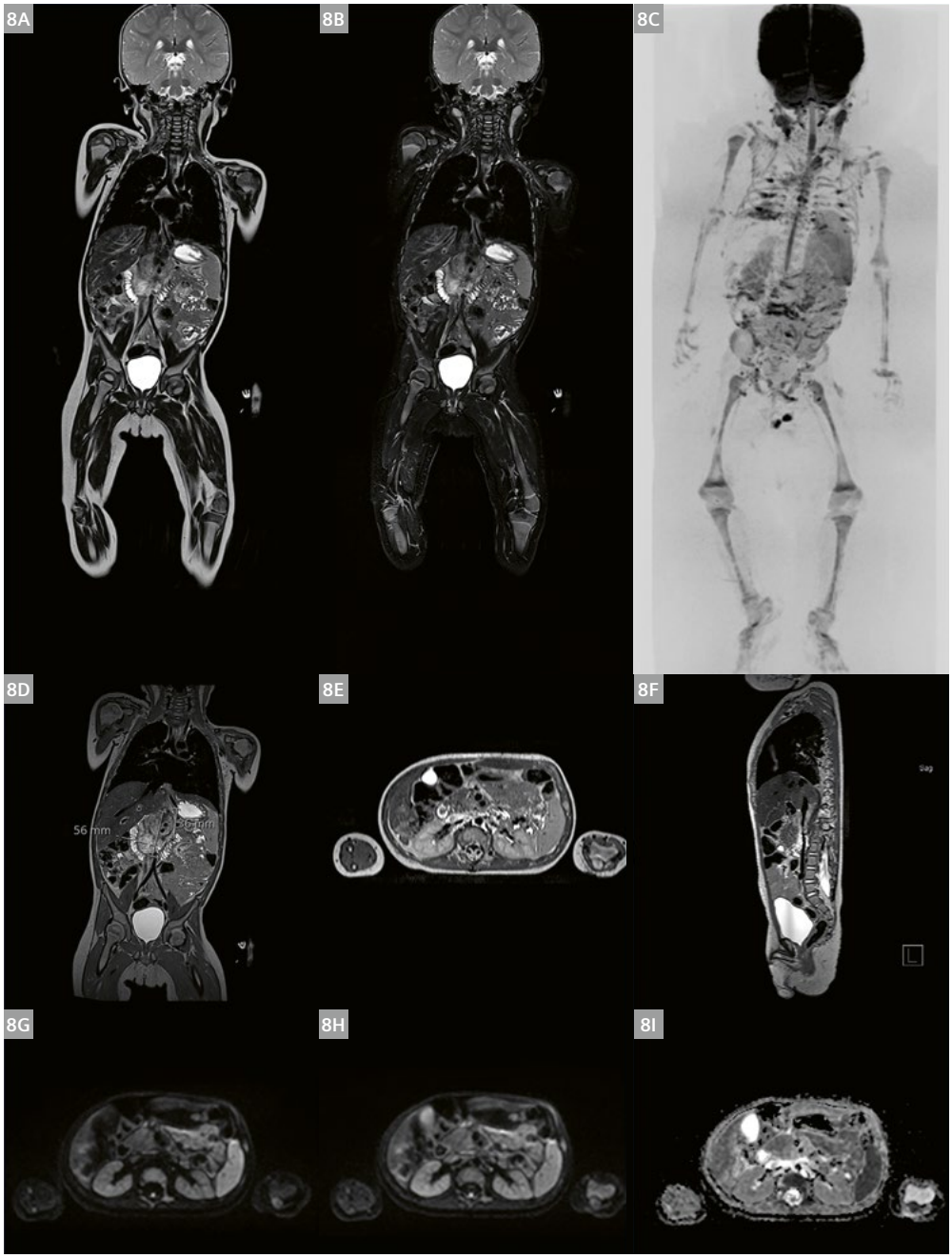


**8** **(8A)** T2w TSE Dixon in-phase coronal, 0.45 × 0.45 × 3.5 mm, TA 2–2.5 min. Multiple steps, composed.
**(8B)** T2w TSE Dixon water-only coronal.
**(8C)** EPI DWI STIR coronal, 1 × 1 × 3 mm, b-value 1000 s/mm$^2$, TA 3–3.5 min. Multiple steps, composed.
**(8D-F)** T2w 3D SPACE coronal with MPR of transversal and sagittal, 1 × 1 × 1 mm isotropic, TA 5 min.
**(8G-I)** EPI DWI transversal, 1 × 1 × 4 mm, TA 3 min.

## Case 3

A 2-year-old girl with neuroblastoma from the left adrenal gland with lymph-node and skeletal metastases. One initial and two follow-up WB-MRI scans were performed under general anesthesia on a 1.5T MAGNETOM Avanto$^{Fit}$. The scans were performed at approximately four-week intervals. The composed WB-DWI images give a good overview of the evolution of the primary tumor arising from the left adrenal gland, and of the lymph-node and skeletal metastases during the treatment course.

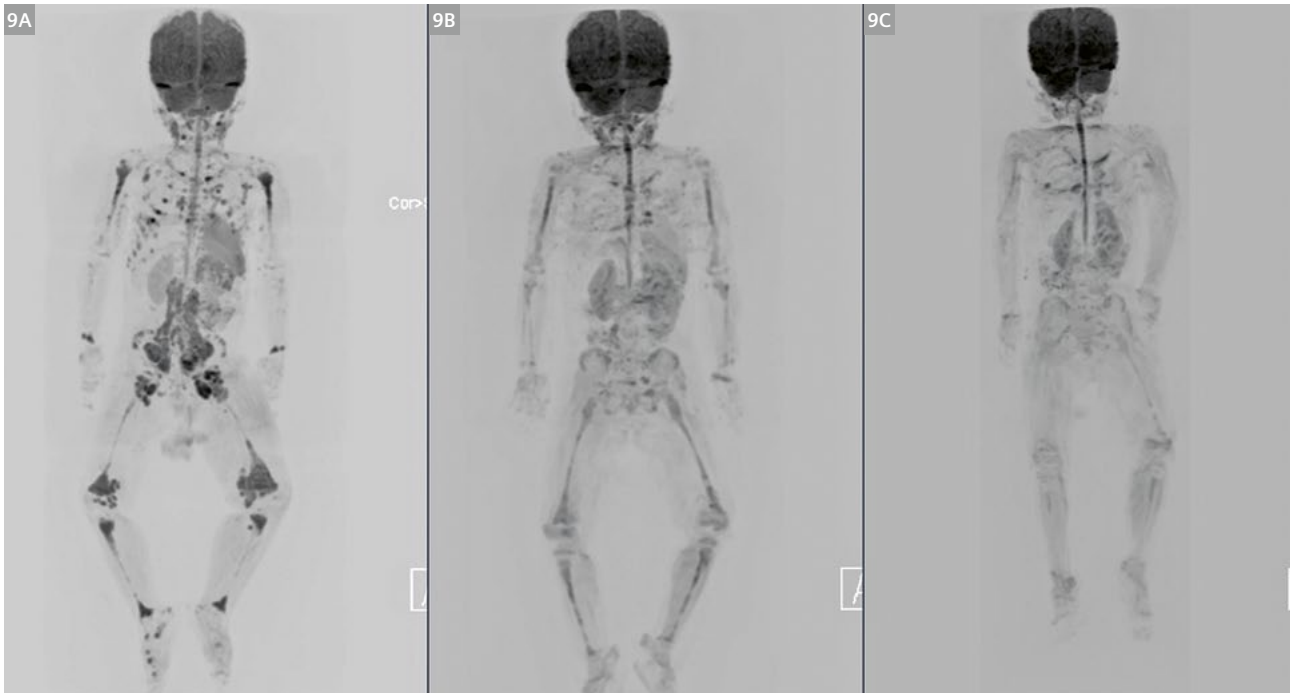


**9** **(9A)** First WB-MRI. EPI DWI STIR coronal, 1 × 1 × 3 mm, b-value 1000 s/mm², TA 3–3.5 min. Multiple steps, composed.
**(9B)** First follow-up WB-MRI. EPI DWI STIR coronal, 1 × 1 × 3 mm, b-value 1000 s/mm², TA 3–3.5 min. Multiple steps, composed.
**(9C)** Second follow-up WB-MRI. EPI DWI STIR coronal, 1 × 1 × 3 mm, b-value 1000 s/mm², TA: 3–3.5 min. Multiple steps, composed.

## Case 4

A 12-year-old boy with relapse of neuroblastoma and progressive disease in his legs, pelvis, and abdominal lymph nodes. The patient was awake during WB-MRI, with the TV screen as entertainment, on a 1.5T MAGNETOM Aera. The examination was aborted due to patient discomfort and pain, so some images are distorted by motion artifacts. Nonetheless, the examination indicates progressive changes in the tibia, lymph-node metastasis, and multiple lesions in the spine.

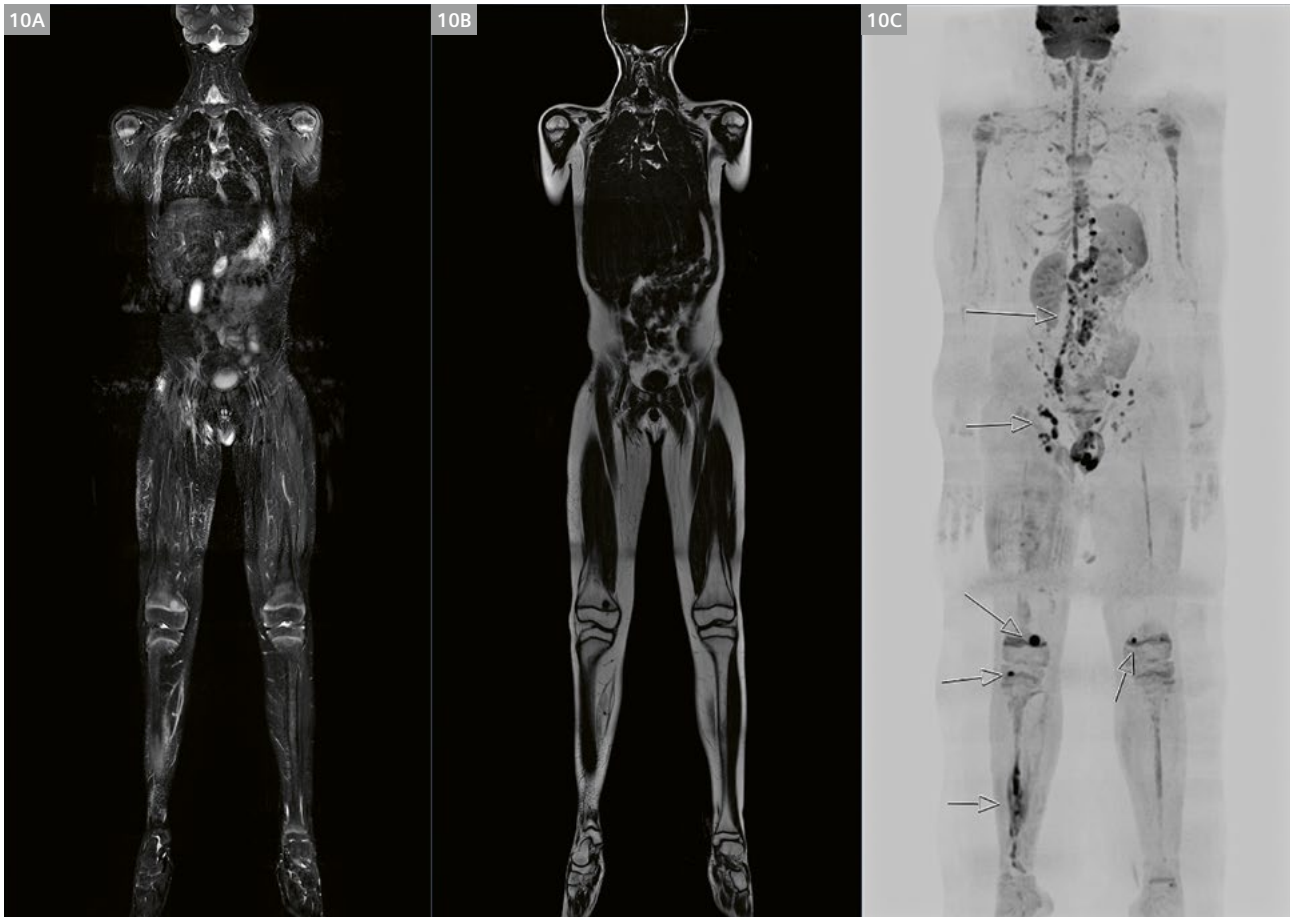


**10** **(10A)** T2w TSE Dixon water-only coronal, 0.45 × 0.45 × 4.5 mm, TA 2–2.5 min. Multiple steps, composed.
**(10B)** T2w TSE Dixon fat-only coronal.
**(10C)** EPI DWI STIR coronal, 1.5 × 1.5 × 4.5 mm, b-value 1000 s/mm², TA 2–2.5 min. Multiple steps, composed.

## Case 5

A 10-year-old boy with shoulder pain. Prior CT examination showed mediastinal lymph nodes and a lesion in the spina scapula. WB-MRI was performed for screening of multifocal disease, malignancy, or other pathology. The patient was awake during WB-MRI, with the TV screen as entertainment, on a 1.5T MAGNETOM Aera. The initial WB-MRI shows additional pathological locations in the skeleton, such as in the left humerus, left tibia, and distal femur. The second WB-MRI was performed approximately 5 months post-treatment and indicates no residual disease and no new pathology.

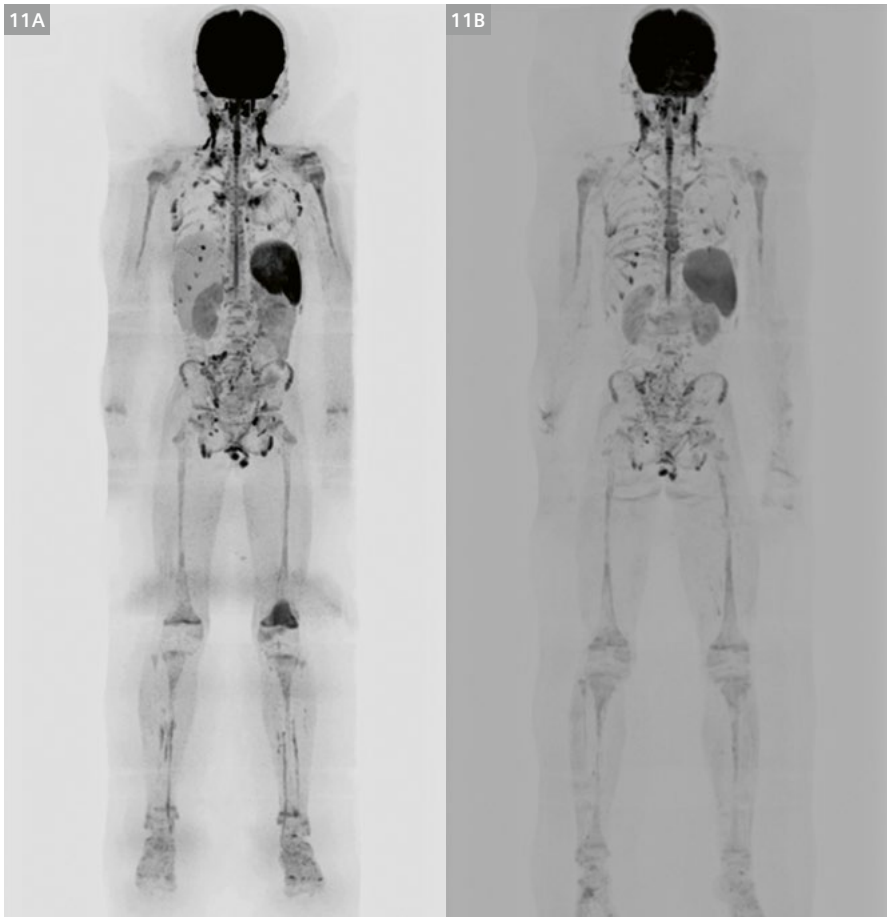


**11** **(11A)** First WB-MRI. EPI DWI STIR coronal, 1.5 × 1.5 × 4.5 mm, b-value 1000 s/mm², TA 2–2.5 min. Multiple steps, composed.
**(11B)** Last WB-MRI. EPI DWI STIR coronal, 1.5 × 1.5 × 4.5 mm, b-value 1000 s/mm², TA 2–2.5 min. Multiple steps, composed.

**References**

1 Zadig P, von Brandis E, Lein RK, Rosendahl K, Avenarius D, Ording Müller LS. Whole-body magnetic resonance imaging in children – how and why? A systematic review. Pediatr Radiol. 2021;51(1):14–24.
2 Maeder Y, Dunet V, Richard R, Becce F, Omoumi P. Bone Marrow Metastases: T2-weighted Dixon Spin-Echo Fat Images Can Replace T1-weighted Spin-Echo Images. Radiology. 2018;286(3):948–959.

## Contact

Bac Nguyen, BSc
Senior MRI Radiographer
Glenneveien 94
1476 Rasta
Norway
Tel.: +47 97702111
og_23@hotmail.com

Lil-Sofie Muller, M.D., Ph.D.
Consultant Paediatric Radiologist
Øvre Smestadvei 37 c
0378 Oslo
Norway
Tel.: +47 92828097
lilsofie.ording@gmail.com

# 3T Cardiac MRI and Acute Myocarditis in the Context of Second-dose mRNA Vaccine. A Case Study

**Erin Robins and Claire Harris**

Perth Children's Hospital, Nedlands, Western Australia

## Abstract

Presentations of acute myocarditis are becoming more common following the second and third dose of mRNA vaccinations. Myocarditis has been recognized as a rare complication of COVID-19 and the mRNA vaccines, especially in young adult and adolescent males. The novelty of this pandemic means we have no standard protocols for imaging this patient cohort. Whether or not to perform MRI remains a little unclear, so we have developed guidelines for which cases to scan. We can, however, be certain that case numbers for these presentations will rise, so robust, quick scanning protocols are important, if we are to manage increasing cases. The representative cohort is favorable for MR imaging in that most patients will be compliant, able to breath hold, and able to withstand the longer exam times of cardiac MRI. Not all patients are equal, however, and keeping scan time short and using some non-breath-hold techniques for those unable to comply, will be discussed. High-quality imaging, especially late gadolinium enhancement (LGE), is crucial for diagnosis. Here we present a case of a fourteen-year-old boy who presented to the ED with severe chest pain and fever two days following his second dose of a COVID-19 mRNA vaccine. He had extremely high troponin levels, an abnormal ECG and echo, and was referred for cardiac MRI (CMRI) for evaluation and as a baseline for monitoring. We have two MAGNETOM Skyra scanners at our site, so all CMRI is performed at 3T.

## Introduction

Myocarditis is an inflammatory disease of the heart caused by infiltrates in cardiac muscle resulting in injury without ischemia. In the developed world, the most common cause of myocarditis is viral. In the general population, 20–50 individuals in every 100,000 will present with myocarditis, especially after other vaccines such as smallpox, influenza, and hepatitis B [1, 2]. The rates for mRNA vaccines are thought to be less, and while several studies have been done to report rates of occurrence, the incidence is difficult to establish. However, the U.S. Centers for Disease Control and Prevention claim myocarditis/pericarditis rates are ~12.6 cases per million doses of second-dose mRNA vaccine among individuals 12 to 39 years of age [1], although some publications state this number could be up to 50 per million [2].

Acute myocarditis following COVID-19 vaccination was first reported on February 1, 2021 in Israel, where a 19-year-old male was admitted to ICU with the condition. His second dose of mRNA vaccine was five days prior. At the time it was not confirmed that the inflammation was attributed to the vaccine, but because the symptoms started immediately after the vaccination, suspicions were raised that an immunological reaction may have caused the condition. Concurrently, several COVID-19-related myocarditis cases had been reported, according to the U.S. National Institutes of Health [10]. Now, over one year later, myocarditis is accepted as a known side effect of COVID-19 and of mRNA (Pfizer and Moderna) vaccines [1, 3, 4], occurring largely after the second dose [6]. These cases, however, are almost always mild and self-resolving, and patients make full recoveries [3–5].

Myocarditis can be difficult to diagnose as presentation ranges from mild to acute [5]. The most common symptoms are pleuritic chest pain, palpitations, shortness of breath, fever, ipsilateral (to vaccination site) lymphadenopathy, and headache. Increased troponin levels can be present in patients presenting with myocarditis. Troponin is a type of protein found in heart muscle. When heart muscle is damaged, troponin is released into the bloodstream. Troponin is measured in nanograms per milliliter (ng/mL) and a level of 0.04 ng/mL or less is considered normal. Troponin typically becomes more elevated over a period of days, before peaking. Once the peak has occurred, patient recovery is usually swift.

ECG may also be normal, although sinus tachycardia and nonspecific ST segment and T wave changes can occur, but usually widespread ST elevations are observed [1, 3]. Patients presenting with preserved left ventricular function on echo typically have an excellent prognosis. Those with impaired LV function on echo may benefit from MRI, particularly from a monitoring perspective. CMRI provides a one-stop shop for diagnosis, and longer-term follow-up by providing data on ventricular function, myocardial injury/edema, and longer-term fibrosis, in the setting of myocarditis. Following diagnosis, patients are generally treated conservatively with anti-inflammatory medicines and beta blockers, while troponin levels are monitored.

At our site, we perform CMRI on patients who have impaired left ventricular function. It Is felt that a baseline is important for ongoing clinical monitoring and is considered best practice for the patient. TrueFISP imaging, for ventricular analysis and kinetic wall studies, SPAIR imaging of left ventricle, and late gadolinium enhancement are performed as a minimum. These sequences can be completed within 30 minutes. First-pass perfusion imaging, early gadolinium enhancement, and T1 imaging are considered bonus sequences. For patients unable to tolerate breath-holds, we perform real-time imaging of LV in place of cine imaging for wall motion and late gadolinium enhancement overview for the late gadolinium views. SPAIR imaging in these patients can be performed as inspiratory breath-holds. T1 mapping is not part of our protocol for acute or subacute myocarditis because of rationale (no expectation of fibrosis), although it might be considered in the unusual scenario of chronic myocarditis.

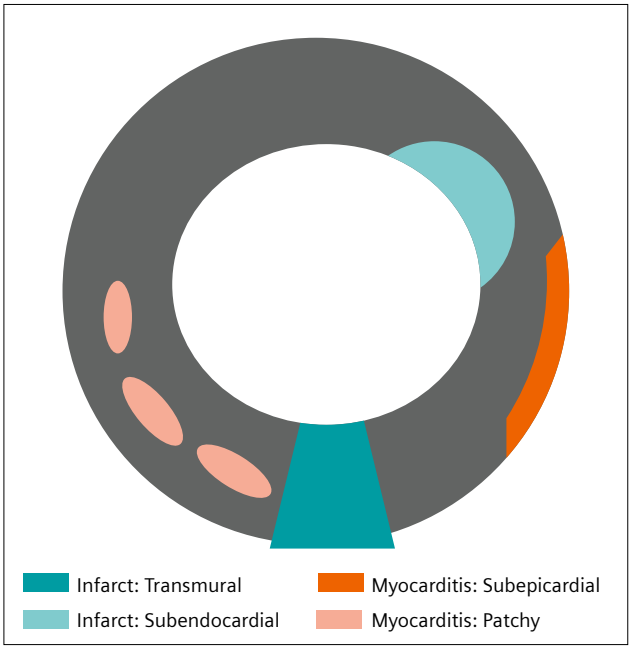


**1** Enhancement patterns of myocarditis vs. ischaemia.

## Perfusion, early, and late gadolinium enhancement

First-pass perfusion deficits are present in ischemia, but not in myocarditis. Early gadolinium enhancement may demonstrate mural thrombus in ischemia, but this would not be usual in myocarditis. So, while useful in aiding a myocarditis vs. ischemia diagnosis, these techniques are not necessary in an assessment of myocardium in the post-mRNA vaccination setting. Late gadolinium enhancement is important is to demonstrate the extent of myocardial inflammation and long-term follow-up of scar (fibrosis). It is useful to note that the enhancement patterns are different depending on the pathology, myocarditis vs. ischemia (Fig. 1).

Gadolinium does not enter normal myocardial cells, but distributes in the extracellular spaces within a few minutes following injection. Both a normal and diseased myocardium will take up contrast, but will wash out again after about five minutes in normal tissue. Diseased tissue will hold onto the contrast, allowing us to capture shortened T1 values resulting in high signal in the diseased tissue on T1-weighted images. Contrast distribution in ischemic tissue tends to pool in the subendocardium and radiate to the epicardium. The abnormalities are also in the coronary artery distributions. For nonischemic pathologies (myocarditis), the enhancement tends to be subepicardial in the lateral ventricle wall and/or patchy in the mid-ventricular wall.

## Case study

Our case involves a 14-year-old boy who presented to a regional emergency department with chest pain, following second-dose of a mRNA vaccine against COVID-19 (Pfizer) three days prior. He described the pain as crushing and constant. The patient had no prior medical history. The pain self-resolved and the patient was discharged. Later the same evening the chest pain recurred and he present-

ed to the ED where blood tests revealed a blood troponin level of 4,000 ng/mL. The patient was transferred via Royal Flying Doctor Service to the Perth Children's Hospital where he underwent an ECG, which demonstrated changes consistent with pericarditis/myocarditis: ST elevation in lateral leads and PR depression in lead 1. The patient was admitted and an echocardiogram was arranged for the following day. Up to then, he had been treated with oral anti-inflammatory drugs.

The echocardiogram showed impaired left ventricular systolic function. Systolic function is assessed by measuring the global longitudinal strain (GLS) of the longitudinal heart muscle in systole compared to diastole. Reduced GLS may reflect abnormal systolic function and is derived from speckle tracking which is software driven from echocardiogram vendors. Normal GLS ranges from 16–22% [11]. Our patient's GLS was 12%, which was considered abnormal and indicated abnormal LV function. The echo also demonstrated mild hypokinetic basal to mid-inferolateral wall contraction. Troponin levels had increased significantly in the 24 hours since the patient was admitted, peaking at 16,400 ng/mL, so at this juncture, it was deemed that CMRI would be useful to assess baseline myocardial damage with plans to follow up the scan in six months if there were significant findings. The patient commenced oral steroids and bisoprolol, a heart medication called a beta-blocker that lowers heart rate.

## Patient preparation

The patient presented in the radiology department and MRI safety and contrast checklists were completed. The patient was changed into appropriate clothing for the scan. Before entering the scan room, we give all our patients thorough, clear instructions for breath-holding. All scans are performed on expiration where possible. Expiration is used as it is easier to reproduce. For patients unable to hold their breath in expiration, we ask that they take a small inspiratory breath in, and that they take the same size breath each time. We find practicing the breath-holds in the waiting room helps. Positioning of ECG placement is explained. We inform patients that the ECG electrodes may get warm and could irritate the skin. We ask that they inform us if this happens.

The patient was positioned supine on the scan table. We ensure the patient is comfortable by placing a pad under the knees and cushions under the elbows. The chest area is cleaned with a skin cleansing agent to lower impedance and improve the ECG signal. We apply four ECG electrodes to the chest (after checking the expiry date and ensuring the electrodes are wet) and attach the ECG device as per scanner graphic user interface. The learning phase is observed. The ECG waveform should always be evaluated to ensure a good waveform is being displayed for adequate gating. If a patient has a *pes excavatum*, leads need to be placed on the same side of the chest. The ECG electrodes should be placed avoiding bony areas and sternal wires.

The Body 18 Coil and Spine Coil are used to obtain images. In order to achieve a good signal-to-noise ratio (SNR), the center of both coils should be aligned with the center of the heart. We always ensure that the coils do not touch the ECG device as this may cause pressure areas and heating. The patient was given headphones for hearing protection and to allow communication for breath-holding. We also provide a mirror so the patient can watch a movie. This is helps the patient to feel relaxed therefore aiding them to maintain the same position throughout the procedure.

## Imaging procedure

The Body 18 Coil is placed over the patient's chest with the center of the coil over the heart. The localizing laser is aligned to center of the coil and the patient is moved into the magnet. Orthogonal localizers are performed. The localizers are used to position the heart in the isocenter. Once this is established, the table position will stay at this position for the remainder of the scan. Localizers are performed in transverse, sagittal, and coronal stacks. From these a 2-chamber, 4-chamber, and short axis oblique (SAO) localizers are prescribed. Before commencing the TrueFISP (true fast imaging with steady-state precession) cine imaging, a shim box is applied for homogeneity to optimize image quality. TrueFISP cine imaging is obtained in 2-chamber, 4-chamber, SAO localizers, covering base to apex approximately 8 slices and left ventricular outflow tract (LVOT). If off-resonance artifact occurs, which we experience at 3T, then a frequency scout can help, although in our experience zero frequency adjust is nearly always the best. If the artifact significantly reduces image quality, we use gradient echo (flash). In myocarditis, the TrueFISP cines are obtained to observe ventricular wall motion and for volumetric analysis. In a cooperative patient, such as our case patient, it takes around ten minutes to complete localizers and TrueFISP cines.

A perfusion scan was set up and prepped prior to contrast injection. Contrast was administered through a 22 g cannula inserted into the right cubital fossa, which was placed prior to commencement of the exam. We used a standard MRI-compatible injector pump; contrast (gadovist) was run at a rate of 2.5 mL/sec and a dose of 7.5 mL was administered, with a 15 ml saline flush.

The perfusion scan (dynamic_tfl_sr_ePAT) was run in SAO (4 slice positions) and 4 chamber. Although not pivotal to the diagnosis, these scans were run opportunistically.

Because the late gadolinium enhancement needs to be performed ten minutes after contrast, we performed

the SPAIR (spectral attenuated inversion recovery) images in between contrast and late gadolinium views to minimize the patient's time in the scanner. SPAIR images were also acquired in the same slice positions to show the extent of the myocardial inflammation. 17 minutes of scanning time had elapsed at this point.

A TI scout was performed ten minutes following contrast injection for the late gadolinium enhancement imaging. This provides the optimal inversion time for the late gadolinium images. A phase-sensitive inversion recovery sequence (PSIR) and fast gradient echo sequence (turboflash) is used for late gadolinium enhancement imaging. We want to achieve an intermediate signal blood pool with the signal nulled in myocardium. This is to show maximum enhancement in the ventricular wall. An inversion time of 330 ms was selected. Once again 2-chamber, 4-chamber, SAO, and LVOT views are acquired with breath-holds. For those patients unable to hold their breath, we run the standard Siemens DE overview sequence, which can be run without breath-holds and gives an overview of the entire ventricle, running several planes simultaneously.

## Findings

Our case patient tolerated the CMRI extremely well with adequate breath-holding and maintained positioning throughout. It is felt that shorter examination time can really improve patient cooperation, enhancing image quality. CMRI demonstrated moderately ill-defined subepicardial and mid-wall enhancement in the late gadolinium enhanced images in the basal mid and apical thirds of the left ventricular myocardium, typical of acute myocarditis. The patient was discharged from hospital following a three-day stay. After troponin levels peaked at 16,400 ng/mL, the patient recovered quickly and responded extremely well to oral steroids. Upon discharge, the patient was advised to not get a third dose (booster) of the mRNA vaccine, and troponin levels, although trending down, were to be monitored back home in his regional hospital. He was to continue low-dose steroids and bisoprolol for two more days. Follow-up MRI in six months was arranged.

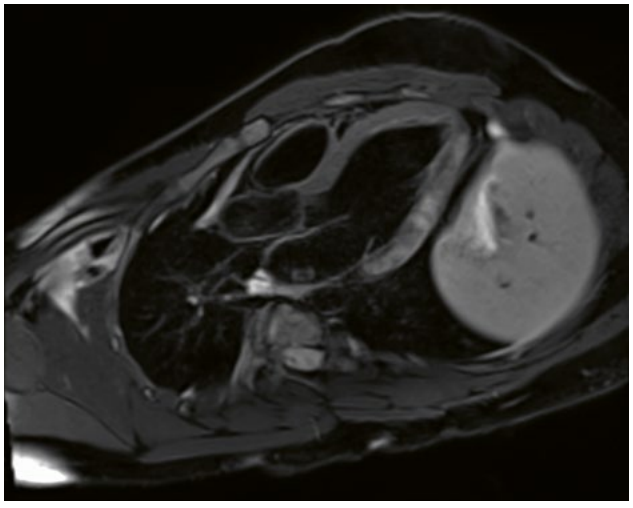

**2** LVOT SPAIR image showing patchy increased T2 signal.

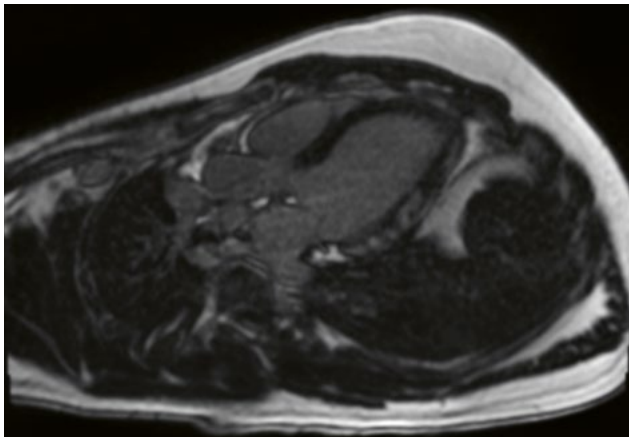

**3** LVOT LGE image showing patchy enhancement in corresponding areas on SPAIR image.

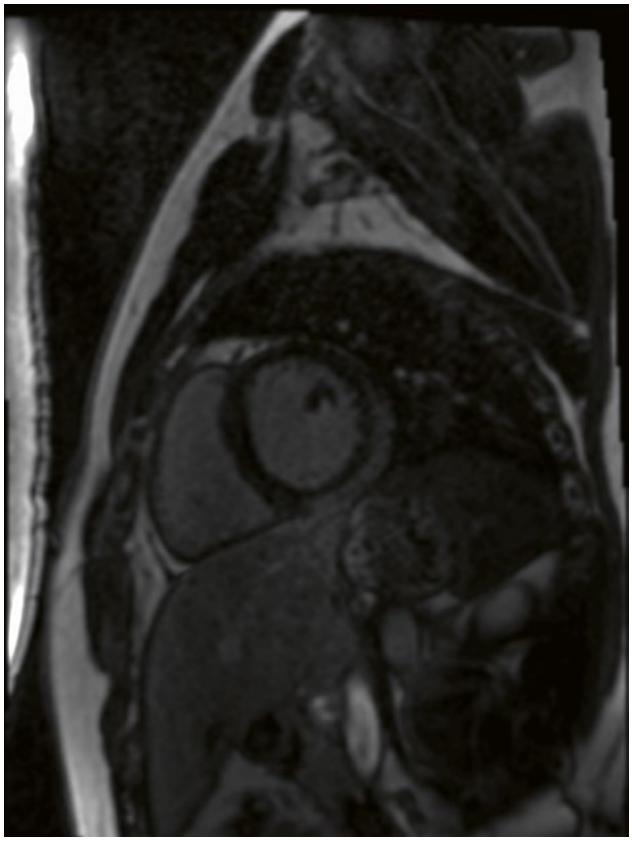

**4** SAO LGE image showing subepicardial enhancement.


**5** Complete CMRI protocol at Perth Children's Hospital for post-vaccination myocarditis.

## Conclusion

In the current situation of mass vaccination, we have seen an increase in patients presenting with vaccine-induced myocarditis. Increased demand for MRI is problematic at most institutions, so a fast, robust protocol is essential and, as shown, possible. Patients at our institution are referred for CMRI if ventricular function is compromised, as determined by reduced GLS in echocardiogram. It is possible to get very high-quality cardiac imaging in under 30 minutes for the assessment of the left ventricle in acute myocarditis, especially if post-vaccination myocarditis diagnosis is likely. The purpose of MRI is to monitor the myocardium over time if left ventricular function is affected. For patients unable to breath hold, real-time cines can be used in place of TrueFISP, and LGE overview scans can be performed instead of conventional breath-hold LGE.

## Acknowledgments

We acknowledge Dr Conor Murray and Dr Pankaj Gupta for their assistance with this article.

## Contact

Erin Robins, MRI Supervisor
Perth Children's Hospital
Hospital Ave
Nedlands 6009
Western Australia
Erin.Robins@health.wa.gov.au

Claire Harris, Senior MRI MIT
Perth Children's Hospital
Hospital Ave
Nedlands 6009
Western Australia
Claire.Harris@health.wa.gov.au

### References

1 Bozkurt B, Kamat I, Hotez P.Circulation: Myocarditis With COVID-19 mRNA Vaccines. Circulation. 2021 Jul;144(6).
2 Stecker E, Mullen B. Vaccine-Associated Myocarditis Risk in Context: Emerging Evidence. ACC. 2022, Feb 09.
3 Wong J, Sharma S, Yao J, Aggarwal A, Grigg L. COVID-19 mRNA vaccine (Comirnaty)-induced myocarditis. Med J Aust. 2022;216(3):122-123. doi: 10.5694/mja2.51394
4 Husby A, Vinsløv Hansen J, Fosbøl E, Myrup Thiesson E, Madsen M, Thomsen R, et al. SARS-CoV-2 Vaccination and Myocarditis or Myopericarditis: Population Based Cohort Study. Br Med J. 2021 Dec;375.
5 Caforio A. Receipt of mRNA Vaccine against Covid-19 and Myocarditis. N Engl J Med. 2021;385:2189-2190.
6 Siripanthong B, Nazarian S, Muser D, Deo R, Santangeli P, Khanji M, et al. Recognizing COVID-19–related myocarditis: The possible pathophysiology and proposed guideline fordiagnosis and management. Heart Rhythm. 2020 Sep;17(9):1463-1471.
7 Singer M, Taub I, Kaelber D. Risk of Myocarditis from COVID-19 Infection in People Under Age 20: A Population-Based Analysis. medRxiv. 2022 Mar.
8 Tijmes F, Thavendiranathan P, Udell J, Seidman M, Hanneman K. Radiology Cardiac MRI Assessment of Nonischemic Myocardial inflammation: State of the Art Review and Update on Myocarditis Associated with COVID-19 Vaccination. Radiol Cardiothorac Imaging. 2021 Nov;3(6).
9 Mather A, Lockie T, Nagel E, Marber M, Perera D, Redwood S, Radjenovic A, et al. Appearance of microvascular obstruction on high resolution first pass perfusion early and late gadolinium enhancement CMR in patients with acute myocardial infarction. J Cardiovasc Magn Reson. 2009 Aug; 11(1):33
10 Kime P. Pentagon Tracking 14 Cases of Heart Inflammation in Troops After COVID-19 Shots. Military.com. April 26, 2021.
11 Yingchoncharoen T, Agarwal S, Popović Z, Marwick T. Normal ranges of left ventricular strain: a meta-analysis. J Am Soc Echocardiogr. 2013; 26(2):185-91.
12 Stirrat J, White J. The Prognostic Role of Late Gadolinium Enhancement Magnetic Resonance Imaging in Patients with Cardiomyopathy. Can J Cardiol. 2013;29(3):329-36.

# Download pediatric protocols

Children are not small adults – they suffer from different types of disease than adults, they demonstrate a different physiology as well as behaviour. This has a direct impact on the way we image them. To support the care of your youngest patients[1] renowned experts in pediatric MR imaging share their optimized protocols.

## Neuro protocols for the brain and spine regions

Using Dot Engines/myExam Assists, strategies for different patient sizes (infant[1], child and teenage) are provided.
For **brain imaging**, strategies for the following clinical indications are provided:

- brain routine
- seizure
- sella
- tumor

Patient size as well as the changes in tissue relaxation times that happen during early brain development are accounted for.

For **spine imaging**, protocols for the C-, T- and L-spine as well as the whole spine are provided for the different patient sizes (infant, child and teenage).

## MSK protocols for various body regions and clinical indications

Using Dot Engines/myExam Assists, strategies for different patient sizes (infant[1], child and teenage) and different coils are provided.
Strategies include routine and arthogram programs for different patient sizes for:

- knee
- foot/ankle
- hand/wrist
- elbow
- shoulder
- pelvis

Additional strategies include tumor and infection programs for various coils such as dedicated MSK coils, UltraFlex 18 Small and Large, Body 18 and Body 30.

## Cardiac protocols – SCMR recommended protocols

To aid standardization of CMR, the Society for Cardiovascular Magnetic Resonance (SCMR) released CMR exam protocol recommendations for the most frequent CMR procedures. Based on the Cardiac Dot Engine / my Exam Assist we have prepared clinically optimized exam protocols for the Siemens MAGNETOM family of MRI scanners.

For ease of use, the protocols are organized by age groups (infant, child, teen/adult), disease-specific indications and strategically sub-organized by the patient's cooperative abilities (breath-hold or free breathing).

**Download .exar1 and PDF files at:**

**www.magnetomworld.siemens-healthineers.com/clinical-corner/protocols/pediatric-mri-protocols/pediatric-protocols**

[1] *MR scanning has not been established as safe for imaging fetuses and infants less than two years of age. The responsible physician must evaluate the benefits of the MR examination compared to those of other imaging procedures.*

# Pediatric Patient Experience: Reshaping the World of Magnetic Resonance Imaging for Children

**Gabriele Hahn, M.D.**

Institute and Polyclinic for Diagnostic and Interventional Radiology, Division of Pediatric Radiology, University Hospital Carl Gustav Carus, Technische Universität Dresden, Germany

## Abstract

In recent years, many healthcare providers have made a shift toward patient orientation. This is certainly a trend worth honoring. However, when it comes to improving patient experience, pediatric patients often seem to take a back seat. Children differ from adults in their emotional and cognitive needs, which means that different approaches to patient preparation are required. In cooperation with Siemens Healthineers, University Hospital Carl Gustav Carus in Dresden has launched a holistic project that aims to prepare children for their imaging procedures in a child-friendly way. The concept includes an interactive children's book, a song, a medal, and tailored in-room design. The overall aim is to reduce sedation rates in children undergoing MRI examinations and to positively impact the clinical workflow, patient throughput, and perceived stress levels of medical staff and parents.

## Why does a pediatric perspective matter?

When children need to be examined and treated in hospitals, they have to cope with a variety of fears, such as the fear of pain, injections, and medicines, and those caused by the symptoms of the disease, a lack of information, and being left alone without their parents [1, 2]. Other fears include nursing procedures, unfamiliar people, and being held [2]. Additionally, different developmental stages have typical fears, such as a fear of darkness [2, 3].

In the hospital context, children can feel restricted in their self-determination and freedom of choice, which makes these unfamiliar situations even more uncomfortable [4].

Children also report feeling anxiety and fear about MRI examinations. Approximately 30% of children and their parents reported that MRI examinations produced significant distress [5]. Insertion of an intravenous line was

**1** The jungle-themed examination room.


**2** Cover of the children's book *Gerda the Brave Giraffe*.

identified as the most aversive component of MRI procedures by both parents (t5%) and children (38%) [5].

MRI is one of the best and safest diagnostic procedures in pediatric care[1]. Worldwide, over 10% of radiological procedures are performed on patients under the age of 18 years [6]. However, combining pediatric care and MRI entails certain difficulties. Children are especially prone to emotions like fear, agitation, and anxiety, making it difficult for them to remain still in the scanner, with image quality compromised as a result [7].

The failure rate associated with pediatric imaging is very high. At least 50% of MRI studies in children aged between 2 and 5 fail [8]. For children aged 6 to 7 years, the failure rate is 35% [8].

Besides motion artifacts that impair image quality, other negative consequences of fear in children include longer examination times and frequent need to repeat scans [9]. Across the board, children below a certain age (usually 6 years) receive sedatives or general anesthesia to minimize motion artifacts [9].

However, although using sedation can improve image quality, it also comes with a risk for the patients, increases examination time, requires more medical staff, and considerably impacts the workflow and costs. A study suggests visit times for children having MRI under sedation are 1.5 times longer than for those who aren't sedated. Visit times for patients under general anesthesia and/or deep sedation are approximately twice that of awake patients [10]. Also, costs have been found to be between 2 and 9 times higher [10].

Moreover, large scientific studies showed that sedation was inadequate in 16% of children and failed in 7% of the cases. Excessive motion was noted in 12% of scans of sedated children and in 0.7% of those under general anesthesia [11].

We have had similar experiences here in Dresden. However, there are ways to avoid the need for sedation. For instance, some 2- or 3-year-olds are already able to understand that nothing bad will happen during the examination, providing we communicate this information in a playful way. By using positive stories and songs, and by creating a friendly environment, children can be prepared for their scan without any sedation. This would be especially beneficial for children who need frequent scans – such as for tumors.

The innovation project "Pediatric Radiology Experience", run in cooperation between University Hospital Dresden and Siemens Healthineers, aims to improve children's experience during MRI scans. It takes a holistic approach to preparing pediatric patients for radiology in a way that minimizes children's fears and anxiety, and helps create a smoother, less stressful workflow for clinical staff.

This is a positive and important development, as it finally brings children into focus. Adults have long received explanatory leaflets and been addressed appropriately. The project shows how hospitals can now also do the same for children.

The aim is to address children's needs beforehand in order to relieve their fears about the upcoming scan. The focus therefore lies on reaching the children and their parents at home, so that there is ample time to prepare the child for the study. By means of child-friendly information embedded in a fun book with interactive elements, children learn about the MRI procedure and what they will experience. The material also provides tips on how parents can best support their child before and during the scan. Additionally, the holistic approach includes patient-friendly room design, a song, and special rewards tailored to children.

## What is our goal?

The mission of the cooperation project between University Hospital Dresden and Siemens Healthineers is to improve medical care for children undergoing imaging procedures.

The project involves a child-centered solution designed to reduce the need for sedation in children, minimize their hospital-related fears, and help them have a more comfortable experience.

The work is based on user-centered research and product design. By conducting workshops with children and parents, we collected information about the difficulties and worries they have regarding diagnostic examinations. This information allowed us to respond to these specific issues and develop optimal solutions.

The project also engages with strategies that lead to satisfied staff, which in turn enable a better workflow and a good reputation. Given that effective preparation of children is likely to reduce stress during the examination, we can expect a smoother workflow, better image quality, and less chance of having to stop scans mid-exam.

The abovementioned mechanisms are depicted in the following figures. The triangle in Figure 3A describes the

[1] *MR scanning has not been established as safe for imaging fetuses and infants less than two years of age. The responsible physician must evaluate the benefits of the MR examination compared to those of other imaging procedures.*

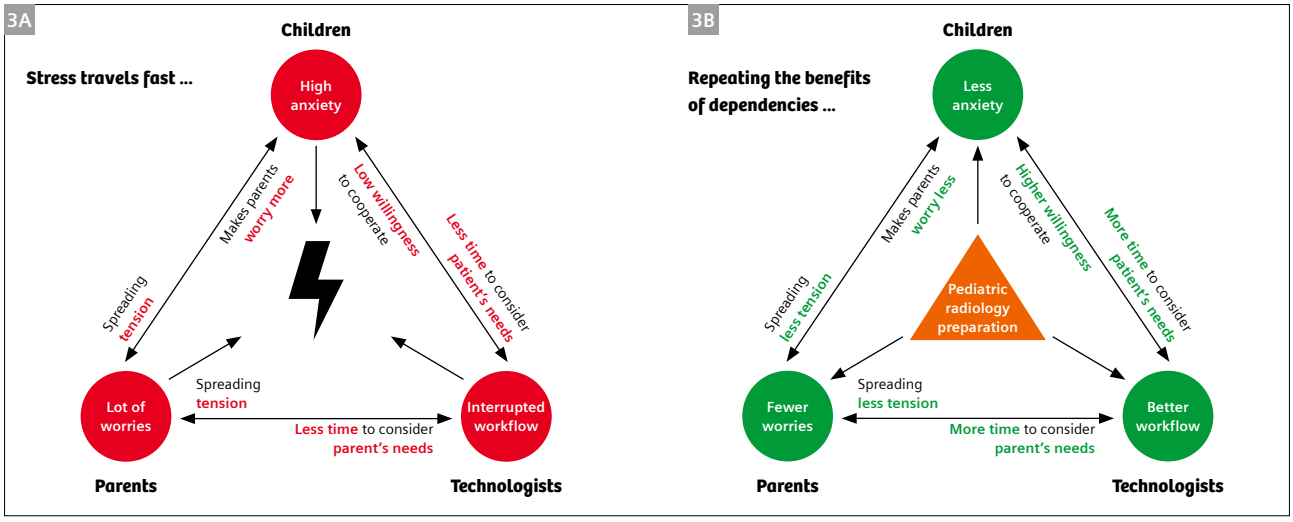


**3** Usual stress cycle **(3A)** and optimized stress cycle **(3B)**.

worst-case scenario: Children are not sufficiently prepared for and educated about their upcoming examination, which makes them feel anxious. The child's tension transfers to the parents, making them feel uneasy, which in turn makes the child worry even more. This vicious circle creates an overall negative atmosphere, that can interrupt the clinical workflow and put staff under a lot of stress. By introducing proper patient preparation, we can create a positive effect (Fig. 3B).

Parents who have been educated about their child's examination feel less anxious. This affects the child's state of mind in a positive and calming way. The child's greater willingness to cooperate allows the technologists to focus on the child and their individual needs.

This is also why, even in the case of very grave findings, we encourage parents not to cry. If the child becomes aware of their parents' anxiety or fear, they are more likely to panic and feel worse. However, if the parents are well-prepared and relaxed, and understand that their child is in good hands, this will help create a calmer atmosphere for them and their child.

Effective preparation of the children themselves also reduces stress for the clinical staff. The technologists will find it easier to work with the children and the interactions become friendlier on both sides. The material we offer in the project helps guide the way staff attend to the children. This is especially useful for those who don't have much experience with children in general. Consequently, the children are not as afraid as they usually are and the technologists are more relaxed.

Finally, as a multidisciplinary team with a diverse background in medicine, design thinking, research, psychology, and drama, we were able to design the project so that it created a holistic experience for our patients.

## Which materials exist?

### Before the examination: Interactive book, *Gerda the Brave Giraffe*

One study found that the essential strategies for coping with the hospital-related fears of children aged between 4 and 6 involved the presence of parents, help from staff, humor, play, and the child's own "security" toys. Play is the factor that most children mentioned as helping them to manage their fears [12]. Based on these findings, our children's book, *Gerda the Brave Giraffe*, was supplemented with playful interactive elements.

The story is about a little giraffe named Gerda. She loves to eat jello. One day, her mom is preparing some when her necklace breaks and the pearls fall into the pot.

Gerda doesn't realize what's happened and eats up all the jello – including the pearls. She gets a really bad stomach ache shortly afterward. Her pediatrician says she needs an MRI examination, so Gerda sets off on her journey to the radiology department.

While accompanying Gerda, the children learn what to expect during the procedure in a playful and child-friendly way.

The principal idea is that children are less afraid in unfamiliar situations when they know what to expect. Therefore, the book talks about different aspects of an MRI scan, such as how the examination proceeds, the use of contrast media, and the noises created by the machine.

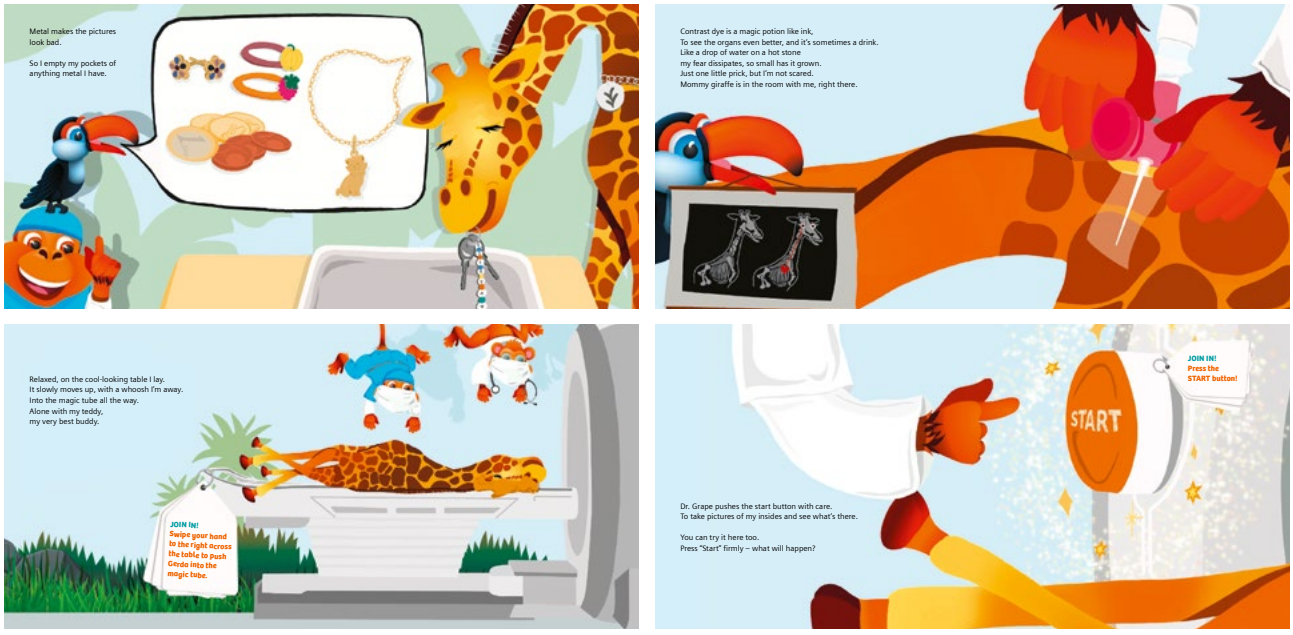


**4** Examples of content of the children's book with interactive elements.

**During the examination: Tailored in-room design**

The design of the room and the medical devices plays an important role in the child's experience. Before an examination, their feelings can fluctuate between insecurity, anxiety, and hope. Room and product designs geared toward these emotional states can serve as a distraction, give joy, and create a sense of security. Patients will feel understood and welcome.

Through our cooperation with Siemens Healthineers, we offer an in-room design that is tailored to a child's needs. From the moment a child enters a hospital, they are usually confronted with lots of cold, sterile, and often lifeless-looking surroundings. We aimed to counter this by creating a more colorful and welcoming atmosphere in the examination room. The jungle-themed design makes the children feel more comfortable – and it also creates a positive association with something the children are already familiar with: Gerda, the little giraffe from the book.

**5** Example of the jungle-themed waiting room.


**6** Ambient lighting at University Hospital Dresden.

**After the examination: A medal**

Each patient receives a medal after completing the scan. By offering the prospect of a reward after a challenge, we aim to create a positive feeling about the examination and increase the child's motivation to cooperate.

By providing a variety of materials, we can accommodate different types of children: Some children are very visual, so the book is ideal for them. There's also a song, which is good for children who like to listen and who respond well to music. Overall, the interior design takes away the children's fears because the colorful pictures remove the expectation of seeing big, noisy machines in the room.

**First experiences at University Hospital Dresden**

Some of our young patients have already had the opportunity to prepare for their MRI examination with Gerda. Ambient lighting during the examination, and the medal as a reward have also proven successful.

Emöke Böhme, one of the technologists who regularly looks after children during their procedures at University Hospital Dresden, says: "There were five-year-olds who didn't have an IV inserted, but still had to lie still during the examination. The parents sat down in the waiting area and read the book with them. The children did a great job of keeping up with [the examination] and then wanted to keep the book. We gave it to them as a reward, of course."

Emöke feels that Gerda, the brave giraffe is a very good way of gently introducing children to their upcoming scan. It provides them with the care and attention they need, and helps create a warm relationship between them and the clinical staff.

The narrative guides children from the beginning of the MRI journey to the end. The idea is that they identify with Gerda as she successfully completes her scan. It should also stop the children from focusing exclusively on the clinical environment and distract them as they wait for their exam.

Qualitative interviews with parents already show that using the book to prepare children for the examination offers a wide range of benefits. The children stated that they were less afraid of the scan. They were also able to imagine in advance what they would encounter during the examination. Furthermore, information provided to parents helps them feel confident and take a more relaxed approach to their child's procedure.

Preparing the patients with the Gerda materials also leads to an effective course of the examinations on a larger scale. This is because it establishes trust and enables good cooperation with the young patients, which is the basis for successful procedures.


**7** Reward medal

Our various preparation materials help us to reduce stress and anxiety in children even before the examination starts. This makes the children more accessible and the hospital staff find it easier to work with them in a child-friendly manner. Reducing the workload involved in patient preparation and enabling a workflow without interruptions or terminations can also reduce stress on employees. In addition to the interpersonal benefits, we believe the project also has advantages at the clinical level: The materials have the potential to minimize movement artifacts and the need for sedation during MRI scans.

## Conclusion

The concept described here is a holistic way of relieving the anxieties of pediatric patients and of decreasing the use of sedation in pediatric MRI. While tools aiming to improve the pediatric patient experience have traditionally focused on distracting children from the aversive clinical environment, our approach also includes the active involvement of the patients and their parents.

This concept has the potential to be expanded to other patient journeys, such as those for inpatients receiving cancer treatment. It could also be extended to include digital media to facilitate greater access to the materials. Our initial work with the Gerda project here at University Hospital Dresden has received very positive feedback from patients, parents, and clinical staff.

**References**

1 Kettwich S, Sibbitt WL Jr, Brandt JR, Johnson CR, Wong CS, Bankhurst, AD. Needle phobia and stress-reducing medical devices in pediatric and adult chemotherapy patients. J Pediatr Oncol Nurs. 2007;24(1):20–28.
2 Salmela M, Salanterä S, Aronen E. Child-reported hospital fears in 4 to 6-year-old children. Pediatr Nurs. 2009;35(5):269–276, 303.
3 Gullone E. The development of normal fear: a century of research. Clin Psychol Rev. 2000;20(4):429–451.
4 Salmela M, Aronen ET, Salanterä S. The experience of hospital-related fears of 4- to 6-year-old children. Child Care Health Dev. 2011;37(5):719–726.
5 Tyc VL, Fairclough D, Fletcher B, Leigh L, Mulhern RK. Children's distress during magnetic resonance imaging procedures. Child Health Care. 1995;24(1):5–19.
6 Pediatric Imaging Market Size, Share & Trends Analysis Report By Modality (X-ray, Ultrasound, MRI, CT), By Application (Gastroenterology, Cardiology, Oncology), By End User, By Region, And Segment Forecasts, 2020 – 2027 [PDF]. Dublin, Ireland: Grand View Research; 2020. Available from: https://www.grandviewresearch.com/industry-analysis/pediatric-imaging-market.
7 Perez M, Cuscaden C, Somers JF, Simms N, Shaheed S, Kehoe LA, et al. Easing anxiety in preparation for pediatric magnetic resonance imaging: a pilot study using animal-assisted therapy. Pediatr Radiol. 2019;49(8):1000–1009.
8 Malisza KL, Martin T, Shiloff D, Yu DC. Reactions of young children to the MRI scanner environment. Magn Reson Med. 2010;64(2):377–381.
9 Oztek MA, Noda S, Beauchemin EA, Otto RK. Gentle Touch: Noninvasive Approaches to Improve Patient Comfort and Cooperation for Pediatric Imaging. Top Magn Reson Imaging. 2020;29(4):187–195.
10 Vanderby S, Babyn PS, Carter MW, Jewell SM, McKeever PD. Effect of anesthesia and sedation on pediatric MR imaging patient flow. Radiology. 2010;256(1):229–237.
11 Malviya S, Voepel-Lewis T, Eldevik OP, Rockwell DT, Wong JH, Tait AR. Sedation and general anaesthesia in children undergoing MRI and CT: adverse events and outcomes. Br J Anaesth. 2000;84(6):743–748.
12 Salmela M, Salanterä S, Aronen ET. Coping with hospital-related fears: experiences of pre-school-aged children. J Adv Nurs. 2010;66(6):1222–1231.

## Contact

Gabriele Hahn, M.D.
Institut und Poliklinik für Diagnostische und Interventionelle Radiologie
Bereich Kinderradiologie
Universitätsklinikum Carl Gustav Carus
TU Dresden
Fetscherstrasse 74
01307 Dresden
Germany
gabriele.hahn@uniklinikum-dresden.de

# Meet Siemens Healthineers

Siemens Healthineers: Our brand name embodies the pioneering spirit and engineering expertise that is unique in the healthcare industry. The people working for Siemens Healthineers are totally committed to the company they work for, and are passionate about their technology. In this section we introduce you to colleagues from all over the world – people who put their hearts into what they do.

## Pedro Itriago Leon

Pedro was born in Caracas, Venezuela. He started his MR career there in 1989, working as a technologist at the first MRI suite in the country: Instituto de Resonancia Magnética (IRM) La Florida. In the 14 years he spent there, Pedro oversaw the introduction of many new MR applications as the institute added new scanners with newer software to its fleet. He was also the technologist in charge of supporting the institute's MRI clinical research group. In 1992, Pedro began working as a freelance MR application specialist for Siemens Venezuela, covering South America. In 1996, he joined the Global Siemens Freelance MR Application Specialist group. Before becoming a U.S. MR collaborations manager based in Houston, TX, USA, in 2018, he supported the Test Team in Erlangen, Germany, in the release of various new systems and software versions from *syngo* MR B13 to *syngo* MR E11A. Pedro also developed protocols for several MR systems from Siemens Healthineers both in Erlangen and Shenzhen, China, and worked in the applications team in Erlangen, where he was involved in the development of the 3T MAGNETOM Vida.



Houston, TX, USA

**How did you first come into contact with MRI?**
I started working as an MR technologist at IRM La Florida on a MAGNETOM 42, also known as GBS II (for the German-speaking readers, GBS stands for *Grundbausatz*, which roughly translates as "MR kit"). It was a completely different experience using an MR scanner back then. Numaris 2 was the software platform, and there were only three local coils available: Head, Spine, and a multi-purpose Helmholtz coil (which had to be manually tuned), plus the Body coil inside the magnet, which was used for all body imaging. We could only scan patients in the isocenter, which made for quite interesting patient positioning in MSK exams. A brain double-echo SE could run for about 8 minutes. You had to wait a couple of minutes for the images to be calculated, and about 10 seconds if you wanted to magnify an image. The only sequences you had were single- and multi-echo SE, and IR – and you could only acquire images in one orientation at a time. Multislice-multiangle (MSMA, an acronym we still use in protocols from Siemens Healthineers today) came in a later software update. The fastest sequences back then were the newly developed FLASH and FISP GRE sequences.

**What do you find motivating about your job?**
Having participated in the clinical side and the development side of MR collaborations, I know that both sides want to improve patient care – but are, in essence, worlds apart. The path of communication between these two sides can be quite difficult, as one speaks in medical terms and the other speaks in physics and engineering terms. Siemens Healthineers speaks both of these languages – and as a collaborations manager, I get to experience the synergy between the clinical input that creates and validates new techniques, and the engineering of those techniques. This combination is what makes innovations a reality. It's amazing to see the two spheres come together for a common goal: improving patient care worldwide. As well as leading to new and exciting applications, this can also lead to new hardware. So I'd say this is the thing I find most motivating.

**What direction do you think the MRI development should take?**
I think we should keep pushing toward improving the overall patient experience – by making exams that are currently

difficult possible and by shortening the amount of time the patient spends in the magnet. We've already seen how newer acquisition techniques help shorten acquisition time. They include iPAT, CAIPIRINHA, Compressed Sensing, Simultaneous Multi-Slice, and Wave CAIPI. And with Deep Resolve, for example, we have witnessed how AI reduces acquisition times whilst also improving image quality. Yet, this is only the beginning of what AI can do to improve patient care. There is also work that needs to be done in motion correction, which will allow us to reduce the number of exams being done under anesthesia, and will help in acquiring clinically useful images for patients unable to hold their breath or stay still. While this will improve many types of exams, pediatric imaging will benefit the most, because this is where anesthesia is used most and makes the prospect of an MRI exam cumbersome and stressful for clinicians and parents alike.

**What would you do if you could spend a month doing whatever you wanted?**
I've spent so much time traveling around the world for work. It allowed me to visit many new places and make some of them recurring backdrops of my life. But suddenly finding myself in one place for what feels like such a long time, even though it's only been four years, I must say that I miss visiting the places I came to cherish as second homes. If I had the time, I would try to visit them again, and travel to some places I've never been before.

# Get to know us

Find more portraits of our colleagues around the world!

**www.magnetomworld.siemens-healthineers.com/meet-siemens-healthineers**

Not for distribution in the US

On account of certain regional limitations of sales rights and service availability, we cannot guarantee that all products included in this brochure are available through the Siemens sales organization worldwide. Availability and packaging may vary by country and is subject to change without prior notice. Some/All of the features and products described herein may not be available in the United States.

The information in this document contains general technical descriptions of specifications and options as well as standard and optional features which do not always have to be present in individual cases, and which may not be commercially available in all countries.

Due to regulatory reasons their future availability cannot be guaranteed. Please contact your local Siemens organization for further details.

Siemens reserves the right to modify the design, packaging, specifications, and options described herein without prior notice. Please contact your local Siemens sales representative for the most current information.

Note: Any technical data contained in this document may vary within defined tolerances. Original images always lose a certain amount of detail when reproduced.

**Siemens Healthineers Headquarters**
Siemens Healthcare GmbH
Henkestr. 127
91052 Erlangen, Germany
Phone: +49 9131 84-0
siemens-healthineers.com

*Published by Siemens Healthcare GmbH · Order No. A91MR-1000-148M-7600 · Printed in Germany · 8705 1120 ·* 